Internal tides off the Amazon shelf Part I: importance for the structuring of ocean temperature during two contrasted seasons

Fernand Assene [1], Ariane Koch-Larrouy [2], Isabelle Dadou [3], Michel Tchilibou [4], Guillaume Morvan [5], Jérôme Chanut [6], Alex Costa da Silva [7], Vincent Vantrepotte [~~7~~8], Damien Allain [~~8~~9], Trung-Kien Tran [~~9~~~~.~~10]

[1, 2, 3, 5, ~~8~~9] Université de Toulouse, LEGOS (CNRS/IRD/UPS/CNES), Toulouse, France~~,~~
[1, 6] Mercator Ocean International, 31400, Toulouse, France~~,~~
[4] Collecte Localisation Satellites (CLS), 31500, Ramonville Saint-Agne, France~~,~~
[7~~, 9~~] Departamento de Oceanografia da Universidade Federal de Pernambuco, DOCEAN/UFPE, Recife, Brazil
[8, 10] Laboratoire d'Océanologie et de Géosciences (LOG), 62930, Wiméreux, France

Correspondence to: Fernand Assene ~~*(assene@legos.obs-mip.fr)*~~*fassene@mercator-ocean.fr*

Abstract

~~Tides and internal tides (IT) in the ocean can significantly affect local to regional ocean temperature, including sea surface temperature (SST), via physical processes such as diffusion (vertical mixing) and advection (vertical and horizontal) of water masses. Offshore of the Amazon River, strong IT have been detected by satellite observations and well modelled; however, their impact on temperature, SST and the identification of the associated processes have not been studied so far. In this work, we use high resolution (1/36°) numerical simulations with and without the tides from an ocean circulation model (NEMO). This model explicitly resolves the internal tides (IT) and is therefore suitable to assess how they can affect ocean temperature in the studied area. We distinguish the analysis for two contrasted seasons, from April to June (AMJ) and from August to October (ASO), since the seasonal stratification off the Amazon River modulates the IT's response and their influence in temperature.~~

~~The generation and the propagation of the IT in the model are in good agreement with observations. The SST reproduced by the simulation including tides is in better agreement with satellite SST data compared to the simulation without tides. During ASO season, stronger meso-scale currents, deeper and weaker pycnocline are observed in contrast to the AMJ season. The observed coastal upwelling during ASO season is better reproduced by the model including tides, whereas the no-tide simulation is too warm by +0.3 °C for the SST. In the subsurface above the thermocline, the tide simulation is cooler by -1.2 °C, and warmer below the~~

Définition du style : Titre 2: Police :14 pt, Gras, Anglais (États-Unis), Espace Avant : 6 pt, Après : 0 pt
Définition du style : Titre 4
Définition du style : Police par défaut
a mis en forme : Police :20 pt, Gras, Couleur de police : Automatique
a mis en forme : Normal, Espace Avant : 0 pt, Après : 0 pt, Interligne : simple
a mis en forme : Français (France)
a mis en forme : Français (France)
a mis en forme : Français (France)
a mis en forme : Français (France)
a mis en forme : Français (France)
a mis en forme : Français (France)
a mis en forme : Français (France)
a mis en forme : Français (France)
a mis en forme : Français (France)
a mis en forme : Français (France)
a mis en forme : Français (France)
a mis en forme : Français (France)
a mis en forme : Français (France)
a mis en forme : Police :12 pt, Non Italique
a mis en forme : Police :12 pt, Non Italique
a mis en forme : Couleur de police : Texte 1
a mis en forme : Espace Avant : 12 pt

~~thermocline by +1.2 °C compared to the simulation without the tides. The IT induce vertical mixing on their generation site along the shelf break and on their propagation pathways towards the open ocean. This process mainly explains the cooler temperature at the ocean surface and is combined with vertical and horizontal advection to explain the cooling in the subsurface water above the thermocline and a warming in the deeper layers below the thermocline. The surface cooling induced in turn an increase of the net heat flux from the atmosphere to the ocean surface, which could induce significant changes in the local and even for the regional tropical Atlantic atmospheric circulation and precipitation.~~

~~We therefore demonstrate that IT, via vertical mixing and advection along their propagation pathways, and tides over the continental shelf, can play a role on the temperature structure off the Amazon River mouth, particularly in the coastal cooling enhanced by the IT.~~

The impact of the tides (internal and barotropic) on the vertical and horizontal structure of temperature off the Amazon River is investigated over two highly contrasting seasons. Twinned regional simulations with and without tides are used to highlight the general effect of tides. The tides tend to cool down the ocean from the surface (~0.3 °C) to above the thermocline (~1.2 °C), and to thaw it below the thermocline (~1.2 °C). The heat budget analysis leads to the conclusion that vertical mixing could represent the dominant process that drives these temperature variations within the mixed layer, while it is associated with both horizontal and vertical advection below to explain temperature variations. The intensified mixing in the simulation including tides is attributed to the breaking of internal tides (ITs), on their generation sites over the shelf break and offshore along their propagation pathways. When over the shelf the mixing is attributed to the dissipation of the barotropic tides. Both horizontal and vertical advections exist in simulations without the tides but are strengthened when including it. Furthermore, vertical heat budget equation terms show a typical mode-1 horizontal propagation wavelength of ITs.

In addition, we found the tides can also have an impact on interactions between the upper ocean interface and the underlying atmosphere. They account for a significant proportion of the net heat flux between the atmosphere and the ocean, with a marked seasonal variation of 33.2% to 7.4% between the first and second seasons. Tidal dynamics could be therefore critical to understand the regional climate. This study highlights the key role of tides, particularly, how ITs-related vertical mixing helps to shape ocean temperature off the Amazon.

Keywords: Amazon shelf break, internal tides, ~~Amazon continental shelf and slope~~mixing, temperature, heat flux, modeling, satellite data~~, mixing, heat flux~~.

I. Introduction

Temperature and its spatial structure ~~play~~carry out a crucial role in ocean dynamics, including water mass formation (Swift and Aagaard, 1981; Lascaratos, 1993; Speer et al~~.~~., 1995), transport and mixing of other tracers in the ocean and exchanges with other biosphere compartments (Archer et al~~.~~., 2004, Rosenthal et al~~.~~., 1997), and most importantly on surface heat exchange at the interface with the atmosphere (~~Calyson~~Clayson and ~~Bagdanoff~~Bogdanoff, 2013; Mei et al~~.~~., 2015) and can thus significantly influence the climate (Li et al~~.~~., 2006; Collins et al~~.~~., 2010). This oceanic thermal structure can be modified at various spatial and temporal scales~~ by~~. Through different processes external to the ocean ~~such as incident~~like solar radiation, heat ~~fluxes~~exchanges with the atmosphere, winds, precipitation, and freshwater inputs from rivers. ~~Processes~~And by its internal ~~to the ocean also play a crucial role in this thermal structure,~~processes such as mass transport by currents and eddies (e.g~~.:~~., Aguedjou et al., 2021), mixing by turbulent diffusion (Kunze et al~~.~~., 2012), ~~tides and~~ internal ~~tidal~~ waves ~~(IT)~~and their dissipation (Barton et al., 2001; Smith et al., 2016; Salamena et al., 2021). ~~The role~~Finally, bottom friction of ~~IT on the thermal structure of the ocean is of increasing interest with many studies in recent years, but remains poorly understood in many ocean regions, and~~ the barotropic tidal currents may also produce intensified mixing especially ~~off the Amazon~~ for shallow water condition (e.g., over a shelf~~.~~, see Lambeck and Runcorn, 1977; Le Provost and Lyard, 1997) and significantly modify ocean temperature in surface layers (Li et al., 2020).

~~In a stratified ocean, the passage of a barotropic tide over a topographic profile with a steep slope (continental slope, seamount, oceanic ridge) generates a disturbance in the flow that gives rise to a so-called baroclinic tide, with the same frequency, but with higher vertical velocities (Zhao et al., 2016). The baroclinic tide, also known as internal tidal waves (IT), thus captures part of the energy of the barotropic tide, propagates it and dissipates it into the global ocean by diapycnal mixing (Zhao et al., 2012), i.e., up to about 1 TW in the deep ocean (Egbert and Ray, 2000; Niwa and Hibiya, 2011) and thus helps to feed the thermohaline circulation (Munk and Wunsch, 1998). These two tidal processes (barotropic tide and IT) thus bring together a set of mechanisms for transferring and redistributing energy from larger to smaller oceanic scales, which can be understood as a tidal energy cascade. The dissipation of IT occurs mainly locally at the generation sites for high-mode IT that are associated with higher vertical shear, while a significant part of the energy dissipates offshore along their propagation path for low-mode IT (Zhao et al., 2016). Results from models in the Indonesian seas (Koch-Larrouy et al., 2007 and Nugroho et al., 2018) and observations in the Celtic Sea (Sharples et al. 2007)~~

a mis en forme : Espace Avant : 12 pt, Après : 6 pt

a mis en forme : Couleur de police : Texte 1

a mis en forme : Couleur de police : Texte 1

a mis en forme : Couleur de police : Texte 1

a mis en forme : Couleur de police : Texte 1

a mis en forme : Couleur de police : Texte 1

a mis en forme : Couleur de police : Texte 1

a mis en forme : Couleur de police : Texte 1

a mis en forme : Couleur de police : Texte 1

a mis en forme : Couleur de police : Texte 1

a mis en forme : Couleur de police : Texte 1

a mis en forme : Couleur de police : Texte 1

a mis en forme : Couleur de police : Texte 1

a mis en forme : Couleur de police : Texte 1

a mis en forme : Couleur de police : Texte 1

a mis en forme : Couleur de police : Texte 1

a mis en forme : Couleur de police : Texte 1

a mis en forme : Couleur de police : Texte 1

a mis en forme : Couleur de police : Texte 1

a mis en forme : Couleur de police : Texte 1

a mis en forme : Couleur de police : Texte 1

a mis en forme : Couleur de police : Texte 1

a mis en forme : Couleur de police : Texte 1

a mis en forme : Couleur de police : Texte 1

a mis en forme : Couleur de police : Texte 1

a mis en forme : Couleur de police : Texte 1

a mis en forme : Couleur de police : Texte 1

a mis en forme : Couleur de police : Texte 1

a mis en forme : Couleur de police : Texte 1

a mis en forme : Couleur de police : Texte 1

a mis en forme : Couleur de police : Texte 1

~~and the Yellow Sea (Xu et al., 2020), point out that IT dissipate most of their energy vertically, where the vertical gradient of stratification is maximal in the water column. IT can also vertically advect water masses during their propagation. They thus induce vertical displacements of the isopycnal levels of several meters to a few tens of meters, observable in the thermocline (Wallace et al., 2008; Xu et al. 2020). Denmann and Garett (1983) and Bordois et al. (2016) point out that the stratification peak acts as a waveguide for the propagation of IT.~~

~~The mixing and advection induced by IT results in a change in temperature structure throughout the water column. In surface waters, Smith et al. (2016) report that IT can induce surface cooling varying between 1 °C and 5 °C depending on the ocean region. Koch-Larrouy et al. (2007) and Nagai and Hibiya (2015) have shown, for the Indonesian region, that IT induces a surface cooling of -0.5 °C on average and that this decreases cloud convection in the atmosphere on a local scale, which in turn reduces precipitation by 20% and thus plays an important role on the climate on a regional scale. Furthermore, Jithin and Francis (2020) showed that IT can also affect the temperature in deep waters (> 1600 m), leading to a warming of the order of 1–2 °C.~~

~~The barotropic tides dissipate most of their energy in shallow coastal waters by bottom friction when the mean ocean depth becomes less than the amplitude of the tide (Lambeck and Runcorn, 1977; Le Provost and Lyard, 1997), and can thus modify temperature. Furthermore, Gonzalez-Haro et al. (2019) showed that barotropic and baroclinic tidal currents can induce temperature fluctuations by horizontal advection of surface water masses over hundreds of kilometers, and thus contribute to modifying the SST. These two tidal processes (barotropic and baroclinic) can also affect other tracers such as nutrients, chlorophyll and sediments (Heathershaw et al., 1987; da Silva et al., 2002; Sharples et al., 2007; Pomar et al., 2012; Muacho et al., 2014; Tuarena et al., 2016; Barbot et al., 2022).~~

The key source for internal waves generation is the barotropic or external tides. The external tides when interacting with sharp topography (e.g., ridge, sea mounts, shelf break) in a stratified ocean generate internal tides also called internal tidal/gravity waves, that may propagate and dissipate in the ocean interior causing diapycnal mixing (Baines, 1982; Munk and Wunsch, 1998; Egbert and Ray, 2000). The precise location of this dissipation is a big unknown. But evidence of dissipation at the generation sites, at the reflection to the bottom or close to the surface when the energy rays interact with the thermocline and pycnocline, have been measured and modelled (among others: Laurent and Garrett, 2002; Sharples et al., 2007, 2009; Koch-Larrouy et al., 2015; Nugroho et al., 2018; Xu et al., 2020 and Whalen et al., 2020).

ITs may also dissipate or lose energy when they encounter others or when they interact with mesoscale or fine-scale structures (Vlasenko and Stashchuk, 2006; Dunphy and Lamb, 2014). Moreover, the surface interactions allow nonlinear internal solitary waves (ISW) to develop and to propagate usually with phase-locked to the ITs troughs (New and Pingree, 1990, 2000; Azevedo et al., 2006; da Silva et al., 2011). Finally, ISW can dissipate and induce mixing (Sandstrom and Oakey, 1995; Feng et al., 2021; Purwandana et al., 2022). Moreover, ITs can vertically advect the water masses following their propagation. The effect is the vertical shifts in isopycnic levels of few meters to tens of meters, which can be observed in the thermocline (Wallace et al., 2008; Xu et al., 2020). But over a tidal cycle, the mean effect on temperature is null except some tidal residual circulation exists (Bessières, 2007).

Our study focuses on the oceanic region of northern Brazil off the Amazon River~~, where IT have been highlighted in previous studies, but their impact on the thermal structure is not currently known.~~. This region ~~is characterized by a broad, shallow continental shelf at the mouth of the Amazon River ended by a steep slope, i.e., a bathymetry~~ exhibits a variation ~~of 200-2000 m over some tens of kilometers (Fig.1). Along this slope, six sites (A to F) of IT generation have been identified (Fig.1), the most intense of which (A and B) are in the south of the region (Magalhaes et al. 2016, Barbot et al. 2021 and Tchilibou et al. 2022). A strong seasonal coastal current, the Brazilian North Current (NBC), strongly influences the study area and flows along the coast from the southeast to the northwest (Johns et al., 1990).~~

~~This region shows a seasonal variation in the~~in the wind position and hence the position of the ~~winds and the~~ Intertropical Convergence Zone (ITCZ) during the year~~, which~~. This directly influences the discharge of the Amazon River, ~~the~~ oceanic circulation ~~(Xie and Carton, 2004), and therefore the stratification. This impacts the activity of internal tidal waves (Barbot et al., 2021). Two seasons can be clearly distinguished by their properties on water masses and currents.~~

~~The first season runs from March to July, during this time the ITCZ is in its most equatorial position and lies in the heart of our region. The increase in rainfall over the ocean leads to a colder and more homogeneous SST far from the coast. The discharge of the Amazon River into the ocean reaches its peak (> 3×10^5 m^3.s^{-1}) and the surface temperature in the coastal zone, although homogeneous, is warmer than offshore. At the end of this season, driven by the strong river discharge, the Amazon plume along the shelf extends beyond 8°N, and sometimes into the Caribbean region (Müller-Karger et al., 1989; Johns et al., 1998). The stratification is somewhat stronger and more homogeneous horizontally, and the maximum of its vertical~~

a mis en forme : Couleur de police : Texte 1

a mis en forme : Couleur de police : Texte 1

a mis en forme : Couleur de police : Texte 1

a mis en forme : Couleur de police : Texte 1

a mis en forme : Couleur de police : Texte 1

a mis en forme : Couleur de police : Texte 1

a mis en forme : Couleur de police : Texte 1

a mis en forme : Couleur de police : Texte 1

~~gradient (pycnocline) is closer to the surface. This latter point leads to a stronger conversion of energy from barotropic to baroclinic, and a stronger local (first 50 km) dissipation of internal tidal wave energy (Barbot et al., 2021; Tchilibou et al., 2022). NBC and~~, eddy kinetic energy (EKE) ~~are weak in the region (Aguedjou et al., 2019). Close to the equator, the NBC develops a retroflection towards 1°N latitude that feeds the Equatorial Under-Current (EUC) transporting water masses eastwards to the Gulf of Guinea (Didden and Schott, 1993, Dimoune at al., 2022).~~

~~Contrasting with this first season, due to different oceanic and atmospheric conditions, the second season extends from~~ and the stratification (Muller-Karger et al., 1988; Johns et al., 1998; Xie and Carton, 2004). Hence, two very contrasting seasons form, April-May-June (AMJ) and August ~~to December. During this season, the ITCZ migrates to its northernmost position around 10°N. In response, rainfall in this area decreases and the Amazon River discharge also decreases to its minimum (~ 10^5 $m^3.s^{-1}$), the extension of the river plume is therefore reduced to no more than 200–300 km offshore from the mouth of the Amazon between November and December (Johns et al., 1998, Garzoli et al., 2003). During this season, cold water (< 27.6 °C) associated with the western extension of the Atlantic cold-water tongue (ACT) enters the region from the south and runs along the edge of the continental shelf to about 3°N (Lentz and Limeburner, 1995; Neto et al., 2014), forming a cold cell often referenced as a seasonal upwelling. The stratification of the study area is strongly modified compared to the previous season. The~~ September-October (ASO). AMJ (vs. ASO) season is characterized by an increasing (vs. decreasing) river discharge, stronger (vs. smaller) and shallower (vs. deeper) pycnocline ~~becomes somewhat deeper. The generation of IT on the slope and their local dissipation~~. The North Brazilian Current (NBC) and eddy kinetic energy (EKE) are weaker ~~compared to the first season (Barbot~~(vs. stronger) (Aguedjou et al., ~~2021;~~2019, Tchilibou et al., 2022). ~~Currents and eddy activity become stronger. The NBC becomes~~ For the ASO season, the stronger~~, farther from the coast and deeper, it~~ NBC develops a retroflection (NBCR) between 5°–8° N that feeds the North Equatorial Counter-Current (NECC) transporting the water masses towards the east of the tropical Atlantic. ~~This~~The retroflexion also generates very large anticyclonic eddies (NBC Rings) exceeding 450 km in diameter (Didden and Schott, 1993; Richardson et al., 1994; Garzoli et al., 2004), which in turn transport water masses towards the Northern Hemisphere (~~Bourlès et al., 1999a; Johns et al., 1998; Schott et al., 2003). In addition, there are more cyclonic/anticyclonic eddies from the Gulf of Guinea during this season. All this contributes to the strengthening of the EKE, which reaches its maximum in this season (Aguedjou~~Bourles et al., 1999a; Johns et al., 1998; Schott et al., 2003). ~~et al., 2019).~~

a mis en forme : Couleur de police : Texte 1

a mis en forme : Couleur de police : Texte 1

a mis en forme : Couleur de police : Texte 1

a mis en forme : Couleur de police : Texte 1

a mis en forme : Couleur de police : Texte 1

a mis en forme : Couleur de police : Texte 1

a mis en forme : Couleur de police : Texte 1

~~When the baroclinic tidal flow interacts with the general circulation, it is deviated from its trajectory, thus we have a so-called incoherent baroclinic tide (Buijsman et al., 2017). This IT-circulation interaction is thus reinforced during this second season because of the more intensified currents and eddy activity (Tchilibou et al., 2022).~~

~~On the Brazilian continental shelf, Geyer et al. (1996) suggests the presence of internal tidal waves from current data. Later, Lentini et al. (2016) based on SAR imagery, shows small-wavelength (~ 10 km) internal solitary waves (ISW) packets propagating along and across the continental shelf, and generated by linear non-hydrostatic interactions between the NBC and barotropic tidal currents. Using a model, Molinas et al. (2020) show that baroclinic tidal currents play an important role on sediment transport on this continental shelf. On a global scale, several studies from altimetry observations (Zhao et al., 2012, 2016; Zaron et al., 2017, 2019) or models (Munk and Wunsch, 1998; Shriver et al., 2012; Arbic et al., 2012; Niwa and Hibiya, 2011, 2014; Buijsman et al. 2016) have shown intense activity of IT along the steep slope of the continental shelf. At the surface, using SAR imagery, Jackson (2007) and Magalhaes et al. (2016) describe longer wavelength ISW (~ 50-150 km) that propagate offshore from the slope. The latter emphasizes the modulation of their propagation by the seasonal variation of the NECC, and from a model, establishes that these ISW originate from instabilities and energy loss of IT coming from the slope, mainly at sites A and B.~~ Internal tides are generated on the sharp shelf break which possesses a depth decreasing of 200-2000 m over some tens of kilometers (Fig.1). Six main sites (A to F) have been identified, with the most intense, A and B, located in the southern part of the region (Fig.1; Magalhaes et al., 2016, Tchilibou et al., 2022). Previous studies have shown that in this region ITs propagation is modulated by the seasonal variation of the currents (Magalhaes et al., 2016; Lentini et al., 2016; Tchilibou et al., 2022; de Macedo et al., 2023). In addition, seasonal variations in stratification induce changes in the internal tide's activity. With in AMJ (vs. ASO) a stronger (vs. smaller) energy conversion and a stronger (vs. smaller) local dissipation of ITs energy (Barbot et al., 2021, Tchilibou et al., 2022). Moreover, the interaction between the weaker (vs. stronger) background circulation and ITs can lead to less (vs. more) incoherent or non-stationary internal tides (Tchilibou et al., 2022). Incoherent ITs can account for about half of the total internal tides in the global ocean and much more when looking at some regional ocean system. For example over 80% in equatorial Pacific (Zaron, 2017) and over 40% off the Amazon (see Fig.11e-f in Tchilibou et al., 2022). But quantifying the associated energy is difficult to determine and is still unknown in our region but is part of the scope of upcoming studies.

The role of ITs on the thermal structure of the ocean is of increasing interest with many studies in recent years. In the Hawaii shallow shelf surface waters, Smith et al. (2016) report that ITs can induce surface cooling from 1 °C to 5 °C. For the Indonesian region, ITs induce an annual mean surface cooling of 0.5 °C (Koch-Larrouy et al., 2007, 2008; Nagai and Hibiya, 2015 and Nugroho et al., 2018), that decreases local atmospheric convection, which in turn reduces precipitation by 20%. They can therefore fulfils a relevant role on regional climate (Koch-Larrouy et al., 2010, Sprintall et al., 2014, 2019). Furthermore, in the Andaman Sea, Jithin and Francis (2020) showed that ITs can affect the temperature in deep waters (> 1600 m), leading to a warming of about 1–2 °C. But off the Amazon plateau, the impact of ITs on the thermal structure of the ocean is still poorly understood.

During the ASO season, cold water (< 27.6 °C) associated with the western extension of the Atlantic Cold-water Tongue (ACT) enter the region from the south and run along the edge of the continental shelf to about 3°N, establishing a cold cell often referred to as seasonal upwelling (Lentz and Limeburner, 1995; Neto and da Silva, 2014). Modelling studies, with and without tides, have shown that this upwelling is affected by the tides. Cooling is more realistic when tides are included (Ruault et al., 2020). However, these analyses cannot determine what processes are at work. For example, it is not yet explicit whether the tidal-induced cooling is due to mixing on the shelf produced by barotropic tides, or to the mixing produced by baroclinic tides at their generation sites and propagation pathways. Neto and da Silva (2014), based on *in situ* observations, suggest instead that it is the vertical advection triggered by the NBC that can explain the cooling observed at the surface. Following on from the latter, we can also examine the role of horizontal advection and its contribution relative to vertical advection.

To ~~Recently, de Macedo et al. (2023) provided a somewhat more comprehensive description of the seasonal characteristics of these ISW, with the predominant origin remaining at sites A and B. Barbot et al. (2021) focused on the influence of stratification on the IT generation on the shelf as well as their propagation offshore. Finally, also in seasonal scale, Tchilibou et al. (2022) looked at the variation of the energy associated with IT from their generation to their dissipation, as well as the interaction of these waves with the general circulation. However, the interactions between IT and tracers such as temperature, salinity or chlorophyll have not received much interest from the scientific community in this region.~~

a mis en forme : Couleur de police : Texte 1

~~Hydrodynamic and biogeochemical conditions on the shelf and off the mouth of the Amazon were studied during the AMASSEDS campaigns in the early 1990s (DeMaster and Pope, 1996; Nittouer and DeMaster, 1996) and the various "*Camadas Finas*" campaigns~~

~~(Araujo et al., 2017, 2021). Furthermore, using data from the two REVIZEE campaigns and TMI SST satellite data, Neto et al. (2014) studied the seasonal cooling of surface waters, which occurs between the months of July and December. They conclude that the NBC is responsible for the upwelling of cold-water masses (< 27.5 °C) to the more superficial layers. Subsequently, Araujo et al. (2016), using in addition a realistic model, suggest that the tide would have a key role to play in intensifying this cooling. Indeed, through twin simulations with and without tide, they show that with tide there is a -0.3 °C cooling of the surface temperature. These analyses remain qualitative and do not allow determining what are the processes at work. Knowing that we are in an area with a strong activity of internal tidal waves, the question remains whether and by what processes these IT can structure the temperature both at the surface and inside the water column.~~

~~In order to~~ answer the ~~above~~previous questions, we used a high-resolution model (1/36°) with and without explicit tidal forcing and a satellite SST product, with the aim of highlighting the impact of ~~IT~~tides on the temperature structure and quantify the associated processes. ~~These observations~~We distinguish the analysis for the two contrasted seasons (AMJ and ASO) described above. The SST product, our ~~modeling, as well as~~model, and the methods used are described in section II. The validation of ~~some~~ certain characteristics of the barotropic and baroclinic ~~tide's characteristics as well as SST are present in~~ tides and of the temperature is presented in section III. The impacts of ~~IT~~ITs on the temperature structure, the influence on heat exchange at the ~~interface between the~~ atmosphere~~ and the ~~-ocean interface, and ~~finally~~ the processes involved, are analyzed in section IV. ~~Summary~~The discussion and ~~discussions~~the summary of the obtained results are presented in ~~a last~~ section V and VI respectively.

II. Data and Methods

II.1. Satellite Data used: TMI SST

This dataset derived from Tropical Rainfall Measurement Mission (TRMM), which performs measurements using onboard TRMM Microwave Imager (TMI). The microwaves can penetrate clouds and are therefore ~~very~~crucially important for data acquisition in low latitude regions, cloudy covered during long periods of raining seasons. We use Remote Sensing Systems (RSS) TMI data products v7.1, which ~~is~~represents the ~~latest~~most recent version of TMI SST. It contains a daily mean of SST with a 0.25°×0.25° grid resolution (~ ~~-~~25 km). This SST is obtained by inter-calibration of TMI data with other microwave radiometers.

a mis en forme : Couleur de police : Texte 1

a mis en forme : Couleur de police : Texte 1

a mis en forme : Couleur de police : Texte 1

a mis en forme : Couleur de police : Texte 1

a mis en forme : Couleur de police : Texte 1

a mis en forme : Couleur de police : Texte 1

a mis en forme : Couleur de police : Texte 1

a mis en forme : Couleur de police : Texte 1

a mis en forme : Couleur de police : Texte 1

a mis en forme : Couleur de police : Texte 1

a mis en forme : Couleur de police : Texte 1

a mis en forme : Couleur de police : Texte 1

a mis en forme : Couleur de police : Texte 1

a mis en forme : Couleur de police : Texte 1

a mis en forme : Couleur de police : Texte 1

a mis en forme : Couleur de police : Texte 1

a mis en forme : Couleur de police : Texte 1

a mis en forme : Couleur de police : Texte 1

a mis en forme : Espace Avant : 12 pt

a mis en forme : Police :14 pt

The TMI SST ~~fully~~full description and inter-calibration algorithm ~~is~~are detailed in Wentz et al~~.~~., (2015).

II.2. The NEMO Model: *AMAZON36* configuration

a mis en forme : Police :14 pt

a mis en forme : Police :14 pt

The numerical model used in this study is the Nucleus for European Modelling of the Ocean (NEMOv4.0.2, Madec et al., 2019). The~~ "*AMAZON36*" model~~ configuration designed for our purpose is called *AMAZON36* and covers the western tropical Atlantic region ~~with a 1/36° horizontal grid, ~~from the Amazon River mouth to the open ocean. ~~Several~~Other configurations ~~with same grid resolution, but for the former NEMOv3.6 (Madec, 2014), exists for the same~~exist in this region, but either ~~includes Caribbean Sea (~~they have a coarse grid (¼°, Hernandez et al., 2016), or ~~are not~~when the grid is fine (1/36°) they do not extend very far ~~extended to the east even used for tides study~~eastwards and therefore exclude most of the site B (Ruault et al., 2020). The ~~present~~current configuration ~~is wider to capture, on their pathways, all the internal tide generating from the Brazilian shelf. Hence,~~avoids these two limitations. The grid resolution is fine (1/36°) and the domain lies between 54.7°W–35.3°W and 5.5°S–10°N (Fig.1). ~~In contrast with former~~In this way, we can capture the internal tides radiating from all the generating sites on the Brazilian shelf break. Unlike previous configurations, we do not use multiple nested grids~~ here~~, but a single fine grid. The vertical grid comprises 75 vertically fixed z-coordinates levels, ~~finer~~with a narrower grid refinement ~~close to~~near the surface with 23 levels in the first 100 m~~, and cell~~. Cell thickness ~~reaching~~reaches 160 m when approaching the bottom. ~~Both~~The horizontal and vertical ~~grid~~ resolutions of the grid are therefore ~~acceptable~~fine enough to resolve low-mode internal tides~~ and were~~. This grid resolution has already been used for ~~that~~this purpose ~~(~~in this region (e.g., Tchilibou et al., 2022).

a mis en forme : Couleur de police : Texte 1

a mis en forme : Couleur de police : Texte 1

A third order upstream biased scheme (UP3) with built-in diffusion is used for momentum advection, while tracer advection relies on a 2nd order Flux Corrected Transport (FCT) scheme~~.~~ (Zalesak, 1979). A Laplacian isopycnal diffusion with a constant coefficient of $20\ m^2.s^{-1}$ is used for tracers. The temporal integration is achieved thanks to a leapfrog scheme combined with an Asselin filter to damp numerical modes~~ (~~, with a baroclinic time step ~~is~~of 150 s~~)~~. The $k-\varepsilon$ turbulent closure scheme is used for the vertical diffusion coefficients. Bottom friction is quadratic with a bottom drag coefficient of 2.5×10^{-3}, while lateral wall free-slip boundary conditions are ~~assumed~~prescribed. A time splitting technique is used to resolve the free surface, with the barotropic part of the dynamical equations integrated explicitly.

We use the 2020's release of the General Bathymetric Chart of the Oceans (GEBCO~~,~~ 2020~~)~~, see details in https://www.gebco.net/data_and_products/gridded_bathymetry_data/gebco_2020/) interpolated onto the model horizontal grid, with the minimal depth ~~equal~~set to 12.8 m. The ~~ocean~~ model is forced at the surface by the ERA-5 atmospheric reanalysis (Hersbach et al., 2020). The river discharges are based on monthly means from hydrology simulation of ~~ISBA model (~~the Interaction Sol-Biosphère-Atmosphère model (ISBA, see description in ~~ISBA – National Centre for Meteorological Research),~~ https://www.umr-cnrm.fr/spip.php?article146&lang=en) and are prescribed as surface mass sources with null salinity, and we use a multiplicative factor of 90% based on a comparison with the HYBAM interannual timeseries (HYBAM, 2018). The model is forced at its open boundaries by (i) the fifteen major ~~high-frequency~~ tidal constituents (M2, S2, N2, K2, 2N2, MU2, NU2, L2, T2, K1, O1, Q1, P1, S1, and M4) and (ii) barotropic currents, both derived from FES2014 atlas (Lyard et al., 2021). ~~At~~In addition to the open boundaries, we prescribe the recent MERCATOR-GLORYS12 v1 assimilation data (Lellouche et al., 2018) for temperature, salinity, sea level, current velocity and derived baroclinic velocity.

The simulation was initialized on the 1st of January 2005, and ran for ~~10~~11 years until December 2015. In this study, we use 3-years model outputs from January 2013 to December 2015. Indeed, the model has reached an equilibrium in terms of seasonal cycle after 2 years ~~(2005-2006)~~ of run. ~~The same~~A twin model configuration without the tides is used to highlight the influence of tides ~~and IT~~ on the temperature structure. To assess the realism of the model, we perform validation of various state variables used in this study such as the current's circulation, temperature, salinity, stratification as well as the barotropic and baroclinic ~~tide~~tides properties.

II.3. Methods

a mis en forme : Police :14 pt

II.3.1. Barotropic/baroclinic tide separation and tide energy budget

a mis en forme : Espace Avant : 6 pt, Après : 6 pt

We follow Kelly et al. (2010)~~ method~~ to separate barotropic and baroclinic tide constituents: pressure, currents and energy flux. ~~No modal~~There is no separation ~~is done, then tidal constituents obtained encompass~~ following vertical propagation modes. Then we analyze the total energy ~~of~~for all ~~propagation's~~the resolved propagation modes for a given harmonic. Note that the barotropic/baroclinic tide separation is performed directly by the model for better accuracy~~, however, by this way~~. Even though, it has the disadvantage of being very costly in terms of computing time. We have therefore ~~analyze~~ only ~~for one~~analyzed the M2 harmonic for the single year ~~(~~2015~~) the M2 frequency, since~~. Note that M2 is the major tidal constituent in this region~~, representing ~~~~ (Prestes et al., 2018; Fassoni-Andrade et al., 2023). It represents ~70% of the tidal energy (Beardsley et al., 1995; Gabioux et al., 2005~~ and Tchilibou et al., 2022~~).

The barotropic and baroclinic tide energy budget equations are obtained by ignoring as ~~the~~a first-order approximation, the energy tendency, the nonlinear advection and the forcing terms (Wang et al., 2016). Then, the remaining equations are reduced to the balance between the energy dissipation, the divergence of the energy flux, ~~the dissipation~~ and the energy conversion from barotropic to baroclinic (e.g., Buijsman et al., 2017; Tchilibou et al., 2018, 2020~~, 2022~~; Jithin and Francis~~,~~ 2020~~ ~~; Peng et al., 2021) :

$$D_{bt} + \nabla_h \cdot F_{bt} + \cancel{CVR}C \approx 0 \qquad \cancel{(\mathrm{W.m^{-2}}),} \qquad (1)$$

$$D_{bc} + \nabla_h \cdot F_{bc} - \cancel{CVR \approx} C \approx 0 \qquad \cancel{(\mathrm{W.m^{-2}}),} \qquad (2)$$

bt and bc indicate the barotropic and baroclinic terms, D is the depth-integrated energy dissipation, which can be understood as a proxy of the real dissipation since D may encompass the energy loss of other tidal harmonics, non-linear terms and/or numerical dissipation (see ~~Nugruho~~Nugroho et al., 2018), $\nabla_h \cdot F$ represents the divergence of the depth-integrated energy flux, whilst ~~CVR~~C is the depth-integrated barotropic-to-baroclinic energy conversion, i.e~~.~~., the amount of incoming barotropic energy ~~which is~~ converted into internal tides energy over the steep topography, with~~ ~~:

$$\cancel{CVR = \langle} C = \langle \nabla H \cdot U^*_{bt} P^*_{bc} \rangle \qquad \cancel{(\mathrm{W.m^{-2}}),} \qquad (3)$$

$$F_{bt} = \cancel{\int_H^{\eta} \langle U_{bt} P_{bt} \rangle \, d_z} \qquad \cancel{(\mathrm{W.m^{-1}}),} \; \langle U^*_{bt} P_{bt} \rangle \qquad (4)$$

$$F_{bc} = \cancel{\int_H^{\eta} \langle U_{bc} P_{bc} \rangle \, d_z} \int_H^{\eta} \langle U^*_{bc} P_{bc} \rangle \, d_z \qquad \cancel{(\mathrm{W.m^{-1}}),} \qquad (5)$$

where the angle bracket ⟨·⟩ denotes the average over a tidal period, ∇H is the slope of the bathymetry, ~~U^*_{bt}~~U^* is the ~~barotropic~~ current ~~and~~ velocity (u, v) respectively in (x, y) directions, P^*_{bc} is the baroclinic pressure perturbation ~~both~~ at the bottom, H is the bottom depth, η the surface elevation, ~~$U(u, v)$ is the horizontal velocity,~~ P is the pressure, then ~~F~~F is the energy

a mis en forme : Espace Après : 6 pt

a mis en forme : Espace Avant : 0 pt

a mis en forme : Police :Times New Roman

a mis en forme : Police :Non Italique

a mis en forme : Police :Non Italique flux and ~~allows~~emphasizes the ~~propagation pathways~~pathway of the ~~given tide to be highlighted.~~respective tides (external or internal).

II.3.2. 3-D heat budget equation for temperature

The three-dimensional temperature budget was computed online and further analyzed. It is the balance between the total temperature trend and the sum of the temperature advection, diffusion and solar radiative and non-solar radiative fluxes (e.g~~.:~~., Jouanno et al., 2011; Hernandez ~~at~~et al., 2017):

$$\partial_t T \;=\; \underbrace{-u\partial_x T - v\partial_y T - w\partial_z T}_{ADV*} \; \underbrace{-\,\partial_z(\cancel{Kz\partial_z}K_z\partial_z T)}_{ZDF} + LDF_T + FOR_Z + Numdiff \qquad \cancel{(°C.s^{-1}),} \qquad (6)$$

~~ADV~~ ~~ZDF~~

~~Where~~

Here *T* is the model potential temperature, ~~,~~ ~~[~~(*u, v, w*~~]~~) are the ~~space dimensional velocity components~~velocities component in the (x, y, z) [respectively eastward, northward and upward] directions, ADV^* *is* the 3-D ~~temperature~~ tendency term from the advection ~~(~~routine of the NEMO code (from the left to right: zonal, meridional and vertical terms~~),~~). Note that this term hides secondary terms that are important to define here. Hence, the total advection tendency of temperature (ADV) is expressed as follows:

$$ADV \;=\; \underbrace{\langle U\cdot\nabla T\rangle}_{ADV*} + \underbrace{\langle U'\cdot\nabla T\rangle + \langle U\cdot\nabla T'\rangle + \langle U'\cdot\nabla T'\rangle}_{Non-Linear\ terms} + Numdiff_{ADV} \qquad (7)$$

where U' is the tidal current, and T' represents the anomaly of temperature that is produced by the tides apart the advection. When comparing the tidal and non-tidal simulation, the residual term could come from at least three possible tidal impacts :

1\) The result of the advection is null over a tidal cycle except in some tidal residual circulation. In our region the residual tidal circulation is limited but might be slightly more important on the shelf (Bessières et al., 2008).

2\) In the nonlinear terms of the previous equation (7), temperature could be modified by other processes than advection, which will count in the total tendency and mark the signature of the impact of the tides.

a mis en forme : Espace Avant : 6 pt, Après : 6 pt

a mis en forme : Espace Après : 12 pt

a mis en forme : Droite, Espace Avant : 0 pt

a mis en forme : Police :Times New Roman, 12 pt

a mis en forme : Police :Times New Roman

a mis en forme : Police :Cambria Math, Italique

a mis en forme : Couleur de police : Texte 1

a mis en forme : Couleur de police : Texte 1

3) Finally, and it might represent the key point, in the model, the advection term leads to some diffusivity of the temperature due to numerical dissipation of the advection scheme ($Numdiff_{ADV}$), in contrast to some non-diffusive advection scheme like in Leclair and Madec (2009). In our case, we are using the FCT advection scheme that includes a diffusive part (Zalesak, 1979). In previous study, this mixing has been quantified to be responsible for 30% of the dissipation (in lower resolution 1/4° resolution, Koch-Larrouy et al., 2008), as part of the high-frequency work of the advection diffusion. We except here at 1/36° that this effect will be smaller but still non negligible. Explicit separation of these 3 impacts is beyond the scope of our study but will be discussed in the last section.

Furthermore, ZDF ~~is~~represents the vertical diffusion, LDF_T is the lateral diffusion, FOR_z is the tendency of temperature due to penetrative solar radiation and ~~has~~includes a vertical decaying structure. At the air-sea interface, the temperature flux is equal to the non-solar heat flux (sum of the latent, sensible, and net infrared fluxes). FOR_z can modify temperature in the thin surface layer but will ~~not~~ be ~~shown~~unshown in the following. $Numdiff$ corresponds to the ~~sum of the~~ numerical diffusion for the temperature~~. In this study, we assume that this last term is of second order and is not highlighted here~~.

~~II.3.3. The atmosphere–ocean net heat flux~~

~~The atmosphere–ocean net heat flux (Qt) reflects the balance of incoming and outgoing heat fluxes across the atmosphere-ocean interface (e.g.: Moisan and Niiler, 1998; Jayakrishnan and Babu, 2013), it is defined as follows:~~

~~$Q_t = Q_{SW} \pm Q_{LW} \pm Q_{SH} \pm Q_{LH}$ $W.m^{-2}$, (7)~~

~~with from left to right: the incident solar radiative flux (Q_{SW}), the net infrared radiative flux (Q_{LW}), the incoming/outgoing sensible heat flux (Q_{SH}) which depends on the temperature difference between the atmosphere and the ocean surface, and the incoming/outgoing latent heat flux (Q_{LH}) which depends on the specific humidity difference between the atmosphere and the ocean surface. All these four components of the Qt influence the variation of the ocean surface temperature (SST). The last two components (Q_{SH} and Q_{LH}) have in addition a direct dependence relationship with the SST. Since IT can change the SST, we are therefore interested in knowing how it affects the net heat flux at the atmosphere-ocean interface.~~

a mis en forme : Couleur de police : Texte 1

a mis en forme : Couleur de police : Texte 1

a mis en forme : Couleur de police : Texte 1

a mis en forme : Retrait : Première ligne : 0 cm, Espace Avant : 6 pt, Après : 0 pt

a mis en forme : Couleur de police : Noir

III. Model validation

In this subsection, we ~~present for the M2 harmonic the~~ assess the quality of our model's simulations by verifying whether they are in good agreement with the observations and other reference data. Firstly, for the barotropic and baroclinic ~~tidal~~ characteristics of the ~~model~~M2 tides for the year 2015, and ~~the SST~~finally for the ~~whole~~ temperature for the period from 2013 to 2015~~, and we verify that they agree with the different observations.~~.

III.1. M2 Tides in the model

~~The~~ We initially examined at the barotropic SSH ~~(Fig.2b) of the model is compared with FES2014 (Lyard et al. 2021) (Fig.2a),~~ and there is a good agreement in ~~terms of~~ both amplitude and phase~~.~~ between FES2014 and the model, Fig2a and Fig.2b respectively. Nevertheless, near the coast, some differences are observed in ~~terms of~~ amplitude. The SSH amplitude of the model is lower (~ +50 ~~m~~cm) north of the mouth of the Amazon. However, ~~inland~~shorewards and on the southern part of the mouth, the model overestimates the amplitude ~~(~ ~~by ~ +20 ~~m~~cm and ~ +40 ~~m~~cm respectively~~). This is in terms~~. These biases are of the same order of magnitude ~~like the biases in the~~ as Ruault et al. (2020~~) configuration that they compared to the FES2012 product (Carrère et al., 2012) over the same region. Along the steep slope of the bathymetry (see Fig.1), a portion of the incident~~). The flux of the barotropic tidal energy ~~(~~flowing inshore is represented by the black arrows in Fig.2c and Fig.2d~~,~~ for FES2014 and the model~~,~~ respectively~~) in the presence~~. A fraction of ~~stratification~~this energy is converted ~~to~~into baroclinic tidal energy~~.~~ over the steep slope of the bathymetry. We compared the depth-integrated barotropic-to-baroclinic energy conversion rate (~~CVR~~C) between FES2014 and the model ~~(~~, color shading in Fig.2c and Fig.2d~~) and FES2014 (Fig.2c).~~ respectively. The model does reproduce the same conversion patterns of FES2014 over the slope, but ~~can~~hardly offshore over the Mid-Atlantic Ridge between 42°W–35°W and 7°N–10°N. This leads to an overall underestimate ~~the CVR by~~of about 30%. ~~The~~ It is worth noting that C increases with bathymetry resolution. The latter therefore plays a critical role in ~~CVR (~~converting barotropic tidal energy into internal tides (see Niwa and Hibiya, 2011~~), then~~). Compared with FES2014 (~1.5 km), the horizontal grid of our model is coarser (~3 km). Meaning that the difference in bathymetry resolution ~~between the model (~ 3 km) and FES2014 (~ 1.5 km)~~ could ~~therefore~~ explains ~~that~~the difference in ~~CVR.~~ energy conversion with FES2014. Later, another part of the barotropic energy is dissipated on the shelf by bottom friction and induces mixing from the bottom (Beardsley et al., 1995; Gabioux et al., 2005; Bessières, 2007; Fontes et al., 2008). Most

a mis en forme : Couleur de police : Texte 1, Anglais (États-Unis)

a mis en forme : Espace Avant : 20 pt, Après : 6 pt

a mis en forme : Couleur de police : Texte 1

a mis en forme ...

a mis en forme : Espace Après : 0 pt

a mis en forme : Police :14 pt

a mis en forme : Police :14 pt

a mis en forme ...

a mis en forme ...

of the dissipation of barotropic energy (D_{bt}) occurs in the middle and inner shelf between 3°S–4°N (Fig.2e) in good agreement with Beardsley et al. (1995) and Bessières (2007). The remaining barotropic energy flows over hundreds of kilometers into the estuarine systems of this region (Kosuth et al., 2009; Fassoni-Andrade et al., 2023).

For the baroclinic tides, the critical parameter, $\gamma = s/\alpha$, is defined as the ratio between the slope of the bathymetry, $s = \nabla H$ (see Fig.1), and the slope of the radiated internal wave, $\alpha = \sqrt{(\omega^2 - f^2)/(N^2 - \omega^2)}$, with ω the tidal frequency for a given wave, f is the Coriolis frequency and N^2 represents the squared Brünt-Väisälä frequency near the bottom (e.g., Nash et al., 2007; Vic et al., 2019). ~~The critical slope for the M2 harmonic on the slope is greater than 1.2 (not shown), consequently, the baroclinic tides (internal tidal waves) thus generated will therefore~~ On the slope where ITs are generated, $\gamma > 1$, meaning that the topography is supercritical. Consequently, the baroclinic tides, once generated, will propagate in the opposite direction to the barotropic tides, i.e., from the slope ~~to~~towards the open ocean~~. The~~, as shown by the model's baroclinic ~~tidal~~energy flux ~~of the model (~~(F_{bc}), black arrows in Fig.~~2e)~~2f. F_{bc} highlights the existence of six main sites of ~~IT~~ITs generation on the ~~continental~~ slope~~, two~~. Two of ~~which~~these are more important (A and B~~), as shown by Maghalaes et al.~~) regarding their higher and far extended energy flux, in good agreement with Magalhaes et al. (2016), Barbot et al. (2021) and Tchilibou et al. (2022). From these two main sites, ~~the flow propagates offshore~~ITs propagate for the nearly 1000 km. ~~On its~~Along the propagation ~~path, the baroclinic tide signs at the surface in SSH. We compared this signature for the model (Fig.2h) with an estimate deduced from the altimeter tracks, produced by Zaron et al. (2019) (Fig.2g). The model is in good agreement with the altimetry observations, with an overestimation of the order of ~ +1.5 cm on the SSH maxima. It is important to note that the baroclinic SSH of the model is an average over the year 2015, whilst the observations are an average over about 20 years. This longer period may smooth the amplitude of the signal obtained from the altimetry observations. Also, the variability contained in the two averages is not the same, and this may explain some differences in the positioning and amplitude of the maxima.~~

pathways, they can dissipate their energy. Color shading in the Figure~~-~~2f shows the ~~full~~model's depth-integrated internal ~~tidal~~tides energy dissipation ~~for~~(D_{bc}). We first look at the ~~model. The estimated~~ local dissipation of this energy ~~is~~ defined as ~~follows:~~

~~$$P = (D_{bc} / CVR) * 100 \qquad (8)$$~~

a mis en forme : Couleur de police : Texte 1

a mis en forme : Couleur de police : Texte 1

a mis en forme : Couleur de police : Texte 1

a mis en forme : Couleur de police : Texte 1

a mis en forme : Couleur de police : Texte 1

a mis en forme : Couleur de police : Texte 1

a mis en forme : Couleur de police : Texte 1

a mis en forme : Police :14 pt, Couleur de police : Texte 1

a mis en forme : Couleur de police : Texte 1

a mis en forme : Couleur de police : Texte 1

a mis en forme : Couleur de police : Texte 1

a mis en forme : Couleur de police : Texte 1

a mis en forme : Couleur de police : Texte 1

a mis en forme : Couleur de police : Texte 1

a mis en forme : Couleur de police : Texte 1

a mis en forme : Couleur de police : Texte 1

a mis en forme : Couleur de police : Texte 1

a mis en forme : Couleur de police : Texte 1

a mis en forme : Couleur de police : Texte 1

a mis en forme : Couleur de police : Texte 1

a mis en forme : Couleur de police : Texte 1

a mis en forme : Couleur de police : Texte 1

a mis en forme : Couleur de police : Texte 1

a mis en forme : Couleur de police : Texte 1

a mis en forme : Couleur de police : Texte 1

a mis en forme : Couleur de police : Texte 1

~~The local dissipation is then~~ $q = D_{bc}/C$ (see Laurent and Garrett, 2002). q is integrated ~~at~~over the ~~embankment level~~slope in the same boxes ~~A1, A2 and B (Fig.2f, see coordinates~~as defined in Table ~~2~~ A1 in Tchilibou et al. (2022~~) and provides information~~). This reveals that a significant part of the energy, about 30%, is dissipated locally in the different boxes~~, i.e., about 30% (not shown). The local dissipation at the generation sites is thus~~ in good agreement with ~~Tchilibou et al. (2022).~~the latter study. The remaining part of the energy is exported offshore, and ~~dissipates~~it is dissipated along the propagation path. This offshore dissipation is more extensive ~~offshore~~ along path A, ~ ~~500~~300 km from the slope, with two patterns spaced approximately ~~120~~by an average wavelength of 120–150 km ~~apart~~ corresponding to mode-1 propagation ~~mode-1, and~~. The offshore dissipation is less extensive ~~offshore~~ along path B, ~~~~~occurring around 100~~-~~–200 km from the slope (Fig.2f).

~~We have presented here only the dissipation for the M2 harmonic, but in the rest of the paper, we will analyze the temperature fields on a seasonal scale and by this fact, the effect of all the tidal harmonics on the temperature are considered.~~

Another critical characteristic of internal tidal waves is their SSH imprints along the propagation pathway. We compared an estimate of this signature deduced from the altimeter tracks (Fig.2g) produced by Zaron (2019) with our model (Fig.2h). The model is in good agreement with this product, with an overestimation of the order of ~ +1.5 cm on the SSH maxima. It is relevant to note the baroclinic SSH of the model is an average over the year 2015, whilst the estimate is an average over about 20 years. This more extended period may lower the amplitude of the signal obtained from the altimetry observations. Furthermore, the variability within the two datasets is not the same. This may explain some differences in the positioning and amplitude of the maxima.

Only the energy dissipation of the M2 tides is presented above. Elsewhere, the harmonic analysis does not consider the incoherent (non-stationary) part of the tidal energy, which has been found to be non-neglectable (Tchilibou et al., 2022). And can therefore influences the structure of the temperature. Further on, the analysis are carried out on a seasonal scale, which means that the mean temperature field obtained could result from the cumulative effect of all coherent and incoherent tidal harmonics.

III.2. ~~SST Validation~~Temperature validation

For the following, it should be noted we obtained the bias between TMI SST and the two model simulations after linear interpolation of the model data into the observation grid.

a mis en forme : Couleur de police : Texte 1

a mis en forme : Couleur de police : Texte 1

a mis en forme : Couleur de police : Texte 1

a mis en forme : Couleur de police : Texte 1

a mis en forme : Couleur de police : Texte 1

a mis en forme : Couleur de police : Texte 1

a mis en forme : Couleur de police : Texte 1

a mis en forme : Couleur de police : Texte 1

a mis en forme : Couleur de police : Texte 1

a mis en forme : Couleur de police : Texte 1

a mis en forme : Couleur de police : Texte 1

a mis en forme : Couleur de police : Texte 1

a mis en forme : Couleur de police : Texte 1

a mis en forme : Couleur de police : Texte 1

a mis en forme : Couleur de police : Texte 1

a mis en forme : Couleur de police : Texte 1

a mis en forme : Couleur de police : Texte 1

a mis en forme : Couleur de police : Texte 1

a mis en forme : Couleur de police : Texte 1

a mis en forme : Couleur de police : Texte 1

a mis en forme : Couleur de police : Texte 1

a mis en forme : Couleur de police : Texte 1

a mis en forme : Couleur de police : Texte 1

a mis en forme : Police :14 pt

a mis en forme : Police :14 pt

Figure 3 shows the mean SST ~~from TMI SST, tidal simulation and non-tidal simulation~~ ~~over~~ over the entire ~~2013-2015~~ period~~. The mean~~ 2013–2015 from TMI SST ~~of~~(Fig.3a), the tidal simulation (Fig.3b) and the non-tidal simulation (Fig.3c). The simulation with tides accurately reproduces ~~well spatially~~ the ~~TMI SST~~spatial distribution of the observations ~~(Fig.3a)~~ both for cooling on the shelf around 47.5°W and to the southeast between 40°W –35°W and 2°S–2°N, ~~which~~ as shown by the weak bias, < ±0.1°C, with TMI (Fig.3d). This cooling is ~~almost absent for~~inaccurately reproduced by the non-tidal simulation ~~(Fig.3e~~which exhibits a warm bias of about 0.3 °C (Fig.3.e). To the northeast, between 50°W–54°W and 3°N–8°N in the Amazon plume, the SST of the non-tidal simulation is in better agreement with the observations, while the SST of the tidal simulation is about ~~1~~> 0.6 °C cooler than TIM SST~~.~~ (Fig.3d). Such a difference ~~is very similar~~fits to what is obtained by other models in the same region (e.g., Hernandez et al., 2016, 2017; Gévaudan et al., 2022). ~~The seasonal cycle of the SST of the three products for the three years 2013-2015 (Fig.3d) is obtained by interpolating the SST of~~Far offshore, between 50°W–40°W and 6°N–10°N, both simulations ~~on the TMI SST grid and averaging~~reveal a negative bias of about 0.2–0.3 °C (Fig.3d-e). We averaged the observations and the interpolated model data in the corresponding dashed ~~boxes around the IT generation areas (Fig.3a, b, and c)~~line box in the upper panels, with ~~the shelf being masked over the~~depth < 200 m ~~isobath.~~masked. This location is around the ITs generation sites and on part of their pathways. Then, we compute the seasonal cycle of the three products (Fig.3f). The tidal and non-tidal simulations of the model reproduce ~~well~~accurately both the seasonal cycle and the standard deviation of the observations, with a low RMSE of ~~approximately~~ ~10^{-2} °C between each simulation and TMI SST (Fig.~~3d), which~~3f). This indicates the ~~good quality~~robustness of our model simulations. Nevertheless, over the seasonal cycle, it appears that between January-April and July-December, the tidal simulation is closer to the observations, while the non-tidal simulation seems ~~slightly~~moderately warmer than the observations~~; and in~~. In May-June, both simulations are colder than TMI SST (Fig.~~3d~~3f).

To gain an insight into our model along the depth, we used the mean model water properties (salinity and temperature) for the three years 2013-2015 in the same region as in Fig.3f. We compared them with the WOA2018 climatological (2005–2017) data (https://www.ncei.noaa.gov/access/world-ocean-atlas-2018/). We used hereabove and elsewhere $\sigma_\theta [\rho - 1000]$ to represent the density, with ρ the water density. Figure 3g shows the Temperature-Salinity (T-S) diagram, with equal density (σ_θ) contours, for WOA2018 (black line), tidal simulation (blue line) and non-tidal simulation (red line). Both simulations

a mis en forme : Espace Après : 0 pt exhibit similar pattern with WOA2018 for deeper waters, i.e., T < 17 °C and σ_θ > 25.6 kg.m^{-3}. However, there exist minor discrepancies for the surface layer waters, i.e., T > 17 °C and 22.4 > σ_θ < 25.6 kg.m^{-3}. At that level, the tidal simulation better reproduces the T-S profiles. The water is slightly more eroded in the non-tidal simulation. These petty differences between WOA2018 observations and the model, even more with the tidal simulation, further demonstrate the ability of our model to reproduce the observed water mass properties.

IV. Results

a mis en forme : Espace Avant : 12 pt, Après : 6 pt

In this section, we ~~will~~ present the influence of ~~IT~~tides on the ~~SST~~temperature, the associated processes, and the impact on the ~~net~~ atmosphere-ocean net heat ~~flux from the model's tidal and non-tidal simulations~~. The analyses were performed on a seasonal scale between April-May-June (AMJ) and August-September-October (ASO) for the three years 2013-2015.

IV.1. Tide-enhanced surface cooling

a mis en forme : Police :14 pt

~~Beginning in July, a tongue of cold water (< 27 °C) begins to form to the southeast and enters the central part of the plateau in August and remains there until October. Figure 3e-g show the SST, averaged over the ASO season. The tidal simulation (Fig.3f) shows that the upwelling cell, represented by the extension of the 27.2 °C isotherm along the slope to about 49°W–3°N, extends further north than in the non-tidal simulation (Fig.3g, 45°W–0°N) which is in better agreement with the TMI SST observations over the same period (Fig.3e).~~

During the first season, warm waters, > 27.6°C, dominate near the coast, especially in the middle shelf and in the south-east. While cold waters are present offshore north of 6°N (Fig.4a-c). Off the mouth of the Amazon River, water colder than 28.2 °C spread between 43°W–51°W for TMI SST (Fig.4a) and the tidal simulation (Fig.4b), whilst warmer waters are present in the same area for the simulation without the tides (Fig.4c). Figures 4d-f show the SST, averaged over the ASO season. The TMI SST observations (Fig.4d) shows an upwelling cell represented by the extension of the 27.2 °C isotherm (white dashed contour) along the slope to about 49°W–3°N towards the north-east of the region, which forms the extension of the ACT. This extension also exists in the tidal simulation (Fig.4e), whereas ≤ 27.2 °C waters are not crossing 45.5°W and remain in the southern hemisphere in the simulation without the tides (Fig.4f). Which means that a lesser upwelling cell may exist without the tides, and it is enhanced by -0.3°C in average due to tidal effect. The tides allow waters colder than 27.2°C to form further north-east. Finally, we can note that the mean SST shows a very contrasting distribution between the two seasons. There are warm waters along the shelf and cold waters offshore during the AMJ season (Fig.4a-c). This is followed by warming along the Amazon plume and offshore, and a upwelling cells in the south-east (Fig.4d-f).

The general impact of the ~~tide~~tides, illustrated by ~~showing~~ the ~~difference in~~ SST anomaly between the tidal and the non-tidal ~~simulations in both seasons (Fig.4c-d, respectively for AMJ and ASO),~~simulation, is a cooling over a large part of the study area with maxima ~~(~~up to ~~-0.3 °C): in the Amazon plume downstream of the river mouth (northeast beyond 3°N), and on the path of propagation of IT for both seasons.~~0.3 °C (Fig.5a-b). For ASO, tides induce a warming (> ~~+~~0.3 °C) on the shelf at the mouth of the Amazon River~~,~~ (Fig.5b), while for AMJ it is a cooling ~~(-0.3 °C). East~~of the same intensity (Fig.5a). That difference will be further discussed. Out of ~~45°W,~~ the ~~tide-induced cooling~~shelf, the temperature anomaly for each ~~of the two seasons~~season has different spatial structures~~, but this~~. This is probably due to a different mesoscale variability between the two seasons.

IV.2. Impact of the tides in the ~~Atmosphere–Ocean Net~~atmosphere-to-ocean net heat flux ~~(Q_T)~~

~~Associated with the cooling~~The atmosphere–ocean net heat flux (Qt) reflects the balance of ~~the SST, the tide induces~~ incoming and outgoing heat fluxes across the atmosphere-ocean interface (see details on Moisan and Niiler, 1998; Jayakrishnan and Babu, 2013). During AMJ, the tides mainly induce positive Qt anomalies ~~whose spatial structure is very similar to the SST. Indeed, the difference in Qt is essentially positive~~ over the whole domain ~~during the AMJ season (Fig.4a) with~~. The average ~~maximum~~ values are around 25 W.m^{-2} in the plume and the Amazon retroflection to the northeast and along A and B~~. During the ASO season, there is as for the temperature at the mouth of the Amazon an inverse anomaly of (-25 W.m^{-2}) (Fig.4b). In each season, the spatial structure of the Qt difference almost perfectly matches that of the SST difference. Knowing~~ (Fig.5c). Negative SST anomalies (~0.3°C) occur throughout the domain in the same location. During the ASO season, at the mouth of the Amazon, there are negative Qt anomalies but of same magnitude as during the previous season (Fig.5d). At this location, positive temperature anomalies (~0.3°C) are observed (Fig.5b). Elsewhere, there are positive Qt anomalies and negative SST anomalies. It therefore appears that negative SST anomalies induce positive Qt anomalies and vice versa. Hence, the spatial structures of Qt anomalies and SST anomalies fit almost perfectly together for the respective season. As it is shown by the correlation among them. There is a strong negative correlation of 0.97 with a

a mis en forme : Police :14 pt

a mis en forme : Police :14 pt

a mis en forme : Police :14 pt

a mis en forme : Police :14 pt

a mis en forme : Couleur de police : Texte 1

a mis en forme : Couleur de police : Texte 1

a mis en forme : Couleur de police : Texte 1

a mis en forme : Couleur de police : Texte 1

a mis en forme : Couleur de police : Texte 1

a mis en forme : Couleur de police : Texte 1

significance of $R^2 = 0.95$ for the AMJ season. And roughly the same intensity and sign for the ASO season with 0.98 and 0.96, respectively for the correlation and its significance (Fig.5e). This is consistent with the fact that the atmosphere and the underlying ocean are ~~in a certain equilibrium~~balanced. Then, the SST cooling ~~of the SST~~induced by ~~the~~upwelled cold water ~~masses arriving at the surface will disturb~~will try upset this balance. ~~In response, a consequent~~As a result of this, an equivalent variation ~~of~~in the net heat flux from the atmosphere to the ocean~~,~~ will ~~try~~attempt to restore ~~the balance. As shown by the very strong and significant negative correlation between the difference in Qt and the difference in SST. For the AMJ season, we have a negative correlation of -0.97 with a significance of $R^2 = 0.95$, and about the same as for the ASO season with -0.98 and 0.96 respectively for negative correlation and its significance (Fig.9f).~~it.

The integral over the entire domain of the net heat flux for each season and for each simulation ~~(Fig.4e) shows that during~~ is shown in Figure 5f. During the AMJ season, ~~the~~ Qt increases from 23.85 TW (1 TW = 10^{12} W) for the non-tidal simulation to 35.7 TW for the tidal simulation, i.e., an increase of ~~±~~33.2 ~~%, two times greater than that found (~~%. The tides are behind a third of Qt variation. This is very large compared to what is observed elsewhere in other ITs hotspots (e.g., 15 ~~%) by~~% in Solomon Sea, Tchilibou et al~~. (~~., 2020~~) in Solomon Sea. Thus, the tide and IT are responsible for a third of the variation in net atmosphere-ocean heat flux during this season. While during the~~). During the second ~~ASO~~ season, there is a smaller increase in Qt of ~~±~~about 7.4~~%,~~% between the two simulations, i.e., ~~a variation~~ from 73.03 TW ~~to 78~~to78.83 TW ~~between~~for the non-tidal and tidal simulations~~.~~ respectively (Fig.5f).

~~We~~Moreover, it is also ~~note~~worth noting the ~~considerable~~significant difference in integrated Qt between the two seasons. ~~We start from~~ The values ~~below~~are less than 36 TW ~~in~~during the AMJ season ~~to values above~~, whereas they are around twice as high, > 73 TW ~~in,~~ during the ASO season~~, i.e., a multiplication by a factor of at least order 2. These larger values could probably be related with the appearance of the upwelling cell described above, knowing~~. Given that ~~cooler~~colder SST induce a stronger Qt, these higher values are likely related to the arrival of water from ACT, which forms upwelling cells (Fig.4d-f) with a secondary tidal effect.

IV.3. Vertical structure of ~~the~~ Temperature along ~~A~~internal tides pathway

To further analyze the temperature changes between both simulations, we made vertical sections following the path of ~~IT~~ITs emanating from sites A and B (~~blue and red line in~~ respectively black and red line in Fig.2e). Hereunder, (i) only the transects following the pathway A will be shown, since the vertical structure is similar following pathway B especially

a mis en forme : Couleur de police : Texte 1

a mis en forme : Couleur de police : Texte 1

a mis en forme : Couleur de police : Texte 1

a mis en forme : Couleur de police : Texte 1

a mis en forme : Couleur de police : Texte 1

a mis en forme : Couleur de police : Texte 1

a mis en forme : Couleur de police : Texte 1

a mis en forme : Couleur de police : Texte 1

a mis en forme : Couleur de police : Texte 1

a mis en forme : Couleur de police : Texte 1

a mis en forme : Couleur de police : Texte 1

a mis en forme : Couleur de police : Texte 1

a mis en forme : Couleur de police : Texte 1

a mis en forme : Couleur de police : Texte 1

a mis en forme : Couleur de police : Texte 1

a mis en forme : Couleur de police : Texte 1

a mis en forme : Couleur de police : Texte 1

a mis en forme : Couleur de police : Texte 1

a mis en forme : Couleur de police : Texte 1

a mis en forme : Couleur de police : Texte 1

a mis en forme : Couleur de police : Texte 1

a mis en forme : Couleur de police : Texte 1

a mis en forme : Couleur de police : Texte 1

a mis en forme : Couleur de police : Texte 1

a mis en forme : Couleur de police : Texte 1

a mis en forme : Couleur de police : Texte 1

a mis en forme : Couleur de police : Texte 1

a mis en forme : Couleur de police : Texte 1

a mis en forme : Couleur de police : Texte 1

a mis en forme : Couleur de police : Texte 1

a mis en forme : Couleur de police : Texte 1

a mis en forme : Couleur de police : Texte 1

a mis en forme : Police :14 pt

a mis en forme : Police :14 pt

a mis en forme : Police :14 pt

a mis en forme : Couleur de police : Texte 1

a mis en forme : Couleur de police : Texte 1

for AMJ season, or because some processes tend to be null along pathway B during the ASO season. (ii) The mixed layer refers to a quasi-homogenous surface layer of temperature-dependent density that interacts with the atmosphere (Kara et al., 2003). Its maximum depth also known as mixed-layer depth (MLD) is defined as the depth where the density increases from the surface value, due to temperature change of $|\Delta T| = 0.2\,^{\circ}C$ with constant salinity (e.g., Dong et al., 2008; Varona et al., 2019).

Figure ~~2e respectively). We will show only the results following path A, but the results are similar for path B.~~

~~Figure 5~~6 shows the vertical sections of temperature for the two seasons following A. For the AMJ season, over the slope and near the coast, cold ~~water~~waters (< 27.6 °C) ~~remains~~remain below the surface at ~~~-~~20 m for the tidal simulation (Fig.~~5a~~6a) and deeper at ~ 60 m for the non-tidal simulation (not shown~~), it then rises~~). Then, cold waters rise to the surface more than 400 km offshore for both simulations. Although at the surface the ~~difference in SST between the two simulations (tide - no-tide)~~SST anomaly is relatively small (~ -0.3 °C, Fig.~~4c~~5a), because the SST is likely damped by the heat fluxes, further down the water column, this ~~difference~~anomaly becomes much larger ~~(> ± 1.2 °C, Fig.5c).~~ (Fig.6b). Note that cyan and yellow dashed lines in Fig.6b and Fig.7b refer to thermocline for tidal and non-tidal simulations respectively. Above ~~the~~that thermocline (< 120 m~~, cyan and yellow lines in Fig.5c~~), the simulation with the tides is colder by -1.2 °C from the slope where the ~~IT~~ITs are generated to the open ocean following their propagation path. Conversely, below the thermocline, the tidal simulation is warmer by ~~+~~approximately the same intensity (1.2 °C) up to ~~~-~~300 m depth and along the ~~same~~ propagation path~~.~~ (Fig.6b). During this AMJ season, the thermocline ~~(~~~~is ~100 m ± 15 m~~, thick dashed black line, Fig.5a)~~ deep and the ~~mixing layer (~~~~MLD is ~40 m ± 20 m~~, thick~~ deep (dashed white line, Fig.~~5a)~~6a). They both have a very weak slope between the coast and the open ocean. ~~Furthermore, the difference in isodensity depths between the two simulations is small (not shown), as are the depths of the thermocline (~ 10 m, Fig.5c) and the mixing layer (not shown), although these different depths are closer to the surface for the tidal simulation (not shown).~~ Over the whole domain~~ (not shown),~~, the thermocline is deeper by about 15 m on average in the non-tidal simulation, following the propagation paths of the ~~IT energy flow~~ITs, on the Amazon shelf and plume~~. While the mixing layer~~ (Fig.6c). Whilst MLD in the non-tidal simulation is deeper by an average of ~~13~~10 m over the shelf, 4 m on average along the ~~IT~~ITs propagation paths and close to zero in the Amazon plume~~.~~ (Fig.6d).

During the ASO season, cold waters ~~(< 27.6 °C)~~ previously confined below the surface during the previous season (AMJ) ~~then~~ rise to the surface. These cold waters extend over the slope and up to about 150 km offshore in the non-tidal simulation (not shown) and up to 250 km offshore in the tidal simulation (Fig.~~5b~~7a). The 27.2 °C isotherm ~~27.2 °C~~only reaches the surface above the slope in the tidal simulation ~~but~~and remains below the surface (~~~-~~30 m) in the non-tidal simulation ~~(not shown). At~~. This aligns with the missing of that isotherm at this location in the corresponding SST map (Fig.4e). For the tidal simulation, at the surface ~~and in the surface layers~~, the temperature ~~in the presence of the tide and IT~~ is therefore ~~cooler.~~colder than in previous season. The temperature ~~difference between the two simulations~~anomaly in the ASO season ~~(Fig.5d)~~ is smaller (< 0.4 °C, Fig.7b) in the surface layers (< 40 m) near the coast compared to the AMJ season (Fig.~~5c~~6b). In contrast, during the ASO season, this cooling ~~reaches~~can reach the surface and results in a colder SST along A (-0.3 °C~~)~~ ~~(~~, Fig.~~4d) along A~~5a) . The strongest cooling ~~(~~~~of ~ -1.2 °C~~)~~ is deeper between 60 and 140 m depth. Below the thermocline, a warming ~~(+~~of about 1.2 °C~~)~~ is also present~~,~~ but extends ~~slightly~~ less ~~(~~~offshore to about 650 km~~) offshore (Fig.5d) compared to the AMJ season (~~~, Fig.7b (vs. ~1000 km, Fig.~~5c~~6b). During this ASO season, the coastward slope of the thermocline and ~~mixing layer~~MLD becomes somewhat steeper compared to the other season. In both simulations, there is a dip of ~~~-~~80 m ~~(~~~, i.e., ~60 m offshore and ~140 m inshore~~) and~~, for the thermocline (dashed black line, Fig.7a). And a dip of ~40 m ~~(~~~, i.e., ~30 m offshore and ~70 m inshore~~), respectively,~~ for ~~the thermocline (thick dashed black line, Fig.5b) and the mixing layer (thick~~ MLD (dashed white line, Fig.~~5b~~7a). Over the entire domain ~~(not shown) between the two simulations (tide - no-tide), the tide deepens~~, the tides shallow the thermocline depth by ~~±~~~6 m on the shelf and ~~±~~~12 m at the plume and far offshore along the propagation path of A (Fig.7c). They shallow MLD in the tidal run by about 10 m along the shelf and ~4 m along the propagation path of A~~.~~ ~~As for the mixing layer, which is deeper in the tidal run by 12 m along the shelf and along the propagation path of A.~~ (Fig.7d).

Between the two seasons, there is also a change in the vertical density gradient (Stratification) between the coast and the open sea. In the tidal simulation ~~with tide (Fig.5a) and without tide (not shown),~~, during the AMJ season, the isodensities are tight near the coast and thicken towards the open sea (Fig.6a). This means that a strong ~~vertical density gradient~~stratification is present near the coast and decreases towards the open sea. In contrast, during the second ASO season, the ~~vertical density gradient~~isodensities are thicker near the coast and tight offshore (Fig.7a). As the result of this, the stratification is weaker inshore than offshore. This clearly highlights a seasonality in the vertical density gradient profile in agreement with Tchilibou et al. (2022). Note that, this behavior also appears in the simulation without the tides (not shown). The ~~transect~~transects of the temperature ~~differences between the two simulations (~~anomaly, Fig.~~5c-d)~~6b and 7b, show that ~~IT (~~ITs and ~~probably~~likely the ~~tide)~~barotropic tides can influence the temperature in the ocean from the surface to the ~~bottom~~deep layers, with a greater effect on the first 300 meters. One question we address in this paper is to better understand what processes are at work that explain these temperature changes.

IV.4. ~~Processes~~What are the processes involved ~~modifying the temperature~~?

To explain the observed surface and water column temperature changes, we ~~calculated~~computed and analyzed the ~~trend~~ terms of the ~~temperature evolution~~heat balance equation (see Section II.3.2, Equation 6) for both seasons (AMJ and ASO) ~~also~~ averaged over the three years from 2013 to 2015.

IV.4.1. Vertical diffusion of Temperature

Figure ~~6~~8 shows the vertical temperature diffusion ~~term (ZDF) for both seasons AMJ (left panel) and ASO (right panel). The~~ tendency (ZDF). ZDF is averaged between 2–20 m, i.e., within the ~~mixing~~ mixed-layer ~~depth range~~. For the AMJ season, ~~the~~ ZDF ~~of the~~in tidal simulation (Fig.~~6a~~8a) shows a negative trend (cooling) in the whole domain~~, which is~~. The maximum ~~on~~values (> |0.4| °C.day^{-1}) are located along the ~~continental~~ slope where the ~~IT~~ITs are generated and on their propagation path ~~(< - 0.4 °C.day^{-1}), with~~. There is a larger horizontal extent along A ~~(~~~of ~700 km from the coasts~~)~~ compared to B ~~(~~~, where it is ~300 km from the coasts~~). Over the rest of the domain~~. Elsewhere, it remains very low ~~(> –~~, > -0.1 °C.day~~$^{-1}$).~~$^{-1}$. For the non-tidal simulation (Fig.~~6c~~8b), the ZDF is very weak ~~(> - 0.1 °C.day^{-1})~~ over the entire domain~~, demonstrating that internal tidal waves would be the main driver of the vertical temperature diffusion in this region during this season.~~ (>> -0.1 °C.day^{-1}). For the ~~second~~ ASO season, the tidal simulation (Fig.~~6b~~8c) shows a decrease of the ZDF ~~along~~near the coast (< 100 km) and a strengthening offshore ~~following A,~~ along A compared to the previous season, but with the same cooling trend (< -0.4 °C.day-^{1}). ~~While along~~Along B, it ~~becomes almost closed~~tends to ~~zero~~be null, both at the coast and offshore (Fig.~~6b).~~ 8c). In addition, the mesoscale circulation ~~intensifies~~and eddy activity intensify during this season. ~~Therefore, to~~To the northeast, approximately between 4°N–8°N, and 47°W–53°W, there is a cooling on the shelf ~~(~ +~~of ~0.3 °C.day~~$^{-1}$)~~$^{-1}$ with ~~NBCR~~eddy-like patterns~~, both~~ in the tidal simulation (Fig.~~6b)~~

a mis en forme : Couleur de police : Texte 1

a mis en forme : Police :14 pt

a mis en forme : Police :14 pt

a mis en forme : Police :14 pt

a mis en forme : Espace Avant : 0 pt

~~and in~~ 8c). The processes by which these features might arise will be examined in more detail in the section V. Unsurprisingly, ZDF is very weak elsewhere for the non-tidal simulation (Fig.~~6d).~~ 8d). Whatever, the ITs could be the dominant driver of vertical diffusion of temperature along the shelf break and offshore, while the barotropic tides could prevail on the shelf to explain the weak ZDF values.

On the vertical following A, we ~~notice an inter~~ have noted inverted ZDF values, with mean magnitude of ~ |0.4| °C.day^{-1}. These values are centered around the thermocline ~~vertical profile~~ for the simulation with ~~tide~~tides in the two seasons AMJ and ASO (respectively Fig.~~6e~~8e and ~~6f), with~~ 8f). There is a cooling ~~tendency (< -0.4 °C.day^{-1})~~trend above the thermocline and a warming ~~(> +0.4 °C.day^{-1})~~trend below~~ the thermocline, with an~~. The average vertical extension ~~of ~~~is up to ~350 m depth for the maximum values~~,~~ but ~~which~~ exceeds 500 m depth for the low values (< ~~+~~0.1 °C.day^{-1}). ~~Over the slope, we see, as~~ As for the horizontal averages~~, this weakening of the ZDF between the AMJ~~ (Fig.~~6e)~~8a and ~~ASO (Fig.6f) seasons~~8c), from one season to another there is a weakening of ZDF above the slope and ~~the~~a strengthening offshore~~. On the other hand, on the vertical, we observe towards the open sea (> 200 km) that the~~, Fig.8e and 8f, for AMJ and ASO respectively. Furthermore, offshore ZDF maxima seem to be discontinuous and spaced of about ~~120–150~~140–160 km during the AMJ season (Fig.~~6e), while we have a~~8e) but are more continuous ~~diffusion~~ for the ASO season (Fig.~~6f). This is consistent with the ZDF vertical averages (Fig.6a-b).~~8f). For the non-tidal simulation, the ~~vertical temperature diffusion~~mean ZDF tends ~~towards 0 °C.day^{-1} within~~to be null in the ~~water column~~ocean interior but remains quite large (> -0.2 °C.day^{-1}) in the thin surface layer ~~(Fig.6g-h).~~

~~During the AMJ season, the ITCZ is close to the equator and thus the trade Winds have their maximum intensity in the heart of the domain, while they migrate northward for the ASO season. As a result, more wind-generated diapycnal mixing is expected in the domain during the AMJ season compared to the ASO season. But the average value of the ZDF (~ -0.2 °C.day^{-1}) is the same between the~~ during the two seasons ~~and for both simulations (not shown) over most of the domain (except for the areas of the NBC backscatter for both simulations, on IT's generation sites and on their propagation path for the tidal simulation). This implies that the ability of the wind to generate diapycnal mixing in the underlying ocean surface layer could be limited by various oceanic processes in this region or is not well considered in the model.~~(Fig.8g-h).

a mis en forme : Couleur de police : Texte 1

a mis en forme : Couleur de police : Texte 1

a mis en forme : Couleur de police : Texte 1

a mis en forme : Couleur de police : Texte 1

a mis en forme : Couleur de police : Texte 1

Furthermore, it is ~~important~~worth to note that along the ~~IT~~ITs propagation's pathway, the maximum of the ZDF follows the maxima of the baroclinic tidal energy dissipation (color shading in Fig.2f). Thus, the dissipation of ~~IT generated on the continental slope generates~~ITs causes vertical mixing that enhances the cooling observed at the surface~~ along the coast~~. In addition, this temperature diffusion contributes to greater subsurface cooling, and warming in the deeper layers beneath the thermocline.

In section IV.3, the seasonality of the ~~vertical gradient of~~ stratification was highlighted, which we recall is stronger at the coast relative to the open ocean during the AMJ season, and reverses during the ASO season to become stronger offshore relative to the coast. This could explain why the ZDF is stronger along the slope and ~~along~~ the near-coastal pathway B during the AMJ season (Fig.~~6a), while~~8a and 8e). And why it is weaker along the slope~~ and closed~~, close to zero following B, and reinforce offshore of A during the ASO season (Fig.~~6b). The vertical gradient of density (and thus~~ 8c and 8f). Previous studies have shown that stratification~~)~~ ~~over the slope~~ influences the generation of ~~IT, by controlling the~~ ITs and controls their propagation ~~mode of the IT that are generated (e.g.: Tchilibou et al., 2020 and Barbot et al., 2021). We~~modes. Here we show ~~here~~ that ~~this vertical gradient~~ stratification also plays a role on the fate of these ~~IT~~ITs, in this case on their dissipation. The ~~vertical gradient of the~~ stratification ~~thus determines~~could determine where ~~the internal tidal~~ITs waves dissipate their energy in the water column~~.~~, as mentioned by de Lavergne et al. (2020).

IV.4.2. Advection of temperature

a mis en forme : Couleur de police : Texte 1

The vertical (z–ADV) or horizontal (h–ADV) terms of the temperature advection tendency are also averaged between 2–20m, for each season over the three years. Remember that when comparing the tidal and non-tidal simulation, a residual term may arise (see equation 7 in the section II.3.2) and must be considered for the following terms, even if it is expected to be low.

IV.4.2.a Vertical advection of Temperature

a mis en forme : Couleur de police : Texte 1

a mis en forme : Titre 4, Espace Avant : 0 pt

~~The vertical temperature advection (z–ADV) averaged between 2–20 m is~~ z-ADV is almost ~~zero~~null in these surface layers throughout the region (Fig.~~7a, b, c, and~~ 9a-d). For both seasons, some weak extreme values are in the northwest on the plateau between 54°W–50°W and 3°N–3°N~~)~~ and are ~~of~~for the same intensity between the two simulations~~. With a slight intensification when moving to the ASO season (~ –0.3 °C.day^{-1}). The z–ADV is zero at the IT generation sites and along their propagation pathways, so the almost zero difference between~~

~~the two simulations for each season shows that the IT~~ with and ~~barotropic tide do not~~without tides. This result suggests that, overall, the tides fail to generate vertical temperature advection within these ocean surface layers. ~~The z–ADV does not contribute to the temperature change in the surface layers of the ocean, and therefore does not influence the cooling observed from the surface on the SST. On the other hand,~~ At deeper~~, under the mixed layer and close to the thermocline, the~~ depth, z–ADV ~~structure is more marked.~~

tendency term is non negligible, and clearly higher in tidal simulation than in non-tidal one. Vertical sections ~~following A~~ (Fig.~~7e, f, g and~~ 9a-h) show an intensification of z~~–~~-ADV of about ±0.8°C.day^{-1} located below the ~~mixing layer~~MLD (magenta dashed line) and ~~near~~seems to be centered around the thermocline ~~between 80 and~~ (black dashed line), with a vertical extension from 20–200 m ~~(~ ± 0.8 °C.day^{-1}). During the AMJ season, over the vertical, the~~depth. z-ADV is stronger in tidal simulation during the both seasons (Fig.9e-f) and mainly presents sparse extrema offshore (> 300 km) for the non-tidal simulation (Fig.9g-h). For the simulation with the tides, z~~–~~-ADV appears to be rather dominated by a cooling trend~~. The tidal simulation (Fig.7e) shows a cooling trend (~ -0.8 °C.day^{-1}),~~ , with a marked hotspot on the slope ~~where the IT are generated, with an average vertical extension from ~ 20 to 200 m depth. Then offshore, two cooling~~ followed by other hotspots ~~(~ -0.8 °C.day^{-1}) followed by a weaker one (~ -0.3 °C.day^{-1})~~ offshore. These extreme values are spaced about 120–150 km apart, ~~interspersed by two warming zones, respectively ~ +0.6 °C.day^{-1} and ~ +0.3 °C.day^{-1} from the coast. For the non-tidal simulation (Fig.7g), the z–ADV is much less intense with lower values (< ± 0.3 °C.day^{-1}) near the coast until ~ 300 km offshore, followed by a cooling hotspot (~ -0.8 °C.day^{-1}) between 300 km and 500 km.~~i.e., the imprint of mode-1 propagation wavelength as for the baroclinic tidal energy dissipation (Fig.2f). For the both simulations~~,~~ (Fig.9e-h), the extreme values ~~appear to be centered around the mean depth of the thermocline (thick black outline) and do not cross the mixing layer depth (thick magenta outline). They are on average located between 40 m and 200 m depth and~~are located within the narrow density (σ_θ) contours [23.8–26.2 kg.m^{-3}], i.e., they follow the ~~position of the~~ maximum ~~vertical density gradient between isodensity anomalies 23.8–26.3 kg.m^{-3}.~~

~~For the ASO season, the simulation with tide (Fig.7f) still shows the same cooling intensity on the slope, although deeper (~ 60 m and 250 m), as well as offshore with this time the third cooling hotspot more intense (~ -0.8 °C.day^{-1}) than during the AMJ season (Fig.7e). The non-tidal simulation (Fig.7h) shows a less intense z–ADV (< ±0.1 °C.day^{-1}) near the slope,~~

~~and a little stronger offshore (~ ±0.3 °C.day^{-1}) between 300 and 600 km from the slope, although less intense than the previous season.~~

~~As in the AMJ season, the extreme values~~ of ~~z–ADV follow the vertical density gradient in both simulations. During the ASO season, the maximum of the vertical density gradient is between 23.8 and 26.2 kg.m^{-3} and is deeper at the coast and is closer to the surface offshore~~the stratification, namely, the pycnocline.

~~Thus, the extreme values of z–ADV are located a little deeper, between 80 and 300 m. Furthermore, for the non-tidal simulation and during both seasons, the position relative to the coast of the extreme values are shifted regarding those ones of the same polarity in the corresponding tidal simulation, which means that the presence of the IT and the tides could modify the intensity and patterns of the z–ADV produced by the other oceanic processes.~~

~~In addition, we averaged the z–ADV between deeper depths above the thermocline depth (20–70 m) and below the thermocline (148–250 m) depth for all simulations and both seasons (not shown). This allows to highlight the NBC's pathway through the extreme values of the z–ADV close to the coast and its retroflection offshore to the northeast for both simulations, but also the propagation of the IT from the coast to the open sea from the two main sites A and B for the simulation with tide. Thus, we see that the IT and the general circulation are the main drivers of the vertical temperature advection in the subsurface and deeper layers in this region.~~

~~-~~IV.4.~~3.~~2.b Horizontal advection of temperature

Horizontal advection of temperature (h–ADV) is defined as the sum of the zonal (x–ADV) and meridional (y–ADV) terms of temperature advection~~. The h–ADV is also averaged between 2–70 m~~ tendency. As for ~~each simulation during both seasons (Fig.8a, b, c and d). As obtained with~~ z–ADV, ~~horizontal advection~~the mean of ~~temperature~~h–ADV tends to ~~zero~~be null over the entire domain in the surface layers for both seasons in both simulations~~, with~~ (Fig.10a-d). Nevertheless, some weak extreme values ~~located~~are in the northwest ~~on~~of the plateau between 54°W–50°W and 3°N–3°N~~) that~~. That intensify during the ASO season ~~(~~~in both simulations, ~ ±0.2 °C.day~~$^{-1}$) (~~$^{-1}$, Fig.~~8b~~ 10c and 10d for the tidal and ~~d). Along the slope between~~non-tidal simulations respectively. During AMJ, h–ADV is slightly stronger, ~0.1 °C.day^{-1}, around sites A and B ~~during the AMJ season, the h–ADV generates a small warming (~ +1 °C.day^{-1}) that is more pronounced~~ in the tidal simulation (Fig.~~8a~~10a) than in the non-tidal simulation (Fig.~~8c), and thus~~10b). This appears to be related to the ~~IT~~ITs generated along

a mis en forme : Police :14 pt, Couleur de police : Texte 1

a mis en forme : Couleur de police : Texte 1

a mis en forme : Titre 4

the slope. On the other hand, the small difference between the two simulations in the surface layers shows that the ~~tidal processes (IT and barotropic tide)~~tides hardly generate ~~horizontal temperature advection. The low values observed here clearly show that the~~ h–ADV. Then, h–ADV could not influence the cold-water tongue observed over the surface SST ~~(Fig.3e-g)~~ during the ASO season~~.~~ (Fig.4d-f). This result aligns with Bessières et al. (2008), which had previously shown that the tidal residual mean transport is null in the upwelling region in the south-east and low (< |0.1| Sverdrup) over the whole shelf.

Along the vertical following A, ~~the~~ h-ADV maxima remain essentially confined below the ~~mixing~~ mixed-layer depth, with much more intense values in the tidal simulation (Fig.10e-f) compared to the non-tidal simulation~~. The~~ (Fig.10g-h). h–ADV contributes to both warming and cooling of the temperature ~~(~~~of ~ ±0.4 °C.day~~$^{-1}$)~~$^{-1}$ from the slope to more than 500 km offshore~~, with an~~. During both seasons, the average vertical extension lies between the surface and 400 m depth for the tidal simulation ~~(Fig.8e and f)~~ and a little less extended between 20–300 m depth for the non-tidal simulation~~(Fig.8g and h)~~. As for z-ADV, h–ADV is also stronger within the pycnocline. For the tidal simulation, there is a warming above the slope (0.4 °C.day^{-1}) reaching the surface in both seasons. This vertical excursion is observed elsewhere for ZDF and z–ADV, and it is probably a marker of local dissipation of ITs at their generation site. The local dissipation of ITs clearly affects both advection and vertical diffusion of the temperature. But there are very low values along the slope when averaging h–ADV or z–ADV between 2–20 m and much more strong values for the ZDF. This means that the energy dissipated by ITs is mostly transferred to mixing.

Furthermore, unlike ZDF and z–ADV, the (horizontal) location of h-ADV maxima mismatch the dissipation hotspots. It is difficult to identify the wave-like characteristic of the propagation of ITs in h-ADV. This probably means that ITs hardly induce any horizontal motion of water mass. We can therefore deduce that the observed increase in h-ADV is mainly because of the barotropic tides.

V. Discussion

V.1. Vertical advection tendency term

Results showed that z-ADV is stronger in the deeper layer, below the MLD and within the pycnocline (Fig.9e-h). As mentioned above, this tendency term includes both nonlinear effect between the temperature and the currents and numerical dissipation of the diffusive part of advection scheme working at high frequencies. The location of the maxima of the vertical advection tendency at the shelf break and along the ITs propagation pathway and its negative sign, suggest that the diffusive part of the advection scheme might be the dominant process compared to nonlinear effects, as the velocity of the (mode-1) internal tidal waves is maximum in the thermocline where exactly z-ADV term is working harder.

V.2. On the role of advection in coastal upwelling

To explain the cooling of the SST at the surface, Neto and da Silva (2014) indicated that the steady flow of the NBC induces northward transport of water masses. This transport is in turn offset by a vertical advection of cool water towards the surface. We demonstrate with our model that the vertical advection hardly modifies the SST. But it is rather working below the mixed layer (Fig.9e-h). The tides-induced vertical diffusion (mixing) extends from the mixed-layer to deeper layers (Fig.8e-f). It is therefore possible for the vertical mixing to bring up to the surface the water masses that are advected into the layers below the mixed layer. The change in SST and temperature within the mixed-layer can then be influence in first order by (i) the vertical diffusion of temperature and secondary by (ii) a cross effect between the latter and the advection (vertical and horizontal) of temperature that mainly takes place below the mixed-layer.

V.3. The mode-1 wave-like patterns in the vertical terms of the heat budget equation

Along the vertical and toward the open ocean, both ZDF and z-ADV tendencies are found to have a wave-like structure. For z-ADV, patches are spaced apart by about 120–150 km and 140–160 km for the AMJ and ASO seasons respectively. Whilst for z-ADV, this wavelength is about 140–160 km during ~~both seasons. The h- ADV~~ the AMJ season and more continuous patches for the ASO season. The wavelength ranges found in temperature tendency terms (3T) are slightly wider (~ 10–20 km, for z-ADV in ASO season and for ZDF) than the purely dynamic tidal coherent wavelength (~ 120–150 km, see section III.1). The difference can be understood as the effect of incoherent ITs, i.e., ITs that are deviated or diffracted by the currents and/or eddies, for which dissipation occurs around where coherent ITs dissipate. They are uncaptured by the harmonic analysis. Hence, the total (coherent + incoherent) dissipation pattern of ITs could be wider than in Figure 2f. When integrating 3T over the season, this cumulative effect is considered and therefore leads to diffuse patterns and wider wavelength. This diffusive effect increases during the ASO season when both background circulation and eddy activity increase.

a mis en forme : Couleur de police : Texte 1

a mis en forme : Couleur de police : Texte 1

Recently, de Macedo et al. ~~is low in the surface layers (2–20 m) but maximum in the subsurface where the~~(2023) gave a detailed description of ISW in this region. They showed an intensification of ISW occurrences along A and B pathways, whose inter-packet distance corresponds to the wavelength of mode-1 ITs. These ISW packets are also colocalized (horizontally) with the deeper 3T patches. Our results are therefore consistent with the observations of the latter study regarding the localization of IT dissipation, particularly where they can generate ISW.

a mis en forme : Couleur de police : Texte 1

V.4. Tidal impact at the mouth of the Amazon River and on the southern shelf: two main competitive processes

Depending on the season, the mean SST anomaly [Tide – No-Tide] at the mouth of the Amazon and southeast of the plateau is either negative (AMJ, fig.5a) or positive (ASO, fig.5b). What we found can be explained by a combination of processes. Note that seasonal variations in solar radiation, river flow and stratification ~~is stronger. We~~over the shelf can also ~~see for~~play significant roles.

In the ~~tidal~~ simulation ~~in both seasons a warming above the slope that reaches~~without the ~~surface~~tides, there is a strong coast-parallel current exiting northwesterly the mouth of the Amazon River (black arrows in Fig.11a, 11b; Ruault et al., 2020) with an average intensity ~~of about +0.4 °C.day^{-1} (Fig.~~> 0.5 m.s^{-1} in the first 50 meters (color shading in Fig.11a, 11b). When including the tides in the model, the latter study had shown that there is an increase in the vertical mixing in the water column due to stratified-shear flow instability. They then show that this weakens the coast-parallel current and favors cross-shore export of water (color shading in Fig.11c, 11d), which is then diverted to the north-west (black arrows in Fig.11c, 11d). We can therefore establish that there are at least two processes at work in producing SST anomalies: (i) vertical mixing and (ii) horizontal transport, reflected respectively by ZDF and h-ADV. We then looked at the latter two processes along the vertical following the cross-shore transect (*C-S*) defined in Figure 10b. Hereinafter, inner mouth refers to the part of the transect before 200 km, whereas outer shelf refers to the part beyond.

During the AMJ season, in the inner mouth, river flow dominates and tide-induced vertical mixing in the narrow water column leads to warming and deepening of the thermocline (cyan and black lines in Fig.12a-b). On the outer shelf, this mixing in the thicker water column leads to cooling above the thermocline and warming below (Fig.12a). Which in turn extends across the shelf and along the pathways of ITs as shown in section IV.4.1 (see Fig.8a, 8c, and 8e~~ and~~

~~f) but remains below the surface (~ 20 m) in the -~~-f). At the same time, the SST on the shelf is somewhat homogeneous (see Fig.4a-c) and solar radiation is lower than 190 W.m^{-2} (not shown). As a result, waters of similar temperature are advected horizontally, i.e., the h-ADV is low (Fig.12b). Thus, for the first season, vertical mixing seems to be the dominant process explaining the average negative SST anomaly on the plateau.

For the second season, solar radiation on the shelf rose sharply with an average value of 60 W.m^{-2} compared with the previous season (Fig.12c). The average depth of the thermocline deepens offshore (cyan and black lines Fig.12d and 12e). Here, mixing leads to warming in the thin surface layer (< 2m, Fig.12d). In contrast to AMJ, there is a significant horizontal variation in SST on the plateau (see Fig.4d-f). The NBC is stronger and can influence transport over the shelf (Prestes et al., 2018). Even it is small, the mean tidal residual transport is added and should be taken into account (Bessières et al., 2008). Warm waters can therefore be advected across the shelf. Consequently, h-ADV is stronger and positive (Fig.12e) and plays a greater role in the fate of SST. For this season, ZDF and h-ADV add to explain the positive SST anomaly on the shelf.

From AMJ to ASO, we can note the deepening of the thermocline depth on the outer shelf. This was previously highlighted by Silva et al. (2005) from REVIZEE (Recursos Vivos da Zona Econômica Exclusiva) campaign data. This is a further contribution to the validation of our model in the section III.2.

V.5. Tidal impact in the NBC retroflection area

To the north-west of the domain [3°N–9°N and 53°W–45°W], in the surface layers (2–20m), eddy-like or circular patterns exist in ZDF during the ASO season for the simulation including tides (Fig.8c). It should be remembered that during this season the NBC intensifies and retroflects, and strong eddy activity takes place there. We therefore assume that they may be the driving force behind these ZDF patterns. However, it is not yet clear how these mesoscale features produce vertical mixing. They may be involved either by fronts or trapping the internal tidal waves.

1) **Fronts**: they exist in such a intensively active mesoscale region. They are associated with significant vertical mixing (see Chapman et al., 2020). We therefore looked at the horizontal temperature gradient (∇T) averaged over the same depth range (2–20m) as the ZDF (Fig.8a-d). During the AMJ season, it is on average equal to 4 10^{-2} °C/10 km. As expected, it does not reveal any circular fronts for the two simulations (Fig.13a-b)

a mis en forme : Paragraphe de liste, Espace Avant : 6 pt, Numéros + Niveau : 1 + Style de numérotation : 1, 2, 3, … + Commencer à : 1 + Alignement : Gauche + Alignement : 0,63 cm + Retrait : 1,27 cm since mesoscale activity is low. Secondly, the horizontal gradient of the temperature increases during the ASO season [> $5\ 10^{-2}$ °C/10 km] in the north-west and exhibits circular and filamentary fronts in both the non-tidal ~~simulation (Fig.8g and h). This vertical excursion that is observed elsewhere for ZDF and z_ADV is a marker of local dissipation of IT at their generation site on the slope, which clearly affects both vertical diffusion and advection of the temperature. But we have almost null values along the slope when averaging h_ADV or z_ADV between 2-20 m and much more strong values for the ZDF (Fig.6a, b, c and d). This means that the IT's energy loss is mostly transferred to the turbulent scale (mixing). Furthermore, unlike the ZDF (Fig.6e) and z_ADV (Fig.7e and f), on the vertical it is difficult to identify a wave structure characteristic of IT propagation in the h_ADV~~(Fig.13c) and tidal (Fig.13d) simulations. Therefore, one would expect to see the same circular patterns in the ZDF for both simulations. This is not actually the case (see Fig.8c and 8d) and invalidates this statement. Furthermore, these values are at least three times smaller compared to other oceanic regions (e.g., Kostianoy et al., 2004 and Bouali et al., 2017), meaning that these fronts are less pronounced.

2) **Trapping internal tidal waves**: stronger mesoscale activity which occurs during this season implies more interaction between the background circulation and ITs (Buijsman et al., 2017 and Tchilibou et al., 2022). The NBC flows along the coast and crosses the sites where ITs are generated (see schematic view in Fig.1). This means that ITs can be trapped and advected along the NBC pathway. When this current destabilizes and retroflects in the north-west, these trapped waves dissipate and therefore generate vertical mixing. This hits the high fraction of the incoherent ITs found here (Tchilibou et al., 2022). But quantifying the impact on temperature of such a wave-mean flow interaction process requires further analysis and is beyond the scope of this study.

Nevertheless, we believe that this second process could be the main cause of vertical diffusion of temperature in that region. Thus, from the section V.3 and the latter, we can conclude that incoherent ITs represent a significant part of the total energy of internal tides. But remains to be quantified in future work. In addition, in parallel with coherent ITs, they might play a critical role on the fate of the temperature in this region.

~~V.~~VI. Summary ~~and Discussions~~

In this paper, ~~the impact of internal tidal waves (IT) on temperature, off the Amazon, especially on the surface and on net heat fluxes is explored through outputs of two~~we used twin oceanic simulations (with and without tides) from a realistic model~~. The~~ to explore the impact of internal tidal waves (ITs) on temperature and associated processes. The impact on the atmosphere-to-ocean net heat fluxes is also covered.

The AMAZON36 configuration~~, based on the 1/36° resolution NEMO model,~~ can reproduce the generation of ~~internal tides (IT), i.e., the conversion of energy from barotropic to baroclinic tides,~~ ITs from two most energetic sites A and B, in good agreement with previous studies ~~(Magalhaes et al., 2016 and Tchilibou et al., 2022). As for dissipation, the model~~. The model well reproduces ~~30% local dissipation, the rest propagating offshore from the different generation sites, the two main ones being A and B (Fig.2e). During their propagation, the IT dissipate most of their energy after~~the local, on-shelf, and offshore dissipation of ITs with two beams of mode-1 ~~reflection~~propagation (120–150 km~~), that is~~). This dissipation occurs less than 300 km from the slope. Then, we assess the ability of the model to reproduce temperature structure. The simulations including tides is in better agreement with SST observations and better reproduce water mass properties along the vertical.

~~The~~Our analyses ~~are~~were based on ~~data from~~ three years (2013 to 2015~~),~~) data averaged over two seasons, AMJ (April-May-June) and ASO (August-September-October~~) which~~). That are highly contrasted in terms of stratification, background circulation and EKE. Results show that for both seasons, the tides create SST cooling of about 0.3 °C in the plume of the Amazon offshore and along the paths of propagation A and B of ITs. During ASO, the cold waters ~~(< 27.5 °C)~~ of the ~~Atlantic Cold Tongue (~~ACT~~)~~ enter our domain along the coast~~,~~ and are affected by ~~IT~~the tides. This enhances that seasonal upwelling and ~~tides, which~~ leads to ~~a~~ cooler ~~seasonal upwelling.~~

~~The impact of the tides on temperature was assessed by comparing our twin simulations with and without tides for each season. For ASO and AMJ, the tides create a cooling of SST of the order of ~ -0.3 °C in the plume of the Amazon offshore and along the paths of propagation A and B of the internal tide. Concerning the Amazon shelf, the tides induce a warming (~ +0.3 °C) in ASO and a cooling (of ~ -0.3 °C) in AMJ. These cooler/warmer waters~~SST. Over the Amazon shelf, the tides induce the same magnitude cooling in AMJ and in turn induce an opposite anomaly (warming) in ASO. These cooling/warming are responsible in the same location for an increase/decrease in the net heat flux from the atmosphere to the ocean~~, leading~~

a mis en forme : Couleur de police : Texte 1

a mis en forme : Couleur de police : Texte 1

a mis en forme : Espace Avant : 12 pt, Après : 6 pt

a mis en forme : Couleur de police : Texte 1

a mis en forme : Couleur de police : Texte 1

a mis en forme : Couleur de police : Texte 1

a mis en forme : Couleur de police : Texte 1

a mis en forme : Couleur de police : Texte 1

a mis en forme : Couleur de police : Texte 1

a mis en forme : Couleur de police : Texte 1

a mis en forme : Couleur de police : Texte 1

a mis en forme : Couleur de police : Texte 1

a mis en forme : Couleur de police : Texte 1

a mis en forme : Couleur de police : Texte 1

a mis en forme : Couleur de police : Texte 1

a mis en forme : Couleur de police : Texte 1

a mis en forme : Couleur de police : Texte 1

a mis en forme : Couleur de police : Texte 1

a mis en forme : Couleur de police : Texte 1

a mis en forme : Couleur de police : Texte 1

a mis en forme : Couleur de police : Texte 1

a mis en forme : Couleur de police : Texte 1

a mis en forme : Couleur de police : Texte 1

a mis en forme : Couleur de police : Texte 1

a mis en forme : Couleur de police : Texte 1

a mis en forme : Couleur de police : Texte 1

a mis en forme : Couleur de police : Texte 1

a mis en forme : Couleur de police : Texte 1

~~to~~ (Qt). However, the overall effect of the tides is an increase ~~(Qt) of +~~of Qt, which lies between [33.2% ~~in AMJ and of +~~ 7.4~~% in ASO between runs with and without tides. In the subsurface, above the thermocline (<120 m), the IT and tides induce a stronger cooling than on the surface of about ~ -1.2 °C and an associated warming of about ~ +1.2 °C under the thermocline (>120 m to 300 m).~~

~~By~~%] from AMJ to ASO. And can be larger than what obtained elsewhere (e.g., in the Solomon Sea). In such a region with large atmospheric convection (marked by the ITCZ), when increasing the atmosphere~~-~~-to~~-~~-ocean net heat flux ~~(Qt),~~, the ~~IT and~~ tides might reduce the cloud convection ~~in~~into the atmosphere~~, as we are in an intertropical convergence zone (ITCZ). Impact on overall atmospheric circulation and precipitation is expected to be significant, as previously shown in other regions such as Indonesia (Tidal induced cooling of -0.3 °C can reduce precipitation by -20%, see~~ (Koch-Larrouy et al., 2010).

Therefore, ~~it becomes important to note that the interannual or even climatic scale evolution of internal~~ this tidal ~~waves activity must be considered to better understand the future evolution of the global~~ effect on the climate~~. Especially since thanks to the CanESM5 global climate model, Yadidya and Rao (2022)~~ might have ~~just shown that in the Andaman Sea and Bay of Bengal, towards the end of this century,~~a key importance for ~~both optimistic and pessimistic SSP scenarios, the increase in depth-averaged stratification will result in an increase in IT activity in these two regions. Knowing that the continental slope of northern Brazil is a place of high generation of IT, which therefore depends on stratification, it is hereby critical to understand how IT activity will evolve in the coming decades in order to better anticipate the climate, and thus better adapt public policies at national and international levels to the global context of~~ the future, taking the climate change~~.~~ into account (Yadidya and Rao, 2022).

~~Another objective of our study was to understand~~In the ~~processes responsible for these temperature changes. For this, we~~subsurface, above the thermocline (< 120 m), the tides induce a stronger cooling (~1.2 °C) than at the surface. And an associated warming of the same magnitude under the thermocline (> 120–300 m). We analyzed the ~~trend~~ terms of the ~~temperature evolution~~heat budget equation~~. Where IT dissipate their energy, there is an intense vertical mixing~~ to identify to processes that ~~generates~~modify the temperature. We found that the vertical diffusion of temperature (ZDF) ~~(~~ is mainly caused by the dissipation of the tides. Horizontal (h-ADV) and vertical (z-ADV) advection can be driven by non-tidal processes but increase when including the tides in the model.

a mis en forme : Couleur de police : Texte 1

a mis en forme : Couleur de police : Texte 1

a mis en forme : Couleur de police : Texte 1

a mis en forme : Couleur de police : Texte 1

a mis en forme : Couleur de police : Texte 1

a mis en forme : Couleur de police : Texte 1

a mis en forme : Couleur de police : Texte 1

a mis en forme : Couleur de police : Texte 1

a mis en forme : Couleur de police : Texte 1

a mis en forme : Couleur de police : Texte 1

a mis en forme : Couleur de police : Texte 1

a mis en forme : Couleur de police : Texte 1

a mis en forme : Couleur de police : Texte 1

a mis en forme : Couleur de police : Texte 1

a mis en forme : Couleur de police : Texte 1

a mis en forme : Couleur de police : Texte 1

a mis en forme : Couleur de police : Texte 1

a mis en forme : Couleur de police : Texte 1

a mis en forme : Couleur de police : Texte 1

a mis en forme : Couleur de police : Texte 1

a mis en forme : Couleur de police : Texte 1

a mis en forme : Couleur de police : Texte 1

a mis en forme : Couleur de police : Texte 1

Over the shelf, barotropic tidal mixing increases ZDF (> |-0.4| °C.day^{-1}) ~~according to pathway A~~and explain the cooling of the water column in AMJ season. During the second season, it combines with h-ADV and to ~~a lesser extent according to pathway B, stronger at shore than offshore during AMJ and inverse during ASO. The ZDF is the only process that reaches the surface layer, and then appears in first approximation to be the main process contributing to the surface cooling observed on SST. The atmospheric heat flux terms (FOR_Z) could also modify this SST but was not highlighted in this study. The~~cause a warming. Off the shelf, the (baroclinic) mixing takes place ~~up~~ from the slope to about ~~800~~700 km ~~off the slope~~ following the path A, and 300 km following ~~B. It is also responsible on a seasonal scale, but also daily for a negative average variation (cooling) of temperature~~ the path B. That mixing induces ZDF with values of about -0.4 °C.day~~$^{-1}$ above the thermocline, and a warming of +0.4 °C.day^{-1}~~$^{-1}$, which is the main process in the upper layer above the mixed layer. But could combine with advection terms (z-ADV and h-ADV) to explain the temperature changes below ~~350 m and decreasing to +0.1 °C.day^{-1} around 500 m depth.~~the mixed layer. Along ITs propagation pathways, some ZDF and z-ADV patches follow the dissipation hotspots of the ITs, i.e., they exhibit the mode-1 propagation of ITs.

~~IT propagation induce vertical advection of water masses around the thermocline level, which has the effect of producing a subsurface mean temperature cooling (~ -0.8 °C.day^{-1}) at a depth varying between 20–200 m AMJ and 60–250 m in ASO, with three extreme values off the coast spaced approximately 120–150 km along of the pathway A, which seem to follow the dissipation patterns, and thus correspond to the horizontal scale of the mode-1 propagation of IT.~~This study highlights the key role of ITs in creating intensified mixing which is important for temperature structure. Other ~~processes such as zonal and meridional advection of temperature~~ analysis we performed with our simulations show that this mixing can also ~~induce temperature change in subsurface and deeper layers. Finally, the horizontal (zonal and meridional) advection of temperature in this region is more related to the general circulation (NBC, mesoscale) but is increased by tides and IT.~~

~~Thus, it is the combination of these different processes that explains the temperature change in the water column in this region. Furthermore, in order to explain the cooling of the SST at the surface, Neto et al. (2014) indicated that the northward transport of water masses by the constant circulation of the NBC was compensated by a vertical advection of colder water masses towards the surface. We now know that this vertical advection process fails to modify the SST but is rather limited below the mixing layer. The same is true for zonal and meridional~~

a mis en forme : Couleur de police : Texte 1

a mis en forme : Couleur de police : Texte 1

a mis en forme : Couleur de police : Texte 1

a mis en forme : Couleur de police : Texte 1

a mis en forme : Couleur de police : Texte 1

a mis en forme : Couleur de police : Texte 1

a mis en forme : Couleur de police : Texte 1

a mis en forme : Couleur de police : Texte 1

a mis en forme : Couleur de police : Texte 1

a mis en forme : Couleur de police : Texte 1

a mis en forme : Couleur de police : Texte 1

a mis en forme : Couleur de police : Texte 1

a mis en forme : Couleur de police : Texte 1

~~advection of temperature (which form horizontal advection). It should be remembered that vertical diffusion extends from the surface, through the mixing layer, into the deep layers. It is therefore possible that water masses cooled by both vertical and horizontal advection below the mixing layer can be recovered and transported vertically to the surface by the effect of vertical mixing. The change in SST and temperature above the mixing layer then comes from (i) vertical diffusion of temperature and (ii) a combination of this vertical diffusion and the advection (vertical and horizontal) of temperature that takes place below the mixing layer.~~

~~This study focuses on temperature, but other analyses we have done on~~impacts salinity ~~show that IT also affects the haline structure of the ocean in this region. A future work would be to look at the impact on salinity, which is also a key parameter in the functioning of the ocean~~. Furthermore, they might be seen as ~~in exchanges with the atmosphere, and thus can play a role on the climate. In addition, internal waves can also influence the biogeochemical cycles of elements and the entire marine ecosystem, since they can induce~~a source of nutrient uptake at tidal frequency and ~~thus participate in structuring~~can have an impact on the spatial distribution of phytoplankton and zooplankton, and ~~in consequence of the rest of the food chain that depends on them.~~

~~It would also be important to compare the results of our model with fields observations. Two high frequency PIRATA anchorages have been installed offshore at the extremity of our region between 35°W–38°W and 0°N–5°N (see~~ therefore on the entire food chain (Sharples et al., 2007, 2009; Xu et al., 2020). These other impacts can be studied through a combined model-in situ data approach. A long-term PIRATA (PredIction and Research moored Array in the Tropical Atlantic) mooring data are available for this goal (Bourlès et al~~.~~., 2019~~) and could be used for this purpose.~~). In addition, recently in late 2021, the ~~"~~"AMAZOn MIXing ("*AMAZOMIX*~~"~~") campaign ~~entirely~~took place in this region. Among other things, this campaign was dedicated to ~~IT (27 August and 8 October 2021) will provide a better~~ITs. It provided a huge set of data, with the aim of understanding ~~of the impact of IT on the marine environment in this region.~~their impact on marine ecosystems (see details in https://en.ird.fr/amazomix-campaign-impact-physical-processes-marine-ecosystem-mouth-amazon). In the meantime, a coupled physical/biogeochemistry simulation (NEMO/PISCES~~),~~) is currently under analysis~~,~~ and will begin to answer these crucial questions~~ of the impact of internal waves on biogeochemistry~~.

Finally, ~~in this first part,~~ we ~~have~~ focused hereabove on describing the ~~effects of internal tidal waves on temperature variation~~impacts of tides on a seasonal scale~~, while~~. A companion

a mis en forme : Couleur de police : Texte 1

a mis en forme : Couleur de police : Texte 1

a mis en forme : Couleur de police : Texte 1

a mis en forme : Couleur de police : Texte 1

a mis en forme : Couleur de police : Texte 1

a mis en forme : Couleur de police : Texte 1

a mis en forme : Couleur de police : Texte 1

a mis en forme : Couleur de police : Texte 1

a mis en forme : Couleur de police : Texte 1

a mis en forme : Couleur de police : Texte 1

a mis en forme : Couleur de police : Texte 1

a mis en forme : Couleur de police : Texte 1

a mis en forme : Couleur de police : Texte 1

a mis en forme : Couleur de police : Texte 1

a mis en forme : Couleur de police : Texte 1

a mis en forme : Couleur de police : Texte 1

a mis en forme : Couleur de police : Texte 1

a mis en forme : Couleur de police : Texte 1

a mis en forme : Couleur de police : Texte 1

paper will then analyze the ~~remainder~~variability of ~~this work will address~~ temperature ~~changes on finer time~~at tidal and subtidal scales~~, notably on the tidal scale~~ using our model simulations and two observational data.

Data availability

The TMI SST v7.1 data are publicly available online from the REMSS platform: https://www.remss.com/missions/tmi/, was accessed on 27 June 2022. The model simulations are available upon request by contacting the corresponding ~~authors~~author.

Authors contributions

Funding acquisition, AKL; Conceptualization and methodology, FA, AKL and ID. Numerical simulations, GM and FA. Formal analysis, FA; FA prepared the paper with contribution from all co-authors.

Competing interests

The authors declare that they have no conflict of interest.

Funding~~Acknowledgments~~

This work is part of the PhD Thesis of Fernand Assene~~ PhD thesis~~, cofounded by Institut de Recherche pour le Développement (IRD) and Mercator Ocean International (MOi~~).~~), under the cobadging of Ariane Koch-Larrouy and Isabelle Dadou. The numerical ~~simulation was~~simulations were founded by CNRS/CNES/IRD via the projects A0080111357 and A0130111357 and were performed ~~tank~~thank to “Jean-Zay”, the CNRS/GENCI/IDRIS platform ~~calculator (Jean-Zay).~~for modelling and computing.

Acknowledgments~~Abbreviations~~

~~The following abbreviations are used in this manuscript:~~

~~AMASSEDS: A Multi-disciplinary Amazon Shelf SEDiment Study~~

~~AMAZOMIX: AMAZOn MIXing~~

~~FES2012 | FES2014: Finite Element Solution 2012 | Finite Element Solution 2014~~

~~NEMO/PISCES: Nucleus for European MOdeling / Pelagic Interactions Scheme for Carbon and Ecosystem Studies~~

~~PIRATA: PredIction and Research moored Array in the Tropical Atlantic~~

a mis en forme : Couleur de police : Texte 1

a mis en forme : Couleur de police : Texte 1

a mis en forme : Couleur de police : Texte 1

a mis en forme : Couleur de police : Texte 1

a mis en forme : Couleur de police : Texte 1

a mis en forme : Couleur de police : Rouge

a mis en forme : Surlignage

a mis en forme : Espace Après : 6 pt

~~REVIZEE : Recursos Vivos da Zona Econômica Exclusiva~~

The authors would like to thank the Editorial team for their availability, and the two reviewers Clément Vic and Nicolas Grissouard for their valuable comments, which enhanced the quality of the present work. We also thank the NOAA Ocean Climate Laboratory for making the WOA2018 products available.

References

Aguedjou, H.M.A., Dadou, I., Chaigneau, A., Morel, Y., Alory, G., 2019. Eddies in the Tropical Atlantic Ocean and Their Seasonal Variability. Geophys. Res. Lett. 46, 12156–12164. https://doi.org/10.1029/2019GL083925

Aguedjou, H.M.A., Chaigneau, A., Dadou, I., Morel, Y., Pegliasco, C., Da-Allada, C.Y., Baloïtcha, E., 2021. What Can We Learn From Observed Temperature and Salinity Isopycnal Anomalies at Eddy Generation Sites? Application in the Tropical Atlantic Ocean. ~~Journal of Geophysical Research: Oceans 126, e2021JC017630. https://doi.org/10.1029/2021JC017630~~J. Geophys. Res. Oceans 126, e2021JC017630. https://doi.org/10.1029/2021JC017630

~~Aguedjou, H.M.A., Dadou, I., Chaigneau, A., Morel, Y., Alory, G., 2019. Eddies in the Tropical Atlantic Ocean and Their Seasonal Variability. Geophysical Research Letters 46, 12156–12164. https://doi.org/10.1029/2019GL083925~~

~~Araujo, M., Dimoune, D.M., Noriega, C., Hounsou-Gbo, G.A., Veleda, D., Araujo, J., Bruto, L., Feitosa, F., Flores-Montes, M., Lefèvre, N., Melo, P., Otsuka, A., Travassos, R.K., Schwamborn, R., Neumann-Leitão, S., 2021. Camadas Finas III - BR cruise: S-ADCP data. https://doi.org/10.17882/80828~~

~~Araujo, M., Noriega, C., Hounsou-gbo, G.A., Veleda, D., Araujo, J., Bruto, L., Feitosa, F., Flores-Montes, M., Lefèvre, N., Melo, P., Otsuka, A., Travassos, K., Schwamborn, R., Neumann-Leitão, S., 2017. A Synoptic Assessment of the Amazon River-Ocean Continuum during Boreal Autumn: From Physics to Plankton Communities and Carbon Flux. Frontiers in Microbiology 8.~~

~~Araujo, J.; Mezilet, Y.; Marin, F.; Jouanno, J.; Araujo, M. On the variability of the upwelling cell off the Amazon River mouth (01072-00001). In: VII Congresso Brasileiro de Oceanografia - CBO2016, 2016, Salvador, BA. Livro de Resumos - CBO2016. Salvador, BA: AOCEANO, 2016. v. 1.~~

a mis en forme : Anglais (États-Unis)

a mis en forme : Anglais (États-Unis)

a mis en forme : Bibliographie, Retrait : Gauche : 0 cm, Première ligne : 0 cm

a mis en forme : Non souligné, Couleur de police : Automatique, Anglais (États-Unis)

a mis en forme : Anglais (États-Unis)

~~Arbic, B., Richman, J., Shriver, J., Timko, P., Metzger, E., Wallcraft, A., 2012. Global Modeling of Internal Tides Within an Eddying Ocean General Circulation Model. Oceanography 25, 20–29. https://doi.org/10.5670/oceanog.2012.38~~

Archer, D., Martin, P., Buffett, B., Brovkin, V., Rahmstorf, S., Ganopolski, A., 2004. The importance of ocean temperature to global biogeochemistry. Earth ~~and Planetary Science Letters 222, 333–348. https://doi.org/10.1016/j.epsl.2004.03.011~~Planet. Sci. Lett. 222, 333–348. https://doi.org/10.1016/j.epsl.2004.03.011

~~Barbot, S., Lagarde, M., Lyard, F., Marsaleix, P., Lherminier, P., Jeandel, C., 2022. Internal Tides Responsible for Lithogenic Inputs Along the Iberian Continental Slope. Journal of Geophysical Research: Oceans 127, e2022JC018816. https://doi.org/10.1029/2022JC018816~~

Azevedo, A., da Silva, J.C.B., New, A.L., 2006. On the generation and propagation of internal solitary waves in the southern Bay of Biscay. Deep Sea Res. Part Oceanogr. Res. Pap. 53, 927–941. https://doi.org/10.1016/j.dsr.2006.01.013

Baines, P.G., 1982. On internal tide generation models. Deep Sea Res. Part Oceanogr. Res. Pap. 29, 307–338. https://doi.org/10.1016/0198-0149(82)90098-X

Barbot, S., Lyard, F., Tchilibou, M., Carrere, L., 2021. Background stratification impacts on internal tide generation and abyssal propagation in the western equatorial Atlantic and the Bay of Biscay. ~~Ocean Science 17, 1563–1583. https://doi.org/10.5194/os-17-1563-2021~~Ocean Sci. 17, 1563–1583. https://doi.org/10.5194/os-17-1563-2021

Barton, E.D., Inall, M.E., Sherwin, T.J., Torres, R., 2001. Vertical structure, turbulent mixing and fluxes during Lagrangian observations of an upwelling filament system off Northwest Iberia. ~~Progress in Oceanography,~~Prog. Oceanogr., Lagrangian studies of the Iberian upwelling system 51, 249–267~~. https://doi.org/10.1016/S0079-6611(01)00069-6~~. https://doi.org/10.1016/S0079-6611(01)00069-6

Beardsley, R.C., Candela, J., Limeburner, R., Geyer, W.R., Lentz, S.J., Castro, B.M., Cacchione, D., Carneiro, N., 1995. The M2 tide on the Amazon Shelf. ~~Journal of Geophysical Research:~~J. Geophys. Res. Oceans 100, 2283–2319~~. https://doi.org/10.1029/94JC01688~~. https://doi.org/10.1029/94JC01688

~~Bordois, L., Auclair, F., Paci, A., Dossmann, Y., Gerkema, T., Nguyen, C., 2016. Tidal energy redistribution among vertical modes in a fluid with a mid-depth pycnocline. Physics of Fluids 28, 101701. https://doi.org/10.1063/1.4964759~~

Bessières, L., 2007. Impact des marées sur la circulation générale océanique dans une perspective climatique (phdthesis). Université Paul Sabatier - Toulouse III.

Bessières, L., Madec, G., Lyard, F., 2008. Global tidal residual mean circulation: Does it affect a climate OGCM? Geophys. Res. Lett. 35. https://doi.org/10.1029/2007GL032644

a mis en forme : Bibliographie, Retrait : Gauche : 0 cm, Première ligne : 0 cm

a mis en forme : Non souligné, Couleur de police : Automatique

a mis en forme : Bibliographie, Retrait : Gauche : 0 cm, Première ligne : 0 cm

a mis en forme : Non souligné, Couleur de police : Automatique

a mis en forme : Non souligné, Couleur de police : Automatique

a mis en forme : Non souligné, Couleur de police : Automatique, Anglais (États-Unis)

Bouali, M., Sato, O.T., Polito, P.S., 2017. Temporal trends in sea surface temperature gradients in the South Atlantic Ocean. Remote Sens. Environ. 194, 100–114. https://doi.org/10.1016/j.rse.2017.03.008

Bourles, B., Molinari, R.L., Johns, E., Wilson, W.D., Leaman, K.D., 1999. Upper layer currents in the western tropical North Atlantic (1989–1991). ~~Journal of Geophysical Research: Oceans 104, 1361–1375. https://doi.org/10.1029/1998JC900025~~J. Geophys. Res. Oceans 104, 1361–1375. https://doi.org/10.1029/1998JC900025

Bourlès, B., Araujo, M., McPhaden, M.J., Brandt, P., Foltz, G.R., Lumpkin, R., Giordani, H., Hernandez, F., Lefèvre, N., Nobre, P., Campos, E., Saravanan, R., Trotte-Duhà, J., Dengler, M., Hahn, J., Hummels, R., Lübbecke, J.F., Rouault, M., Cotrim, L., Sutton, A., Jochum, M., Perez, R.C., 2019. ~~Buijsman, M.C., Ansong, J.K., Arbic, B.K., Richman, J.G., Shriver, J.F., Timko, P.G., Wallcraft, A.J., Whalen, C.B., Zhao, Z., 2016. Impact of Parameterized Internal Wave Drag on the Semidiurnal Energy Balance in a Global Ocean Circulation Model. Journal of Physical Oceanography 46, 1399–1419. https://doi.org/10.1175/JPO-D-15-0074.1~~

PIRATA: A Sustained Observing System for Tropical Atlantic Climate Research and Forecasting. Earth Space Sci. 6, 577–616. https://doi.org/10.1029/2018EA000428

Buijsman, M.C., Arbic, B.K., Richman, J.G., Shriver, J.F., Wallcraft, A.J., Zamudio, L., 2017. Semidiurnal internal tide incoherence in the equatorial Pacific. ~~Journal of Geophysical Research: Oceans 122, 5286–5305. https://doi.org/10.1002/2016JC012590~~J. Geophys. Res. Oceans 122, 5286–5305. https://doi.org/10.1002/2016JC012590

~~Carrere, L., Lyard, F., Cancet, M., Guillot, A., & Roblou, L. (2012). FES 2012: A new global tidal model taking advantage of nearly 20 years of altimetry, in 20 Years of Progress in Radar Altimetry.~~

C., Le Provost, Florent, Lyard, 1997. Energetics of the M2 barotropic ocean tides: an estimate of bottom friction dissipation from a hydrodynamic model - ScienceDirect. Prog. Oceanogr. 37–52.

Chapman, C.C., Lea, M.-A., Meyer, A., Sallée, J.-B., Hindell, M., 2020. Defining Southern Ocean fronts and their influence on biological and physical processes in a changing climate. Nat. Clim. Change 10, 209–219. https://doi.org/10.1038/s41558-020-0705-4

Clayson, C.A., Bogdanoff, A.S., 2013. The Effect of Diurnal Sea Surface Temperature Warming on Climatological Air–Sea Fluxes. J. Clim. 26, 2546–2556. https://doi.org/10.1175/JCLI-D-12-00062.1

~~Clayson, C.A., Bogdanoff, A.S., 2013. The Effect of Diurnal Sea Surface Temperature Warming on Climatological Air–Sea Fluxes. American Meteorological Society.~~

Collins, M., An, S.-I., Cai, W., Ganachaud, A., Guilyardi, E., Jin, F.-F., Jochum, M., Lengaigne, M., Power, S., Timmermann, A., Vecchi, G., Wittenberg, A., 2010. The

a mis en forme : Bibliographie, Retrait : Gauche : 0 cm, Première ligne : 0 cm

a mis en forme : Non souligné, Couleur de police : Automatique, Anglais (États-Unis)

a mis en forme : Anglais (États-Unis)

a mis en forme : Bibliographie, Retrait : Gauche : 0 cm, Première ligne : 0 cm

a mis en forme : Non souligné, Couleur de police : Automatique,

a mis en forme : Bibliographie, Retrait : Gauche : 0 cm, Première ligne : 0 cm

a mis en forme : Non souligné

a mis en forme : Bibliographie, Retrait : Gauche : 0 cm, Première ligne : 0 cm

impact of global warming on the tropical Pacific Ocean and El Niño. ~~Nature Geosci 3, 391–397. https://doi.org/10.1038/ngeo868~~Nat. Geosci. 3, 391–397. https://doi.org/10.1038/ngeo868

da Silva, J.C.B., New, A.L., ~~Srokosz,~~ Magalhaes, J.M~~.A., Smyth, T.J., 2002.~~., 2011. On the ~~observability~~structure and propagation of internal ~~tidal~~solitary waves generated at the Mascarene Plateau in ~~remotely-sensed ocean colour data. Geophysical Research Letters 29, 10-1-10-4. https://doi.org/10.1029/2001GL013888~~the Indian Ocean. Deep Sea Res. Part Oceanogr. Res. Pap. 58, 229–240. https://doi.org/10.1016/j.dsr.2010.12.003

de Lavergne, C., Vic, C., Madec, G., Roquet, F., Waterhouse, A.F., Whalen, C.B., Cuypers, Y., Bouruet-Aubertot, P., Ferron, B., Hibiya, T., 2020. A Parameterization of Local and Remote Tidal Mixing. J. Adv. Model. Earth Syst. 12, e2020MS002065. https://doi.org/10.1029/2020MS002065

de Macedo, C.R., Koch-Larrouy, A., da Silva, J.C.B., Magalhães, J.M., Lentini, C.A.D., Tran, T.K., Rosa, M.C.B., Vantrepotte, V., 2023. Spatial and temporal variability of mode-1 and mode-2 internal solitary waves from MODIS/TERRA sunglint off the Amazon shelf. EGUsphere 1–27~~. https://doi.org/10.5194/egusphere-2022-1482.~~ https://doi.org/10.5194/egusphere-2022-1482

~~Demaster, D.J., Pope, R.H., 1996. Nutrient dynamics in Amazon shelf waters: results from AMASSEDS. Continental Shelf Research 16, 263–289. https://doi.org/10.1016/0278-4343(95)00008-O~~

~~Denman, K.L., Gargett, A.E., 1983. Time and space scales of vertical mixing and advection of phytoplankton in the upper ocean. Limnology and Oceanography 28, 801–815. https://doi.org/10.4319/lo.1983.28.5.0801~~

Didden, N., Schott, F., 1993. Eddies in the North Brazil Current retroflection region observed by Geosat altimetry. ~~Journal of Geophysical Research: Oceans 98, 20121–20131. https://doi.org/10.1029/93JC01184~~ J. Geophys. Res. Oceans 98, 20121–20131. https://doi.org/10.1029/93JC01184

~~Dimoune, D. M., Birol, F., Hernandez, F., Léger, F., Araujo, M., 2022. Revisiting the tropical Atlantic western boundary circulation from a 25-year time series of satellite altimetry data. *EGUsphere*, 1-42.~~

Dong, S., Sprintall, J., Gille, S.T., Talley, L., 2008. Southern Ocean mixed-layer depth from Argo float profiles. J. Geophys. Res. Oceans 113. https://doi.org/10.1029/2006JC004051

Dunphy, M., Lamb, K.G., 2014. Focusing and vertical mode scattering of the first mode internal tide by mesoscale eddy interaction. J. Geophys. Res. Oceans 119, 523–536. https://doi.org/10.1002/2013JC009293

Egbert, G.D., Ray, R.D., 2000. Significant dissipation of tidal energy in the deep ocean inferred from satellite altimeter data. Nature 405, 775–778~~. https://doi.org/10.1038/35015531.~~ https://doi.org/10.1038/35015531

a mis en forme : Non souligné, Couleur de police : Automatique

a mis en forme : Non souligné, Couleur de police : Automatique

a mis en forme : Bibliographie, Retrait : Gauche : 0 cm, Première ligne : 0 cm

a mis en forme : Non souligné, Couleur de police : Automatique

a mis en forme : Bibliographie, Retrait : Gauche : 0 cm, Première ligne : 0 cm

a mis en forme : Non souligné, Couleur de police : Automatique

a mis en forme : Bibliographie, Retrait : Gauche : 0 cm, Première ligne : 0 cm

a mis en forme : Non souligné, Couleur de police : Automatique

Fassoni-Andrade, A.C., Durand, F., Azevedo, A., Bertin, X., Santos, L.G., Khan, J.U., Testut, L., Moreira, D.M., 2023. Seasonal to interannual variability of the tide in the Amazon estuary. Cont. Shelf Res. 255, 104945. https://doi.org/10.1016/j.csr.2023.104945

Feng, Y., Tang, Q., Li, J., Sun, J., Zhan, W., 2021. Internal Solitary Waves Observed on the Continental Shelf in the Northern South China Sea From Acoustic Backscatter Data. Front. Mar. Sci. 8.

Fontes, R.F.C., Castro, B.M., Beardsley, R.C., 2008. Numerical study of circulation on the inner Amazon Shelf. Ocean Dyn. 58, 187–198. https://doi.org/10.1007/s10236-008-0139-4

Gabioux, M., Vinzon, S.B., Paiva, A.M., 2005. Tidal propagation over fluid mud layers on the Amazon shelf. ~~Continental Shelf Research 25, 113–125. https://doi.org/10.1016/j.csr.2004.09.001~~Cont. Shelf Res. 25, 113–125. https://doi.org/10.1016/j.csr.2004.09.001

a mis en forme : Bibliographie, Retrait : Gauche : 0 cm, Première ligne : 0 cm

a mis en forme : Non souligné, Couleur de police : Automatique

Garzoli, S.L., Ffield, A., Johns, W.E., Yao, Q., 2004. North Brazil Current retroflection and transports. ~~Journal of Geophysical Research: Oceans 109. https://doi.org/10.1029/2003JC001775~~J. Geophys. Res. Oceans 109. https://doi.org/10.1029/2003JC001775

a mis en forme : Non souligné, Couleur de police : Automatique

~~Garzoli, S.L., Ffield, A., Yao, Q., 2003. North Brazil Current rings and the variability in the latitude of retroflection, in: Goni, G.J., Malanotte-Rizzoli, P. (Eds.), Elsevier Oceanography Series, Interhemispheric Water Exchange in the Atlantic Ocean. Elsevier, pp. 357–373. https://doi.org/10.1016/S0422-9894(03)80154-X~~

Gévaudan, M., Durand, F., Jouanno, J., 2022. Influence of the Amazon-Orinoco Discharge Interannual Variability on the Western Tropical Atlantic Salinity and Temperature. ~~Journal of Geophysical Research: Oceans 127, e2022JC018495. https://doi.org/10.1029/2022JC018495~~J. Geophys. Res. Oceans 127, e2022JC018495. https://doi.org/10.1029/2022JC018495

a mis en forme : Français (France)

a mis en forme : Bibliographie, Retrait : Gauche : 0 cm, Première ligne : 0 cm

a mis en forme : Non souligné, Couleur de police : Automatique

~~Geyer et al., 1996. Physical oceanography of the Amazon shelf. Continental Shelf Research 16, 575–616. https://doi.org/10.1016/0278-4343(95)00051-8~~

~~González-Haro, C., Ponte, A., Autret, E., 2019. Quantifying Tidal Fluctuations in Remote Sensing Infrared SST Observations. Remote Sensing 11, 2313. https://doi.org/10.3390/rs11192313~~

a mis en forme : Anglais (États-Unis)

~~Heathershaw, A.D., New, A.L., Edwards, P.D., 1987. Internal tides and sediment transport at the shelf break in the Celtic Sea. Continental Shelf Research 7, 485–517. https://doi.org/10.1016/0278-4343(87)90092-6~~

Hernandez, O., Jouanno, J., Durand, F., 2016. Do the Amazon and Orinoco freshwater plumes really matter for hurricane-induced ocean surface cooling? ~~Journal of Geophysical Research: Oceans 121, 2119–2141. https://doi.org/10.1002/2015JC011021~~J. Geophys. Res. Oceans 121, 2119–2141. https://doi.org/10.1002/2015JC011021

a mis en forme : Bibliographie, Retrait : Gauche : 0 cm, Première ligne : 0 cm

a mis en forme : Non souligné, Couleur de police : Automatique, Hernandez, O., Jouanno, J., Echevin, V., Aumont, O., 2017. Modification of sea surface temperature by chlorophyll concentration in the Atlantic upwelling systems. ~~Journal of Geophysical Research: Oceans 122, 5367–5389. https://doi.org/10.1002/2016JC012330~~J. Geophys. Res. Oceans 122, 5367–5389. https://doi.org/10.1002/2016JC012330

Hersbach, H., Bell, B., Berrisford, P., Hirahara, S., Horányi, A., Muñoz-Sabater, J., Nicolas, J., Peubey, C., Radu, R., Schepers, D., Simmons, A., Soci, C., Abdalla, S., Abellan, X., Balsamo, G., Bechtold, P., Biavati, G., Bidlot, J., Bonavita, M., De Chiara, G., Dahlgren, P., Dee, D., Diamantakis, M., Dragani, R., Flemming, J., Forbes, R., Fuentes, M., Geer, A., Haimberger, L., Healy, S., Hogan, R.J., Hólm, E., Janisková, M., Keeley, S., Laloyaux, P., Lopez, P., Lupu, C., Radnoti, G., de Rosnay, P., Rozum, I., Vamborg, F., Villaume, S., Thépaut, J.-N., 2020. The ERA5 global reanalysis. ~~Quarterly Journal of the Royal Meteorological Society 146, 1999–2049. https://doi.org/10.1002/qj.3803~~Q. J. R. Meteorol. Soc. 146, 1999–2049. https://doi.org/10.1002/qj.3803

HYBAM (2018) Contrôles géodynamique, hydrologique et biogéochimique de l'érosion/altération et des transferts de matière dans les bassins de l'Amazone, de l'Orénoque et du Congo~~. http://www.ore-hybam.org.~~ http://www.ore-hybam.org, Accessed 10 December 2021

~~Jackson, C., 2007. Internal wave detection using the Moderate Resolution Imaging Spectroradiometer (MODIS). Journal of Geophysical Research: Oceans 112. https://doi.org/10.1029/2007JC004220~~

Jayakrishnan, P.R., Babu, C.A., 2013. Study of the Oceanic Heat Budget Components over the Arabian Sea during the Formation and Evolution of Super Cyclone, Gonu 2013~~.~~ ~~https://doi.org/10.4236/acs.2013.33030.~~ https://doi.org/10.4236/acs.2013.33030

Jithin, A.K., Francis, P.A., 2020. Role of internal tide mixing in keeping the deep Andaman Sea warmer than the Bay of Bengal. ~~Sci Rep 10, 11982. https://doi.org/10.1038/s41598-020-68708-6~~Sci. Rep. 10, 11982. https://doi.org/10.1038/s41598-020-68708-6

Johns, W.E., Lee, T.N., Beardsley, R.C., Candela, J., Limeburner, R., Castro, B., 1998. Annual Cycle and Variability of the North Brazil Current. ~~Journal of Physical Oceanography 28, 103–128. https://doi.org/10.1175/1520-0485(1998)028<0103:ACAVOT>2.0.CO;2~~J. Phys. Oceanogr. 28, 103–128. https://doi.org/10.1175/1520-0485(1998)028<0103:ACAVOT>2.0.CO;2

~~Johns, W.E., Lee, T.N., Schott, F.A., Zantopp, R.J., Evans, R.H., 1990. The North Brazil Current retroflection: Seasonal structure and eddy variability. Journal of Geophysical Research: Oceans 95, 22103–22120. https://doi.org/10.1029/JC095iC12p22103~~

Jouanno, J., Marin, F., ~~Du~~du Penhoat, Y., Sheinbaum, J., ~~& ~~Molines, J~~. ~~.-M., 2011. Seasonal heat balance in the upper 100 m of the equatorial Atlantic Ocean. ~~Journal of Geophysical Research:~~J. Geophys. Res. Oceans 116. https://doi.org/10.1029/2010JC006912

a mis en forme

a mis en forme : Non souligné, Couleur de police : Automatique

a mis en forme : Non souligné, Couleur de police : Automatique, Anglais (États-Unis)

a mis en forme : Français (France)

a mis en forme : Bibliographie, Retrait : Gauche : 0 cm, Première ligne : 0 cm

a mis en forme : Non souligné, Couleur de police : Automatique

a mis en forme : Non souligné, Couleur de police : Automatique

a mis en forme : Non souligné, Couleur de police : Automatique

a mis en forme : Anglais (États-Unis)

a mis en forme

a mis en forme

a mis en forme

a mis en forme

Kara, A.B., Rochford, P.A., Hurlburt, H.E., 2003. Mixed layer depth variability over the global ocean. J. Geophys. Res. Oceans~~, 116(C9).~~ 108. https://doi.org/10.1029/2000JC000736

Kelly, S.M., Nash, J.D., Kunze, E., 2010. Internal-tide energy over topography. ~~Journal of Geophysical Research: Oceans 115. https://doi.org/10.1029/2009JC005618~~

~~Koch-Larrouy, A., Lengaigne, M., Terray, P., Madec, G., Masson, S., 2010. Tidal mixing in the Indonesian Seas and its effect on the tropical climate system. Clim Dyn 34, 891–904. https://doi.org/10.1007/s00382-009-0642-4~~

~~Koch-Larrouy, A., Madec, G., Iudicone, D., Atmadipoera, A., Molcard, R., 2008. Physical processes contributing to the water mass transformation of the Indonesian Throughflow. Ocean Dynamics~~J. Geophys. Res. Oceans 115. https://doi.org/10.1029/2009JC005618~~ 58, 275–288. https://doi.org/10.1007/s10236-008-0154-5~~

Koch-Larrouy, A., Madec, G., Bouruet-Aubertot, P., Gerkema, T., Bessières, L., Molcard, R., 2007. On the transformation of Pacific Water into Indonesian Throughflow Water by internal tidal mixing. ~~Geophysical Research Letters 34. https://doi.org/10.1029/2006GL028405~~Geophys. Res. Lett. 34. https://doi.org/10.1029/2006GL028405

Koch-Larrouy, A., Madec, G., Iudicone, D., Atmadipoera, A., Molcard, R., 2008. Physical processes contributing to the water mass transformation of the Indonesian Throughflow. Ocean Dyn. 58, 275–288. https://doi.org/10.1007/s10236-008-0154-5

Koch-Larrouy, A., Lengaigne, M., Terray, P., Madec, G., Masson, S., 2010. Tidal mixing in the Indonesian Seas and its effect on the tropical climate system. Clim. Dyn. 34, 891–904. https://doi.org/10.1007/s00382-009-0642-4

Koch-Larrouy, A., Atmadipoera, A., van Beek, P., Madec, G., Aucan, J., Lyard, F., Grelet, J., Souhaut, M., 2015. Estimates of tidal mixing in the Indonesian archipelago from multidisciplinary INDOMIX in-situ data. Deep Sea Res. Part Oceanogr. Res. Pap. 106, 136–153. https://doi.org/10.1016/j.dsr.2015.09.007

Kostianoy, A.G., Ginzburg, A.I., Frankignoulle, M., Delille, B., 2004. Fronts in the Southern Indian Ocean as inferred from satellite sea surface temperature data. J. Mar. Syst. 45, 55–73. https://doi.org/10.1016/j.jmarsys.2003.09.004

Kosuth, P., Callède, J., Laraque, A., Filizola, N., Guyot, J.L., Seyler, P., Fritsch, J.M., Guimarães, V., 2009. Sea-tide effects on flows in the lower reaches of the Amazon River. Hydrol. Process. 23, 3141–3150. https://doi.org/10.1002/hyp.7387

Kunze, E., MacKay, C., McPhee-Shaw, E.E., Morrice, K., Girton, J.B., Terker, S.R., 2012. Turbulent Mixing and Exchange with Interior Waters on Sloping Boundaries. ~~Journal of Physical Oceanography 42, 910–927. https://doi.org/10.1175/JPO-D-11-075.1~~J. Phys. Oceanogr. 42, 910–927. https://doi.org/10.1175/JPO-D-11-075.1

Lambeck, K., Runcorn, S.K., 1977. Tidal dissipation in the oceans: astronomical, geophysical and oceanographic consequences. ~~Philosophical Transactions of the Royal Society of~~

a mis en forme : Bibliographie, Retrait : Gauche : 0 cm, Première ligne : 0 cm

a mis en forme : Bibliographie, Retrait : Gauche : 0 cm, Première ligne : 0 cm

a mis en forme : Non souligné

a mis en forme : Non souligné, Couleur de police : Automatique

a mis en forme : Bibliographie, Retrait : Gauche : 0 cm, Première ligne : 0 cm

a mis en forme : Non souligné, Couleur de police : Automatique

~~London. Series A, Mathematical and Physical Sciences 287, 545–594. https://doi.org/10.1098/rsta.1977.0159~~Philos. Trans. R. Soc. Lond. Ser. Math. Phys. Sci. 287, 545–594. https://doi.org/10.1098/rsta.1977.0159

a mis en forme : Non souligné, Couleur de police : Automatique

Lascaratos, A., 1993. Estimation of deep and intermediate water mass formation rates in the Mediterranean Sea. ~~Deep Sea Research Part II: Topical Studies in Oceanography 40, 1327–1332. https://doi.org/10.1016/0967-0645(93)90072-U~~Deep Sea Res. Part II Top. Stud. Oceanogr. 40, 1327–1332. https://doi.org/10.1016/0967-0645(93)90072-U

a mis en forme : Non souligné, Couleur de police : Automatique

~~Le Provost, C., Lyard, F., 1997.~~Laurent, L.S., Garrett, C., 2002. The Role of Internal Tides in Mixing the Deep Ocean. J. Phys. Oceanogr. 32, 2882–2899. https://doi.org/10.1175/1520-0485(2002)032<2882:TROITI>2.0.CO;2

Leclair, M., Madec, G., 2009. A conservative leapfrog time stepping method. Ocean Model. 30, 88–94. https://doi.org/10.1016/j.ocemod.2009.06.006

~~Energetics of the M2 barotropic ocean tides: an estimate of bottom friction dissipation from a hydrodynamic model - ScienceDirect. Progress in Oceanography 37–52.~~

a mis en forme : Bibliographie, Retrait : Gauche : 0 cm, Première ligne : 0 cm

a mis en forme : Non souligné

Lellouche, J.-M., Greiner, E., Le Galloudec, O., Garric, G., Regnier, C., Drevillon, M., Benkiran, M., Testut, C.-E., Bourdalle-Badie, R., Gasparin, F., Hernandez, O., Levier, B., Drillet, Y., Remy, E., Le Traon, P.-Y., 2018. Recent updates to the Copernicus Marine Service global ocean monitoring and forecasting real-time 1/12° high-resolution system. ~~Ocean Science 14, 1093–1126. https://doi.org/10.5194/os-14-1093-2018~~Ocean Sci. 14, 1093–1126. https://doi.org/10.5194/os-14-1093-2018

a mis en forme : Non souligné, Couleur de police : Automatique

Lentini, C.A.D., Magalhães, J.M., da Silva, J.C.B., Lorenzzetti, J.A., 2016. Transcritical Flow and Generation of Internal Solitary Waves off the Amazon River: Synthetic Aperture Radar Observations and Interpretation. Oceanography 29, 187–195.

Lentz, S.J., Limeburner, R., 1995. The Amazon River Plume during AMASSEDS: Spatial characteristics and salinity variability. ~~Journal of Geophysical Research: Oceans 100, 2355–2375. https://doi.org/10.1029/94JC01411~~J. Geophys. Res. Oceans 100, 2355–2375. https://doi.org/10.1029/94JC01411

a mis en forme : Non souligné, Couleur de police : Automatique

Li, C., Zhou, W., Jia, X., Wang, X., 2006. Decadal/interdecadal variations of the ocean temperature and its impacts on climate. Adv. ~~Atmos. Sci. 23, 964–981. https://doi.org/10.1007/s00376-006-0964-7~~Atmospheric Sci. 23, 964–981. https://doi.org/10.1007/s00376-006-0964-7

a mis en forme : Non souligné, Couleur de police : Automatique

Li, Y., Curchitser, E.N., Wang, J., Peng, S., 2020. Tidal Effects on the Surface Water Cooling Northeast of Hainan Island, South China Sea. J. Geophys. Res. Oceans 125, e2019JC016016. https://doi.org/10.1029/2019JC016016

Lyard, F.H., Allain, D.J., Cancet, M., Carrère, L., Picot, N., 2021. FES2014 global ocean tide atlas: design and performance. ~~Ocean Science 17, 615–649. https://doi.org/10.5194/os-17-615-2021~~Ocean Sci. 17, 615–649. https://doi.org/10.5194/os-17-615-2021

a mis en forme : Bibliographie, Retrait : Gauche : 0 cm, Première ligne : 0 cm

a mis en forme : Non souligné, Couleur de police : Automatique

Madec, G., Bourdallé-Badie, R., Chanut, J., Clementi, E., Coward, A., Ethé, C., Iovino, D., Lea, D., Lévy, C., Lovato, T., Martin, N., Masson, S., Mocavero, S., Rousset, C., Storkey, D., Vancoppenolle, M., Müeller, S., Nurser, G., Bell, M., & Samson, G., (2019). NEMO ocean engine. In Notes du Pôle de modélisation de l'Institut Pierre-Simon Laplace (IPSL) (v4.0, Number 27). Zenodo~~.~~ ~~https://doi.org/10.5281/zenodo.3878122.~~ https://doi.org/10.5281/zenodo.3878122

~~Madec, G. (2014), "NEMO ocean engine" (Draft edition r5171), *Note du Pôle de modélisation 27*, Inst. Pierre-Simon Laplace, France, ISSN No 1288-1619.~~

Magalhaes, J.M., da Silva, J.C.B., Buijsman, M.C., Garcia, C. a. E., 2016. Effect of the North Equatorial Counter Current on the generation and propagation of internal solitary waves off the Amazon shelf (SAR observations). ~~Ocean Science 12, 243–255. https://doi.org/10.5194/os-12-243-2016~~Ocean Sci. 12, 243–255. https://doi.org/10.5194/os-12-243-2016

Mei, W., Xie, S.-P., Primeau, F., McWilliams, J.C., Pasquero, C., 2015. Northwestern Pacific typhoon intensity controlled by changes in ocean temperatures. ~~Science Advances 1, e1500014. https://doi.org/10.1126/sciadv.1500014~~Sci. Adv. 1, e1500014. https://doi.org/10.1126/sciadv.1500014

Moisan, J.R., Niiler, P.P., 1998. The Seasonal Heat Budget of the North Pacific: Net Heat Flux and Heat Storage Rates (1950–1990). ~~Journal of Physical Oceanography 28, 401–421. https://doi.org/10.1175/1520-0485(1998)028<0401:TSHBOT>2.0.CO;2~~J. Phys. Oceanogr. 28, 401–421. https://doi.org/10.1175/1520-0485(1998)028<0401:TSHBOT>2.0.CO;2

~~Molinas, E., Carneiro, J.C., Vinzon, S., 2020. Internal tides as a major process in Amazon continental shelf fine sediment transport. Marine Geology 430, 106360. https://doi.org/10.1016/j.margeo.2020.106360~~

~~Muacho, S., da Silva, J.C.B., Brotas, V., Oliveira, P.B., 2013. Effect of internal waves on near-surface chlorophyll concentration and primary production in the Nazaré Canyon (west of the Iberian Peninsula). Deep Sea Research Part I: Oceanographic Research Papers 81, 89–96. https://doi.org/10.1016/j.dsr.2013.07.012~~

Muller-Karger, F.E., McClain, C.R., Richardson, P.L., 1988. The dispersal of the Amazon's water. Nature 333, 56–59~~. https://doi.org/10.1038/333056a0~~. https://doi.org/10.1038/333056a0

Munk, W., Wunsch, C., 1998. Abyssal recipes II: energetics of tidal and wind mixing. Deep Sea ~~Research~~Res. Part ~~I: Oceanographic Research Papers~~Oceanogr. Res. Pap. 45, 1977–2010~~. https://doi.org/10.1016/S0967-0637(98)00070-3~~. https://doi.org/10.1016/S0967-0637(98)00070-3

Nagai, T., Hibiya, T., 2015. Internal tides and associated vertical mixing in the Indonesian Archipelago. ~~Journal of Geophysical Research : Oceans 120, 3373–3390. https://doi.org/10.1002/2014JC010592~~J. Geophys. Res. Oceans 120, 3373–3390. https://doi.org/10.1002/2014JC010592

a mis en forme : Non souligné, Couleur de police : Automatique

a mis en forme : Bibliographie, Retrait : Gauche : 0 cm, Première ligne : 0 cm

a mis en forme : Non souligné, Couleur de police : Automatique

a mis en forme : Non souligné, Couleur de police : Automatique

a mis en forme : Français (France)

a mis en forme : Non souligné, Couleur de police : Automatique

a mis en forme : Bibliographie, Retrait : Gauche : 0 cm, Première ligne : 0 cm

a mis en forme : Non souligné, Couleur de police : Automatique

a mis en forme : Non souligné, Couleur de police : Automatique

a mis en forme : Non souligné, Couleur de police : Automatique

Nash, J.D., Alford, M.H., Kunze, E., Martini, K., Kelly, S., 2007. Hotspots of deep ocean mixing on the Oregon continental slope. Geophys. Res. Lett. 34. https://doi.org/10.1029/2006GL028170

Neto, A.V.N., da Silva, A.C., 2014. Seawater temperature changes associated with the North Brazil current dynamics. ~~Ocean Dynamics 64, 13–27. https://doi.org/10.1007/s10236-013-0667-4~~Ocean Dyn. 64, 13–27. https://doi.org/10.1007/s10236-013-0667-4

New, A.L., Pingree, R.D., 2000. An intercomparison of internal solitary waves in the Bay of Biscay and resulting from Korteweg-de Vries-Type theory. Prog. Oceanogr. 45, 1–38. https://doi.org/10.1016/S0079-6611(99)00049-X

New, A.L., Pingree, R.D., 1990. ~~Nittrouer, C.A., DeMaster, D.J., 1996. The Amazon shelf setting: tropical, energetic, and influenced by a large river. Continental Shelf Research 16, 553–573. https://doi.org/10.1016/0278-4343(95)00069-0~~

~~Niwa, Y., Hibiya, T., 2014. Generation of baroclinic tide energy in a global three-dimensional numerical model with different spatial grid resolutions. Ocean Modelling 80, 59–73. https://doi.org/10.1016/j.ocemod.2014.05.003~~

Large-amplitude internal soliton packets in the central Bay of Biscay. Deep Sea Res. Part Oceanogr. Res. Pap. 37, 513–524. https://doi.org/10.1016/0198-0149(90)90022-N

Niwa, Y., Hibiya, T., 2011. Estimation of baroclinic tide energy available for deep ocean mixing based on three-dimensional global numerical simulations. ~~J Oceanogr 67, 493–502. https://doi.org/10.1007/s10872-011-0052-1~~J. Oceanogr. 67, 493–502. https://doi.org/10.1007/s10872-011-0052-1

Nugroho, D., Koch-Larrouy, A., Gaspar, P., Lyard, F., Reffray, G., Tranchant, B., 2018. Modelling explicit tides in the Indonesian seas: An important process for surface sea water properties. ~~Marine Pollution Bulletin,~~Mar. Pollut. Bull., Special Issue: Indonesia seas management 131, 7–18~~. https://doi.org/10.1016/j.marpolbul.2017.06.033~~. https://doi.org/10.1016/j.marpolbul.2017.06.033

Peng, S., Liao, J., Wang, X., Liu, Z., Liu, Y., Zhu, Y., Li, B., Khokiattiwong, S., Yu, W., 2021. Energetics Based Estimation of the Diapycnal Mixing Induced by Internal Tides in the Andaman Sea. ~~Journal of Geophysical Research: Oceans 126. https://doi.org/10.1029/2020JC016521~~J. Geophys. Res. Oceans 126. https://doi.org/10.1029/2020JC016521

~~Pomar, L., Morsilli, M., Hallock, P., Bádenas, B., 2012. Internal waves, an under-explored source of turbulence events in the sedimentary record. Earth Science Reviews 111, 56–81. https://doi.org/10.1016/j.earscirev.2011.12.005~~

Prestes, Y.O., Silva, A.C. da, Jeandel, C., 2018. Amazon water lenses and the influence of the North Brazil Current on the continental shelf. Cont. Shelf Res. 160, 36–48. https://doi.org/10.1016/j.csr.2018.04.002

a mis en forme : Bibliographie, Retrait : Gauche : 0 cm, Première ligne : 0 cm

a mis en forme : Non souligné, Couleur de police : Automatique

a mis en forme : Anglais (États-Unis)

a mis en forme : Bibliographie, Retrait : Gauche : 0 cm, Première ligne : 0 cm

a mis en forme : Non souligné, Couleur de police : Automatique

a mis en forme : Non souligné, Couleur de police : Automatique

a mis en forme : Non souligné, Couleur de police : Automatique,

Purwandana, A., Cuypers, Y., Bourgault, D., Bouruet-Aubertot, P., Santoso, P.D., 2022. Fate of internal solitary wave and enhanced mixing in Manado Bay, North Sulawesi, Indonesia. Cont. Shelf Res. 245, 104801. https://doi.org/10.1016/j.csr.2022.104801

Richardson, P.L., Hufford, G.E., Limeburner, R., Brown, W.S., 1994. North Brazil Current retroflection eddies. ~~Journal of Geophysical Research: Oceans 99, 5081-5093. https://doi.org/10.1029/93JC03486~~J. Geophys. Res. Oceans 99, 5081–5093. https://doi.org/10.1029/93JC03486

a mis en forme : Bibliographie, Retrait : Gauche : 0 cm, Première ligne : 0 cm

a mis en forme : Non souligné, Couleur de police : Automatique

Rosenthal, Y., Boyle, E.A., Slowey, N., 1997. Temperature control on the incorporation of magnesium, strontium, fluorine, and cadmium into benthic foraminiferal shells from Little Bahama Bank: Prospects for thermocline paleoceanography. ~~Geochimica et Cosmochimica Acta 61, 3633-3643. https://doi.org/10.1016/S0016-7037(97)00181-6~~Geochim. Cosmochim. Acta 61, 3633–3643. https://doi.org/10.1016/S0016-7037(97)00181-6

a mis en forme : Non souligné, Couleur de police : Automatique

Ruault, V., Jouanno, J., Durand, F., Chanut, J., Benshila, R., 2020. Role of the Tide on the Structure of the Amazon Plume: A Numerical Modeling Approach. ~~Journal of Geophysical Research: Oceans 125, e2019JC015495. https://doi.org/10.1029/2019JC015495~~J. Geophys. Res. Oceans 125, e2019JC015495. https://doi.org/10.1029/2019JC015495

a mis en forme : Non souligné, Couleur de police : Automatique

Salamena, G.G., Whinney, J.C., Heron, S.F., Ridd, P.V., 2021. Internal tidal waves and deep-water renewal in a tropical fjord: Lessons from Ambon Bay, eastern Indonesia. ~~Estuarine, Coastal and Shelf Science 253, 107291. https://doi.org/10.1016/j.ecss.2021.107291~~Estuar. Coast. Shelf Sci. 253, 107291. https://doi.org/10.1016/j.ecss.2021.107291

a mis en forme : Non souligné, Couleur de police : Automatique

Sandstrom, H., Oakey, N.S., 1995. Dissipation in Internal Tides and Solitary Waves. J. Phys. Oceanogr. 25, 604–614. https://doi.org/10.1175/1520-0485(1995)025<0604:DIITAS>2.0.CO;2

Schott, F.A., Dengler, M., Brandt, P., Affler, K., Fischer, J., Bourlès, B., Gouriou, Y., Molinari, R.L., Rhein, M., 2003. The zonal currents and transports at 35°W in the tropical Atlantic. ~~Geophysical Research Letters 30. https://doi.org/10.1029/2002GL016849~~Geophys. Res. Lett. 30. https://doi.org/10.1029/2002GL016849

a mis en forme : Bibliographie, Retrait : Gauche : 0 cm, Première ligne : 0 cm

a mis en forme : Non souligné, Couleur de police : Automatique

Sharples, J., Moore, C.M., Hickman, A.E., Holligan, P.M., Tweddle, J.F., Palmer, M.R., Simpson, J.H., 2009. Internal tidal mixing as a control on continental margin ecosystems. Geophys. Res. Lett. 36. https://doi.org/10.1029/2009GL040683

Sharples, J., Tweddle, J.F., Green, J.A.M., Palmer, M.R., Kim, Y.-N., Hickman, A.E., Holligan, P.M., Moore, C.M., Rippeth, T.P., Simpson, J.H., Krivtsov, V., 2007. Spring-neap modulation of internal tide mixing and vertical nitrate fluxes at a shelf edge in summer. ~~Limnology and Oceanography 52, 1735-1747. https://doi.org/10.4319/lo.2007.52.5.1735~~Limnol. Oceanogr. 52, 1735–1747. https://doi.org/10.4319/lo.2007.52.5.1735

a mis en forme : Bibliographie, Retrait : Gauche : 0 cm, Première ligne : 0 cm

a mis en forme : Non souligné, Couleur de police : Automatique

~~Shriver, J., Arbic, B., Richman, J., Ray, R., Metzger, E., Wallcraft, A., Timko, P., 2012.~~

~~An evaluation of the barotropic and internal tides in a high-resolution global ocean~~

~~circulation model. Journal of Geophysical Research 117, C10024. https://doi.org/10.1029/2012JC008170~~

Silva, A., Araujo, M., Medeiros, C., Silva, M., Bourles, B., 2005. Seasonal changes in the mixed and barrier layers in the western Equatorial Atlantic. Braz. J. Oceanogr. 53, 83–98.

Smith, K.A., Rocheleau, G., Merrifield, M.A., Jaramillo, S., Pawlak, G., 2016. Temperature variability caused by internal tides in the coral reef ecosystem of Hanauma bay, Hawaiʻi. ~~Continental Shelf Research 116, 1–12. https://doi.org/10.1016/j.csr.2016.01.004~~Cont. Shelf Res. 116, 1–12. https://doi.org/10.1016/j.csr.2016.01.004

Speer, K.G., Isemer, H.-J., Biastoch, A., 1995. Water mass formation from revised COADS data. ~~Journal of Physical Oceanography~~J. Phys. Oceanogr. 25, 2444–2457.

Sprintall, J., Gordon, A.L., Koch-Larrouy, A., Lee, T., Potemra, J.T., Pujiana, K., Wijffels, S.E., 2014. The Indonesian seas and their role in the coupled ocean–climate system. Nat. Geosci. 7, 487–492. https://doi.org/10.1038/ngeo2188

Sprintall, J., Gordon, A.L., Wijffels, S.E., Feng, M., Hu, S., Koch-Larrouy, A., Phillips, H., Nugroho, D., Napitu, A., Pujiana, K., Susanto, R.D., Sloyan, B., Peña-Molino, B., Yuan, D., Riama, N.F., Siswanto, S., Kuswardani, A., Arifin, Z., Wahyudi, A.J., Zhou, H., Nagai, T., Ansong, J.K., Bourdalle-Badié, R., Chanut, J., Lyard, F., Arbic, B.K., Ramdhani, A., Setiawan, A., 2019. Detecting Change in the Indonesian Seas. Front. Mar. Sci. 6.

Swift, J.H., Aagaard, K., 1981. Seasonal transitions and water mass formation in the Iceland and Greenland seas. ~~Deep Sea Research Part A. Oceanographic Research Papers 28, 1107–1129. https://doi.org/10.1016/0198-0149(81)90050-9~~Deep Sea Res. Part Oceanogr. Res. Pap. 28, 1107–1129. https://doi.org/10.1016/0198-0149(81)90050-9

~~Tchilibou, M., Koch-Larrouy, A., Barbot, S., Lyard, F., Morel, Y., Jouanno, J., Morrow, R., 2022. Internal tides off the Amazon shelf during two contrasted seasons: interactions with background circulation and SSH imprints. Ocean Science 18, 1591–1618. https://doi.org/10.5194/os-18-1591-2022~~

Tchilibou, M., Gourdeau, L., Lyard, F., Morrow, R., Koch Larrouy, A., Allain, D., Djath, B., 2020. Internal tides in the Solomon Sea in contrasted ENSO conditions. ~~Ocean Science 16, 615–635. https://doi.org/10.5194/os-16-615-2020~~Ocean Sci. 16, 615–635. https://doi.org/10.5194/os-16-615-2020

Tchilibou, M., Gourdeau, L., Morrow, R., Serazin, G., Djath, B., Lyard, F., 2018. Spectral signatures of the tropical Pacific dynamics from model and altimetry: a focus on the meso-/submesoscale range. ~~Ocean Science 14, 1283–1301. https://doi.org/10.5194/os-14-1283-2018~~Ocean Sci. 14, 1283–1301. https://doi.org/10.5194/os-14-1283-2018

~~Tuerena, R.E., Williams, R.G., Mahaffey, C., Vic, C., Green, J.A.M., Naveira-Garabato, A., Forryan, A., Sharples, J., 2019. Internal Tides Drive Nutrient Fluxes into the Deep~~

a mis en forme : Bibliographie, Retrait : Gauche : 0 cm, Première ligne : 0 cm

a mis en forme : Non souligné, Couleur de police : Automatique

a mis en forme : Bibliographie, Retrait : Gauche : 0 cm, Première ligne : 0 cm

a mis en forme : Non souligné, Couleur de police : Automatique

a mis en forme : Bibliographie, Retrait : Gauche : 0 cm, Première ligne : 0 cm

a mis en forme : Non souligné, Couleur de police : Automatique

a mis en forme : Non souligné, Couleur de police : Automatique

~~Chlorophyll Maximum Over Mid-ocean Ridges. Global Biogeochemical Cycles 33, 995–1009. https://doi.org/10.1029/2019GB006214~~

Tchilibou, M., Koch-Larrouy, A., Barbot, S., Lyard, F., Morel, Y., Jouanno, J., Morrow, R., 2022. Internal tides off the Amazon shelf during two contrasted seasons: interactions with background circulation and SSH imprints. Ocean Sci. 18, 1591–1618. https://doi.org/10.5194/os-18-1591-2022

Varona, H.L., Veleda, D., Silva, M., Cintra, M., Araujo, M., 2019. Amazon River plume influence on Western Tropical Atlantic dynamic variability. Dyn. Atmospheres Oceans 85, 1–15. https://doi.org/10.1016/j.dynatmoce.2018.10.002

Vic, C., Naveira Garabato, A.C., Green, J.A.M., Waterhouse, A.F., Zhao, Z., Melet, A., de Lavergne, C., Buijsman, M.C., Stephenson, G.R., 2019. Deep-ocean mixing driven by small-scale internal tides. Nat. Commun. 10, 2099. https://doi.org/10.1038/s41467-019-10149-5

Vlasenko, V., Stashchuk, N., 2006. Amplification and Suppression of Internal Waves by Tides over Variable Bottom Topography. J. Phys. Oceanogr. 36, 1959–1973. https://doi.org/10.1175/JPO2958.1

Wallace, M.I., Meredith, M.P., Brandon, M.A., Sherwin, T.J., Dale, A., Clarke, A., 2008. On the characteristics of internal tides and coastal upwelling behaviour in Marguerite Bay, west Antarctic Peninsula. ~~Deep Sea Research Part II: Topical Studies in Oceanography 55, 2023–2040. https://doi.org/10.1016/j.dsr2.2008.04.033~~Deep Sea Res. Part II Top. Stud. Oceanogr. 55, 2023–2040. https://doi.org/10.1016/j.dsr2.2008.04.033.

a mis en forme : Bibliographie, Retrait : Gauche : 0 cm, Première ligne : 0 cm

a mis en forme : Non souligné, Couleur de police : Automatique

Wang, X., Peng, S., Liu, Z., Huang, R.X., Qian, Y.-K., Li, Y., 2016. Tidal Mixing in the South China Sea: An Estimate Based on the Internal Tide Energetics. ~~Journal of Physical Oceanography 46, 107–124. https://doi.org/10.1175/JPO-D-15-0082.1~~J. Phys. Oceanogr. 46, 107–124. https://doi.org/10.1175/JPO-D-15-0082.1.

a mis en forme : Non souligné, Couleur de police : Automatique

Wentz, F.J., C. Gentemann, K.A. Hilburn, 2015: Remote Sensing Systems TRMM TMI [~~indicate whether you used~~ Daily~~, 3-Day, Weekly, or Monthly~~] Environmental Suite on 0.25 deg grid, Version 7.1~~, [indicate subset if used]~~. Remote Sensing Systems, Santa Rosa, CA. Available online at ~~ www.remss.com/missions/tmi.~~ www.remss.com/missions/tmi.

a mis en forme : Non souligné

Whalen, C.B., de Lavergne, C., Naveira Garabato, A.C., Klymak, J.M., MacKinnon, J.A., Sheen, K.L., 2020. Internal wave-driven mixing: governing processes and consequences for climate. Nat. Rev. Earth Environ. 1, 606–621. https://doi.org/10.1038/s43017-020-0097-z

Xie, S.-P., Carton, J.A., 2004. Tropical Atlantic variability: Patterns, mechanisms, and impacts. ~~Washington DC American Geophysical Union Geophysical Monograph Series 147, 121–142. https://doi.org/10.1029/147GM07~~Wash. DC Am. Geophys. Union Geophys. Monogr. Ser. 147, 121–142. https://doi.org/10.1029/147GM07.

a mis en forme : Anglais (États-Unis)

a mis en forme : Bibliographie, Retrait : Gauche : 0 cm, Première ligne : 0 cm

a mis en forme : Non souligné, Couleur de police : Automatique

Xu, P., Yang, W., Zhu, B., Wei, H., Zhao, L., Nie, H., 2020. Turbulent mixing and vertical nitrate flux induced by the semidiurnal internal tides in the southern Yellow Sea.

~~Continental Shelf Research 208, 104240. https://doi.org/10.1016/j.csr.2020.104240~~Cont. Shelf Res. 208, 104240. https://doi.org/10.1016/j.csr.2020.104240.

Yadidya, B., Rao, A.D., 2022. Projected climate variability of internal waves in the Andaman Sea. ~~Commun Earth Environ 3, 1–12. https://doi.org/10.1038/s43247-022-00574-8~~Commun. Earth Environ. 3, 1–12. https://doi.org/10.1038/s43247-022-00574-8.

Zalesak, S.T., 1979. Fully multidimensional flux-corrected transport algorithms for fluids. J. Comput. Phys. 31, 335–362. https://doi.org/10.1016/0021-9991(79)90051-2

Zaron, E.D., 2017. Mapping the nonstationary internal tide with satellite altimetry. J. Geophys. Res. Oceans 122, 539–554. https://doi.org/10.1002/2016JC012487

Zaron, E.D., 2019. Baroclinic Tidal Sea Level from Exact-Repeat Mission Altimetry. ~~Journal of Physical Oceanography~~J. Phys. Oceanogr. 49, 193–210~~.~~ ~~https://doi.org/10.1175/JPO-D-18-0127.1.~~ https://doi.org/10.1175/JPO-D-18-0127.1.

a mis en forme : Non souligné, Couleur de police : Automatique

a mis en forme : Non souligné

a mis en forme : Bibliographie, Retrait : Gauche : 0 cm, Première ligne : 0 cm

a mis en forme : Non souligné, Couleur de police : Automatique,

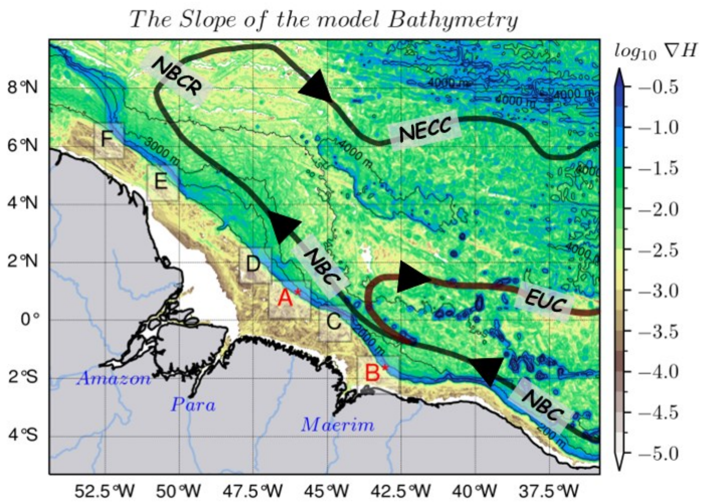

~~Zaron, E.D., 2017. Mapping the nonstationary internal tide with satellite altimetry. Journal of Geophysical Research: Oceans 122, 539–554. https://doi.org/10.1002/2016JC012487~~

~~Zhao, Z., Alford, M.H., Girton, J.B., Rainville, L., Simmons, H.L., 2016. Global Observations of Open-Ocean Mode-1 M2 Internal Tides. Journal of Physical Oceanography 46, 1657–1684. https://doi.org/10.1175/JPO-D-15-0105.1~~

~~Zhao, Z., Alford, M.H., Girton, J.B., 2012. Mapping Low-Mode Internal Tides from Multisatellite Altimetry. Oceanography 25, 42–51.ls~~

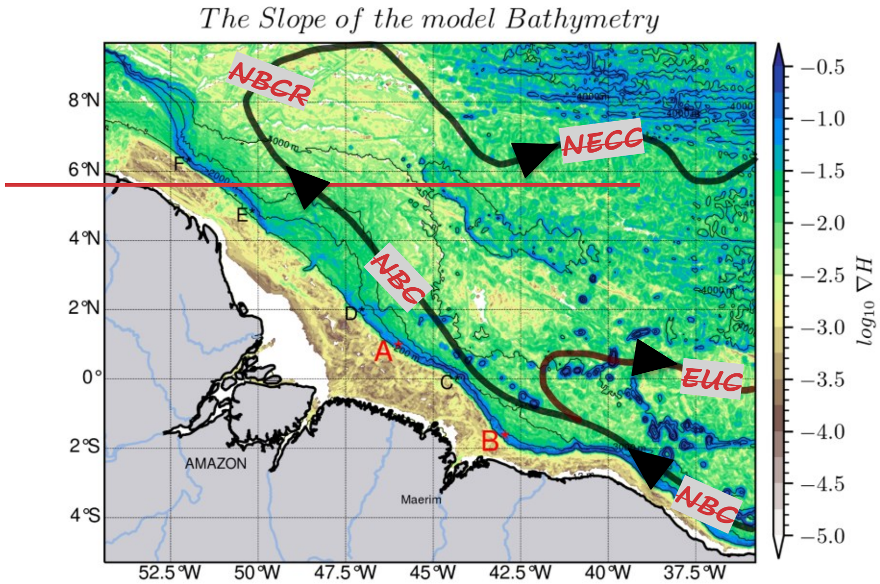

Figure 1: The horizontal gradient (~~∇H~~∇H) of the model's bathymetry with different internal tides generation sites (A, B*, C~~*,~~, D~~*,~~, E~~*~~ and F~~*)~~) along the high slope (blue color shading) of the shelf break, with the two main sites ~~(in red) being~~ A* and B~~*,~~* (in red), as ~~mentioned~~reported in Magalhaes et al. (2016) and Tchilibou et al. (2022). Solid bold lines represent a schematic view of the circulation (as described by Didden and Schott, 1993; Richardson et al., 1994; ~~Bourlès et al., 1999a;~~ Johns et al., 1998; Bourles et al., 1999a; Schott et al., 2003; Garzoli et al., 2004) with NBC, NBCR and NECC ~~pathways~~tracks in black, and the EUC ~~pathway~~track in brown red. Tin black contours are 200 m, 2000 m, 3000 m and 4000 m isobaths.*

a mis en forme : Retrait : Gauche : 0 cm

a mis en forme : Police :Italique

1778

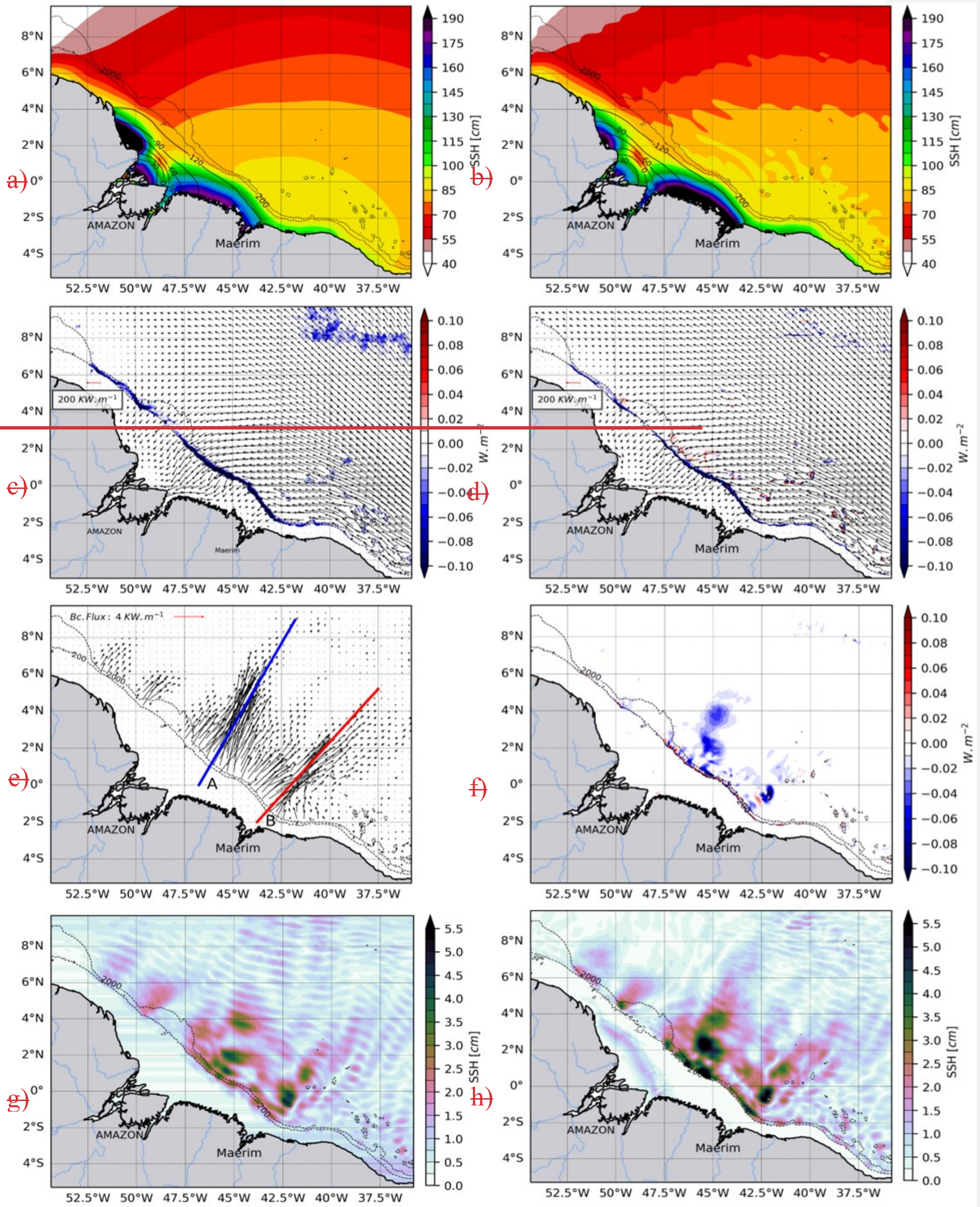
~~a)~~
~~b)~~
~~c)~~
~~d)~~
~~e)~~
~~f)~~
~~g)~~
~~h)~~
SSH [cm]
W.m^{-2}
200 KW.m^{-1}
Bc.Flux : 4 KW.m^{-1}
A
B
AMAZON
Maerim
2000
200
120
90
8°N
6°N
4°N
2°N
0°
2°S
4°S
52.5°W
50°W
47.5°W
45°W
42.5°W
40°W
37.5°W
190
175
160
145
130
115
100
85
70
55
40
0.10
0.08
0.06
0.04
0.02
0.00
−0.02
−0.04
−0.06
−0.08
−0.10
5.5
5.0
4.5
4.0
3.5
3.0
2.5
2.0
1.5
1.0
0.5
0.0

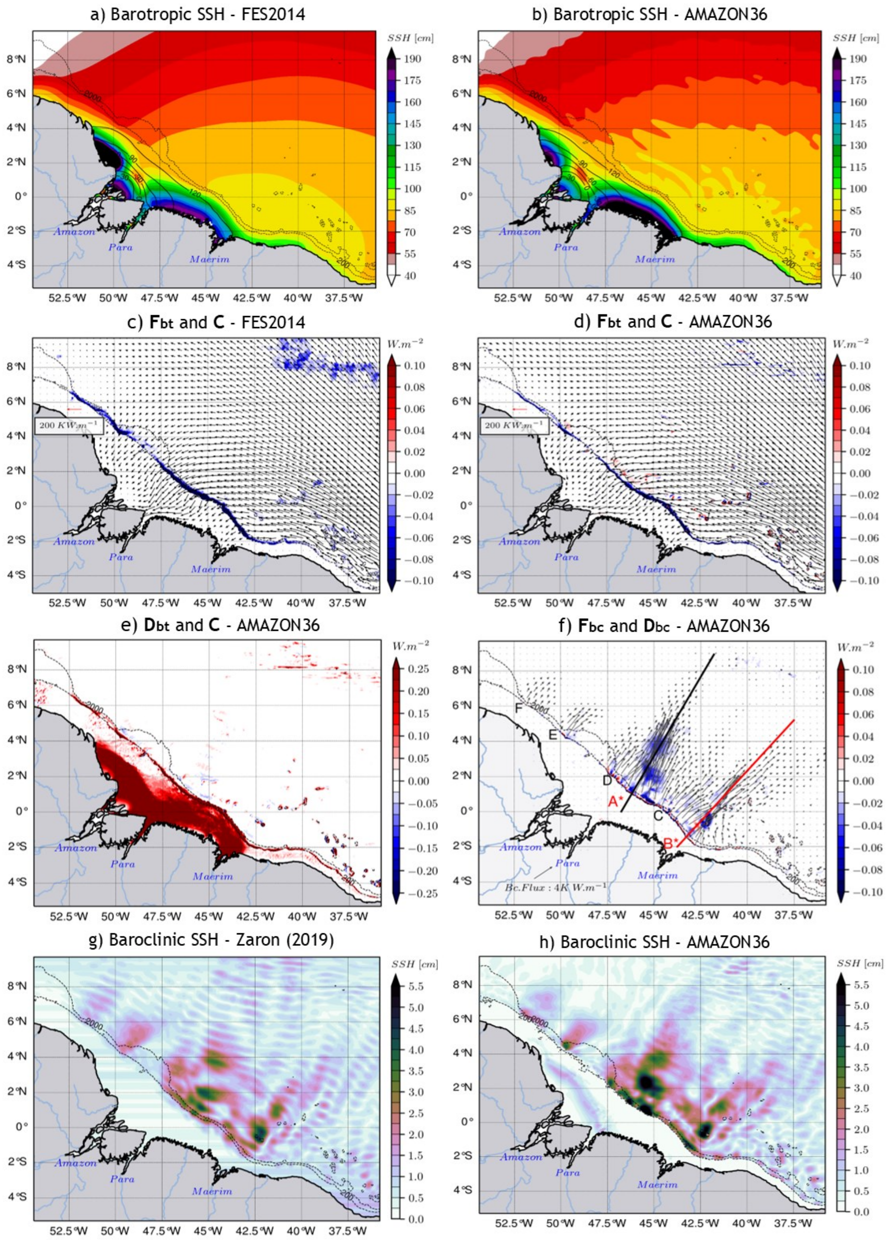

bt : barotropic ; **bc** : baroclinic

F : energy flux ; **C** : barotropic-to-baroclinic energy conversion ; **D** : energy dissipation

Figure 2: ~~M2 tides (coherent~~Coherent (or stationary) characteristics~~.~~ of the M2 tides. Barotropic sea surface height ~~for~~ (color shading) and its phase (solid tin contours) for (a) FES2014 ~~(a)~~ and (b) the model ~~(b), depth-integrated~~ , barotropic energy flux (black arrows) with the energy conversion rate (~~CVR) (~~color shading) for (c) FES2014 ~~(c)~~ and (d) the model ~~(d) with~~, (e) the model depth-integrated barotropic energy ~~flux black arrows,~~dissipation, (f) the model depth-integrated baroclinic energy flux (black ~~(e)~~ arrows ~~with transect lines along A (blue) and B (red) IT's pathways, model~~) and the depth-integrated baroclinic energy dissipation (~~f), and~~ color shading) with transect lines along ITs trajectories A* (black) and B* (red), the baroclinic sea surface height from ~~observation (~~(g) Zaron~~,~~ (2019) ~~(g)~~ and (h) the model ~~(h).~~ . Data from the model are the mean value over the year 2015. For all panels, dashed black lines represent the 200 m and 2000 m isobaths of the model bathymetry.

a mis en forme : Couleur de police : Texte 1

a mis en forme : Couleur de police : Texte 1

a mis en forme : Couleur de police : Texte 1

a mis en forme : Couleur de police : Texte 1

a mis en forme : Couleur de police : Texte 1

a mis en forme : Couleur de police : Texte 1

a mis en forme : Couleur de police : Texte 1

a mis en forme : Couleur de police : Texte 1

a mis en forme : Couleur de police : Texte 1

a mis en forme : Couleur de police : Texte 1

a mis en forme : Couleur de police : Texte 1

a mis en forme : Couleur de police : Texte 1

a mis en forme : Couleur de police : Texte 1

a mis en forme : Couleur de police : Texte 1

a mis en forme : Couleur de police : Texte 1

a mis en forme : Couleur de police : Texte 1

a mis en forme : Couleur de police : Texte 1

a mis en forme : Couleur de police : Texte 1

a mis en forme : Couleur de police : Texte 1

a mis en forme : Couleur de police : Texte 1

a mis en forme : Police :Italique, Couleur de police : Texte 1

a mis en forme : Couleur de police : Texte 1

1805

1806

1807

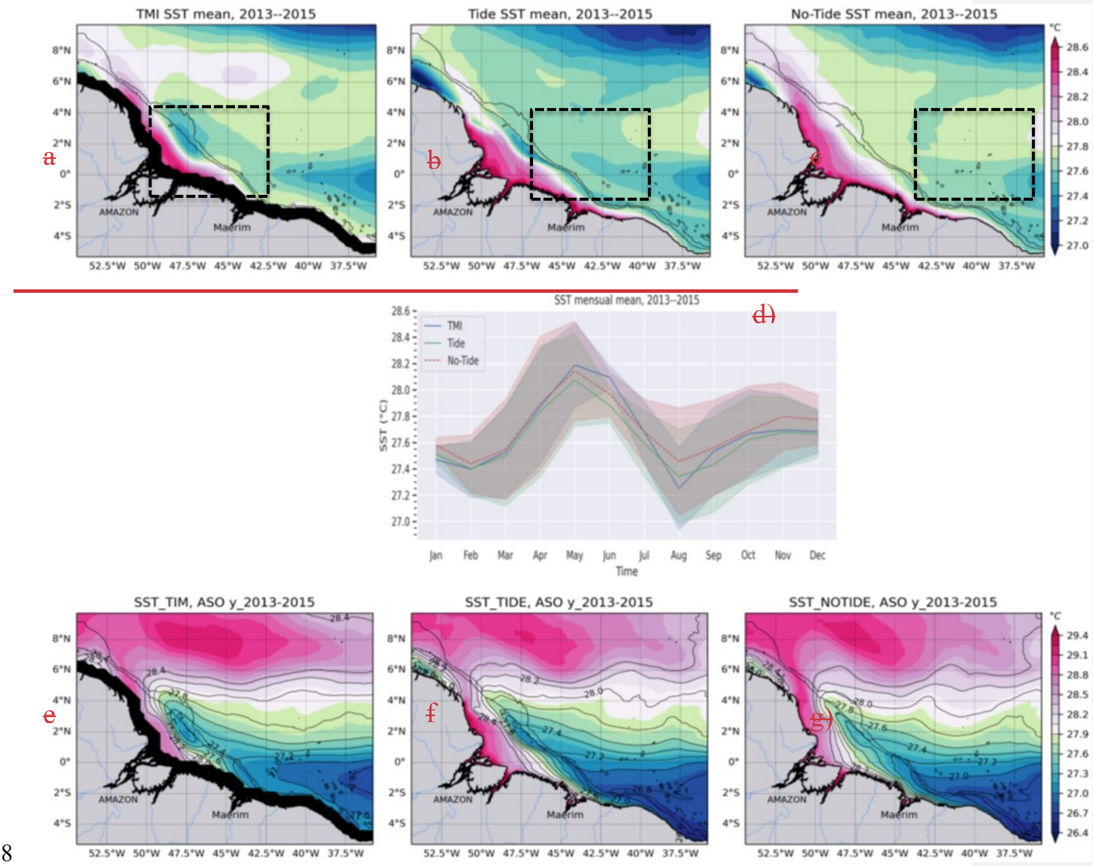
TMI SST mean, 2013--2015
Tide SST mean, 2013--2015
No-Tide SST mean, 2013--2015
~~a~~
~~b~~
~~c~~
AMAZON
Maerim
8°N
6°N
4°N
2°N
0°
2°S
4°S
52.5°W
50°W
47.5°W
45°W
42.5°W
40°W
37.5°W
°C
28.6
28.4
28.2
28.0
27.8
27.6
27.4
27.2
27.0
SST mensual mean, 2013--2015
~~d)~~
TMI
Tide
No-Tide
SST (°C)
Jan
Feb
Mar
Apr
May
Jun
Jul
Aug
Sep
Oct
Nov
Dec
Time
SST_TIM, ASO y_2013-2015
SST_TIDE, ASO y_2013-2015
SST_NOTIDE, ASO y_2013-2015
e
f
g)
29.4
29.1
28.8
28.5
28.2
27.9
27.6
27.3
27.0
26.7
26.4

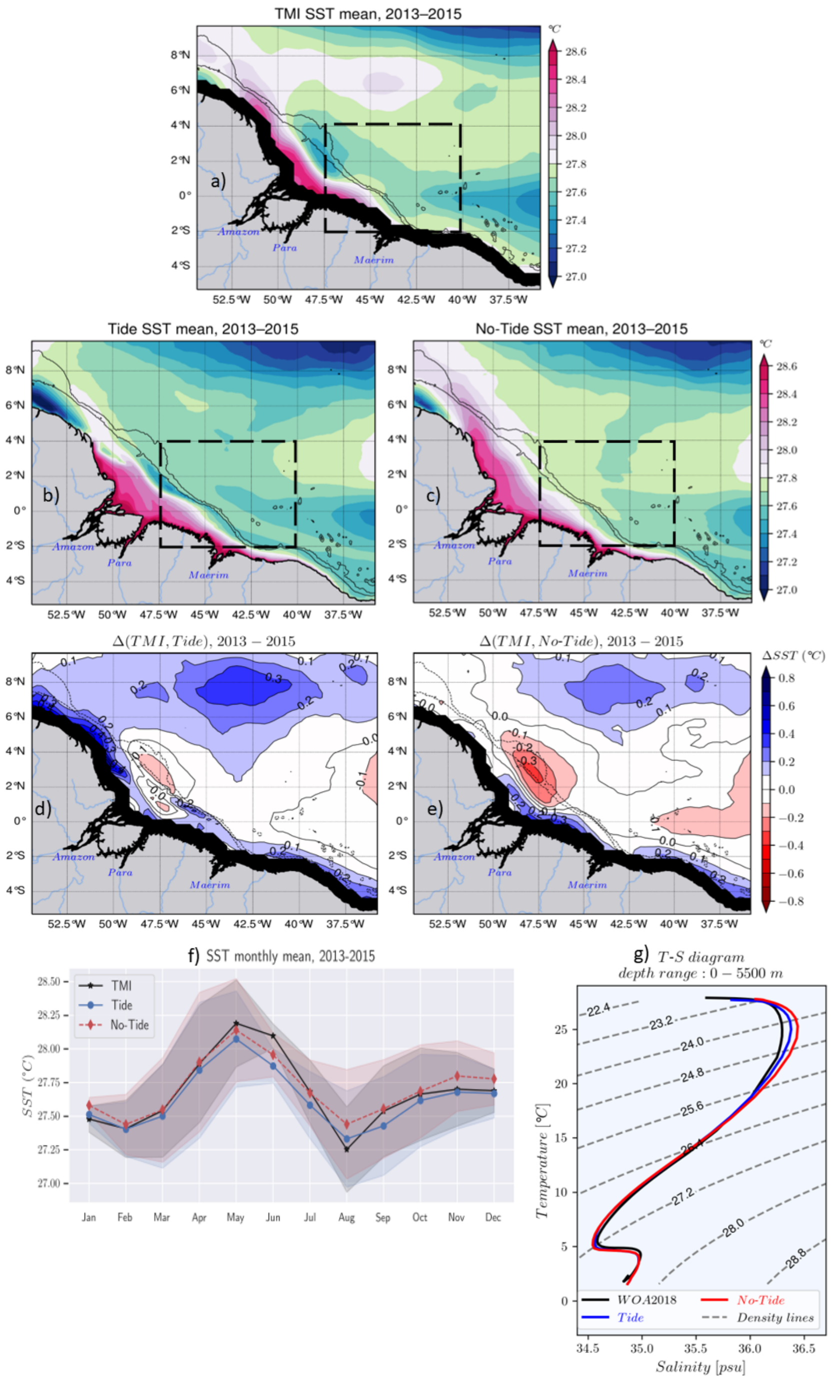
TMI SST mean, 2013–2015
a)
Tide SST mean, 2013–2015
b)
No-Tide SST mean, 2013–2015
c)
Δ(TMI, Tide), 2013 – 2015
d)
Δ(TMI, No-Tide), 2013 – 2015
e)
ΔSST (℃)
℃
Amazon
Para
Maerim
8°N
6°N
4°N
2°N
0°
2°S
4°S
52.5°W
50°W
47.5°W
45°W
42.5°W
40°W
37.5°W
28.6
28.4
28.2
28.0
27.8
27.6
27.4
27.2
27.0
0.8
0.6
0.4
0.2
0.0
−0.2
−0.4
−0.6
−0.8
f) SST monthly mean, 2013-2015
TMI
Tide
No-Tide
SST (°C)
Jan
Feb
Mar
Apr
May
Jun
Jul
Aug
Sep
Oct
Nov
Dec
g) T-S diagram
depth range : 0 – 5500 m
WOA2018
Tide
No-Tide
Density lines
Temperature [℃]
Salinity [psu]
22.4
23.2
24.0
24.8
25.6
26.4
27.2
28.0
28.8

Figure 3: ~~Mean SST~~Validation of the model temperature for the whole period 2013~~ to ~~-2015 ~~from~~. Mean SST for (a) TMI ~~SST (a)~~ with ~~a~~its black coastal mask, (b) the ~~model's~~ tidal simulation~~ (b),~~, (c) the ~~model's~~ non-tidal simulation~~ (c),~~, the difference (bias) in SST between TMI and (d) the tidal simulation and (e) the non-tidal simulation, (f) the seasonal cycle of the SST of the three products averaged ~~inside~~within the ~~dotted~~dashed line box in upper panels (covering ~~IT~~ITs pathways emanating from the main generation sites A and B) with ~~shelf~~values masked ~~over~~below the 200 m isobath, ~~the~~ bands ~~give the~~indiciate variability according to standard deviation~~ (d).~~, (g) Temperature-Salinity (T-S) diagram of the mean properties in the same area as (e) from observed WOA2018 climatology (black line), the tidal simulation (blue line) and non-tidal simulation (red line) for the water column from surface to 5500 m depth, dashed gray lines represent density (σ_θ) contours. For panels a-e and hereinafter (unless otherwise stated), the solid black lines represent the 200 m and 2000 m isobaths from the model bathymetry.

a mis en forme : Couleur de police : Texte 1

a mis en forme : Couleur de police : Texte 1

a mis en forme : Couleur de police : Texte 1

a mis en forme : Couleur de police : Texte 1

a mis en forme : Couleur de police : Texte 1

a mis en forme : Couleur de police : Texte 1

a mis en forme : Couleur de police : Texte 1

a mis en forme : Couleur de police : Texte 1

a mis en forme : Couleur de police : Texte 1

a mis en forme : Couleur de police : Texte 1

a mis en forme : Couleur de police : Texte 1

a mis en forme : Couleur de police : Texte 1

a mis en forme : Couleur de police : Texte 1

a mis en forme : Couleur de police : Texte 1

a mis en forme : Couleur de police : Texte 1

a mis en forme : Couleur de police : Texte 1

a mis en forme : Couleur de police : Texte 1

a mis en forme : Couleur de police : Texte 1

a mis en forme : Couleur de police : Texte 1

a mis en forme : Couleur de police : Texte 1

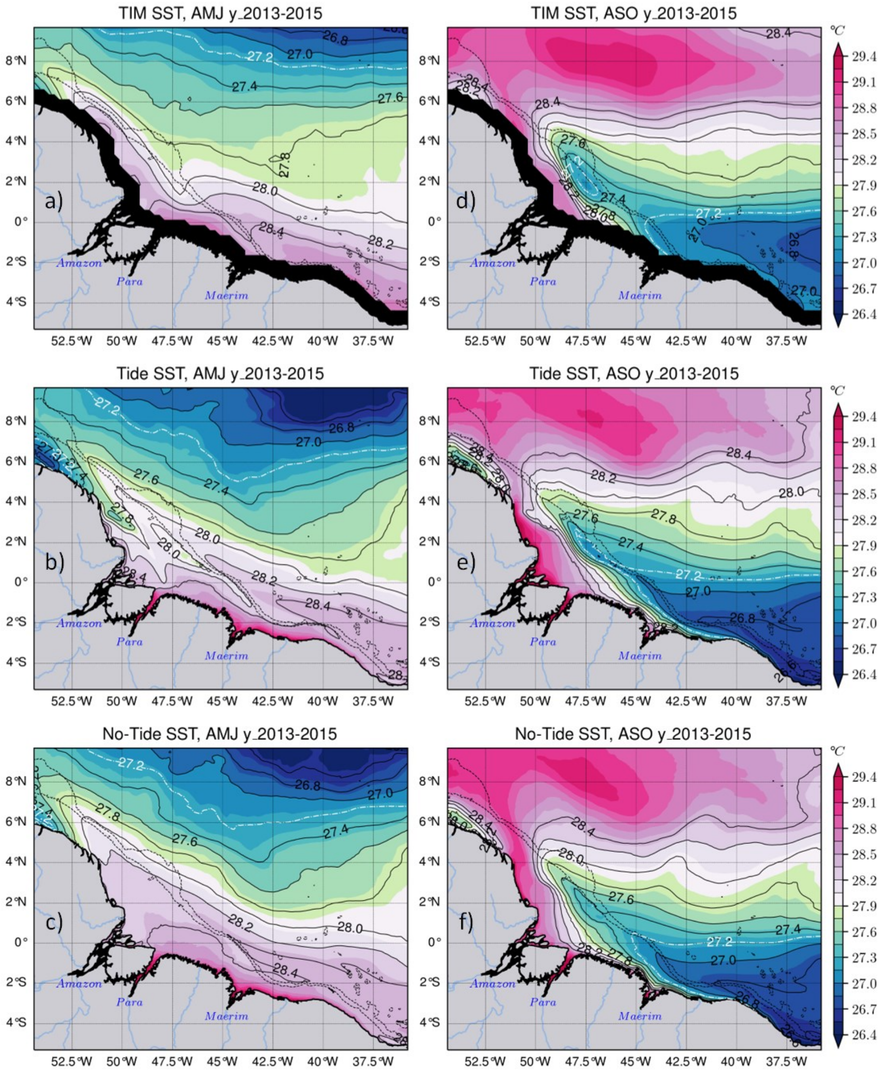

Figure 4: 2013-2015 seasonal SST mean. The ~~lower~~left panels ~~present the SST averaged~~stand for the ~~ASO (August-September-October)~~AMJ season ~~over the years 2013 - 2015~~ for TMI ~~SST (e)~~ with ~~a white~~its black coastal mask, the ~~model's~~ tidal simulation ~~(f)~~ and the ~~model's~~ non-tidal simulation~~ (g), with the~~, respectively for the upper-left, center-left and lower-left panel; the same in the panels on the right but for the ASO season. The dashed white ~~thin~~and black

a mis en forme : Couleur de police : Texte 1

a mis en forme : Couleur de police : Texte 1

a mis en forme : Couleur de police : Texte 1

a mis en forme : Couleur de police : Texte 1

a mis en forme : Couleur de police : Texte 1

a mis en forme : Couleur de police : Texte 1

a mis en forme : Couleur de police : Texte 1

a mis en forme : Couleur de police : Texte 1

a mis en forme : Couleur de police : Texte 1

a mis en forme : Couleur de police : Texte 1

a mis en forme : Couleur de police : Texte 1

solid lines ~~representing~~represent the temperature contours. ~~The~~Dashed black ~~tin~~ lines stand for the 200 m and 2000 m isobaths~~.~~

a mis en forme : Couleur de police : Texte 1

a mis en forme : Couleur de police : Texte 1

a mis en forme : Couleur de police : Texte 1

a mis en forme : Couleur de police : Texte 1

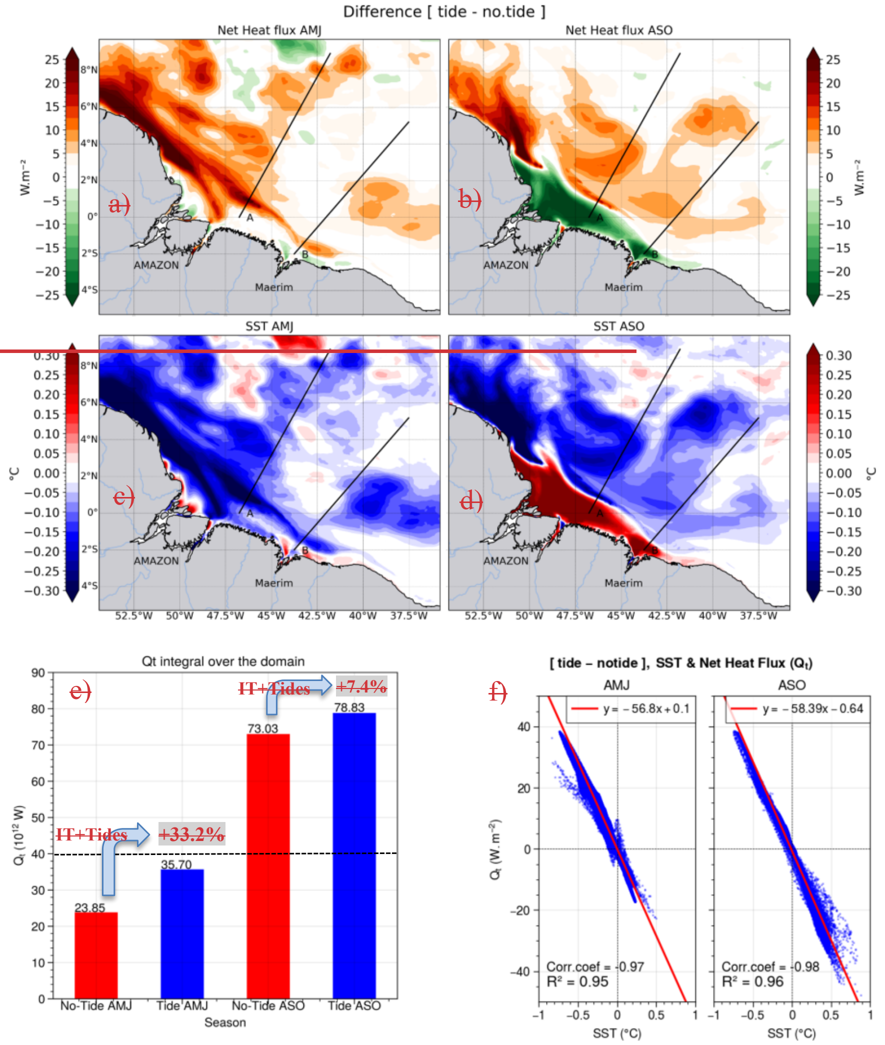

from the model bathymetry.

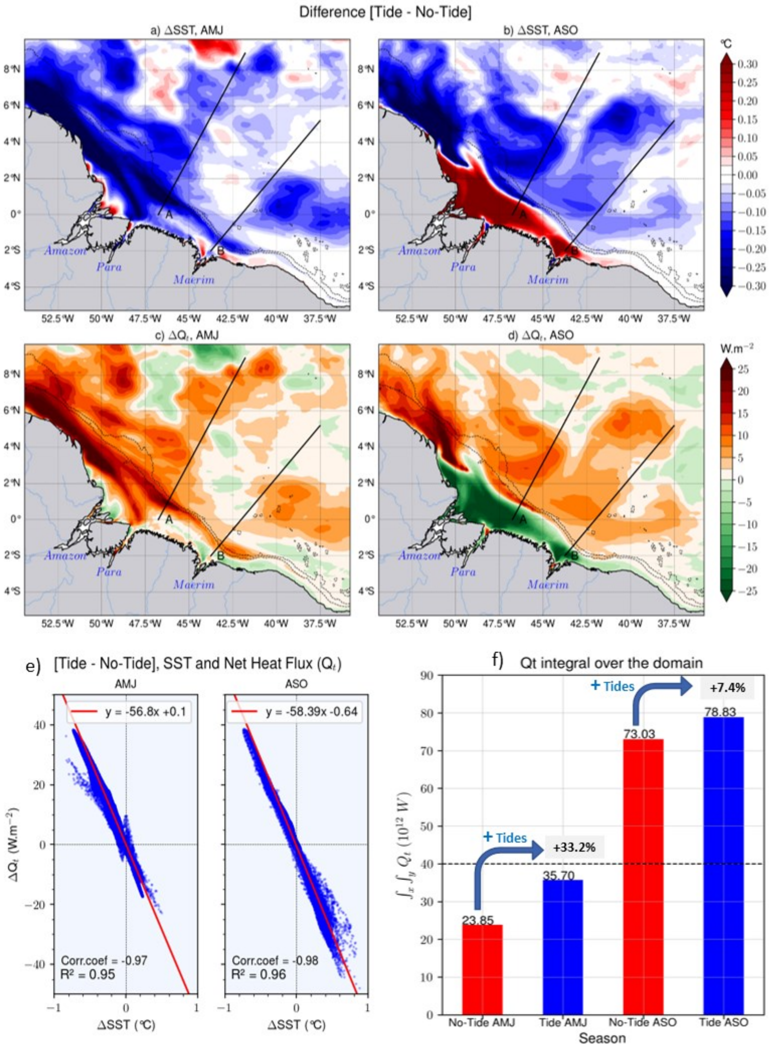

Figure ~~4~~5: Relationship between the SST and the atmosphere-to-ocean net heat flux (Qt~~) and the~~): SST~~: the Qt difference between tide and no-tide simulations~~ anomaly [Tide - No-Tide] in AMJ (a) and ASO (b) ~~season, and SST difference~~seasons, Qt anomaly in AMJ (c) and ASO (d~~),~~) seasons, (e) correlation between Qt anomaly and SST anomaly for each season, (f) domain integrated Qt ~~(e)~~ for both seasons ~~for~~of each simulation. ~~Correlation between Qt difference and SST difference for each season (f).~~ Hereinafter, -anomaly- refers to what is described hereabove.

1843
1844
1845

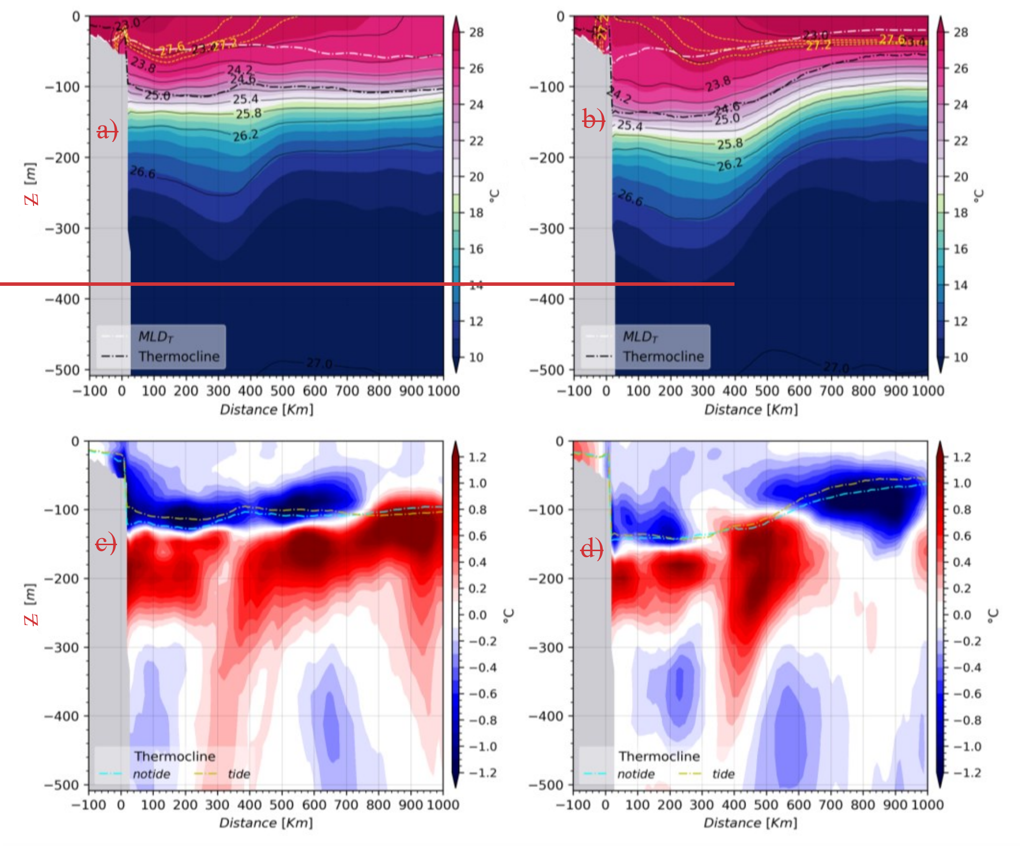
~~a)~~
~~b)~~
~~c)~~
~~d)~~
Z [m]
Distance [Km]
°C
MLD_T
Thermocline
notide
tide
23.0
23.8
24.2
24.6
25.0
25.4
25.8
26.2
26.6
27.0
27.2
27.6
0
−100
−200
−300
−400
−500
−100 0 100 200 300 400 500 600 700 800 900 1000
28 26 24 22 20 18 16 14 12 10
1.2 1.0 0.8 0.6 0.4 0.2 0.0 −0.2 −0.4 −0.6 −0.8 −1.0 −1.2

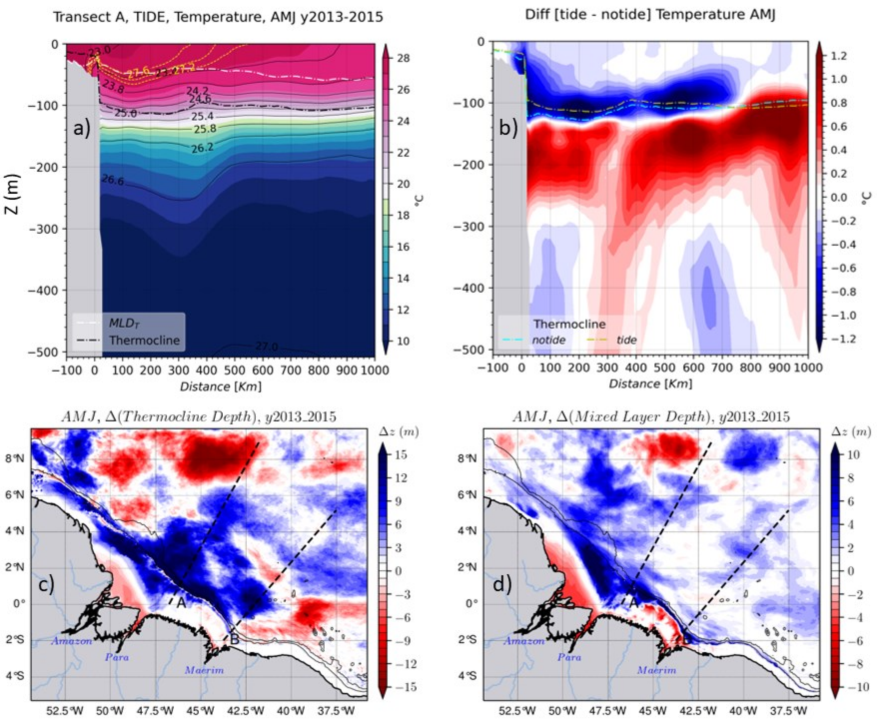

Figure ~~5: Vertical sections of tidal simulation's temperature following IT's pathway A~~6: Some water mass properties for the AMJ season: (a) ~~and ASO (b) seasons. Difference of~~ vertical section of the temperature ~~between tidal and non-tidal simulations for AMJ (c) and ASO (d) seasons. The~~of the tidal simulation following the transect A, the yellow ~~dotted~~dashed and the solid black ~~tin~~ lines ~~in the upper panels~~ are~~, respectively, for~~ the temperature and density ~~anomaly isocontours~~(σ_θ) isolines respectively, the black and white ticker ~~dot~~ dashed lines are ~~respectively~~the thermocline and ~~mixed layer depths. The~~MLD respectively, (b) the temperature anomaly for the same vertical section, yellow and cyan ~~ticker dot~~ dashed lines ~~in the lower panel~~ are the thermocline depth ~~respectively for tidal and non-tidal simulations~~for the tidal and non-tidal simulations respectively, (c) thermocline depth anomaly and (d) MLD anomaly for the whole domain. When the MLD or the Thermocline depth anomaly are colored in blue (vs red) it means that the tides rise (vs deepen) them.

a mis en forme : Police :13 pt, Non Italique

1861

1862

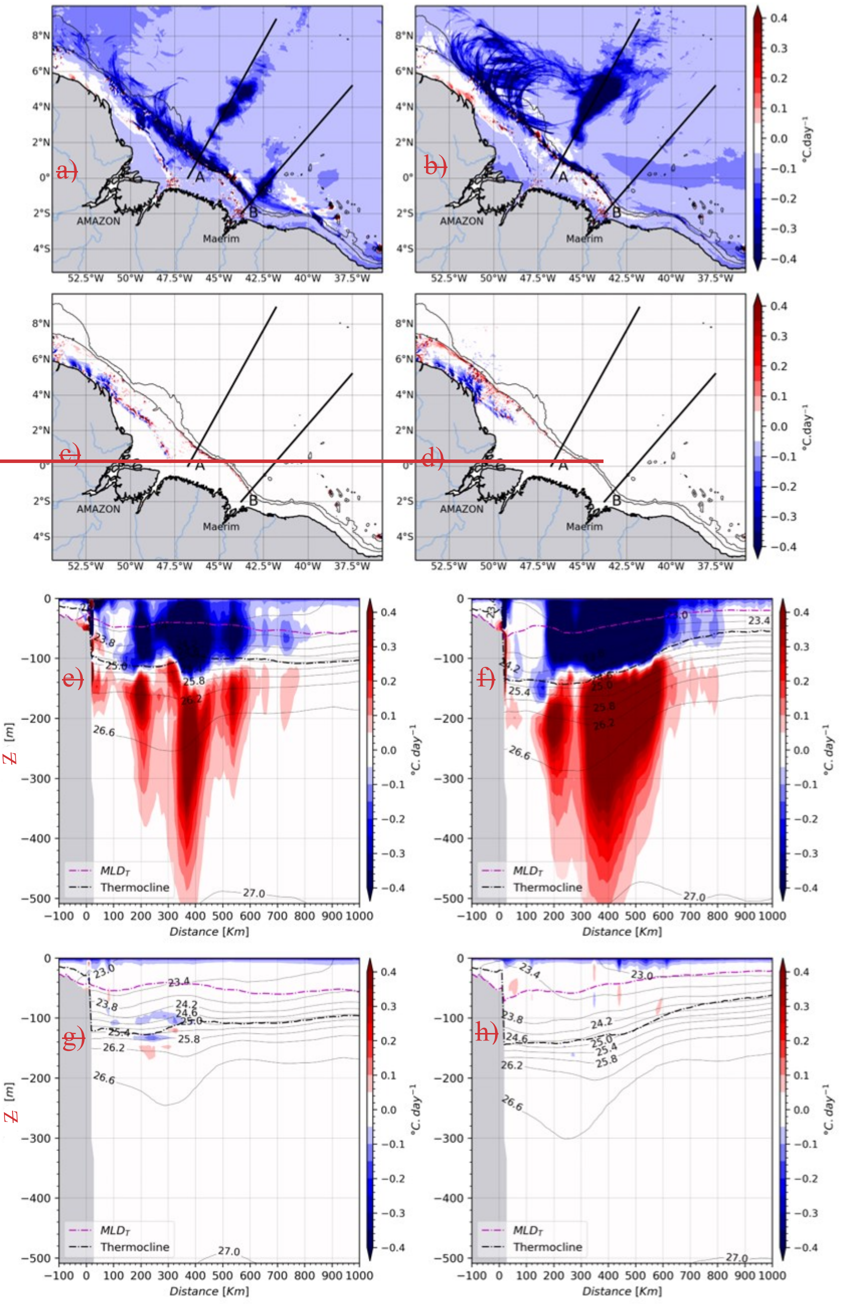
~~a)~~
~~b)~~
~~c)~~
~~d)~~
~~e)~~
~~f)~~
~~g)~~
~~h)~~
8°N
6°N
4°N
2°N
0°
2°S
4°S
52.5°W
50°W
47.5°W
45°W
42.5°W
40°W
37.5°W
A
B
AMAZON
Maerim
°C.day⁻¹
0.4
0.3
0.2
0.1
0.0
−0.1
−0.2
−0.3
−0.4
~~z~~ [m]
Distance [Km]
−100
0
100
200
300
400
500
600
700
800
900
1000
−500
°C. day⁻¹
MLD_T
Thermocline
23.0
23.4
23.8
24.2
24.6
25.0
25.4
25.8
26.2
26.6
27.0

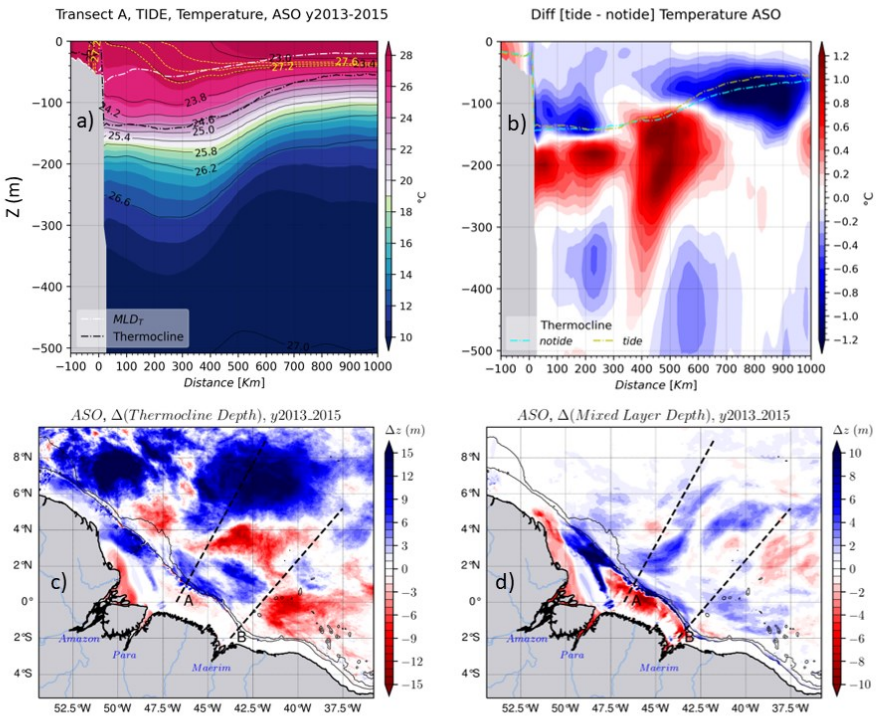

Figure 7 : same as figure 6 but for the ASO season.

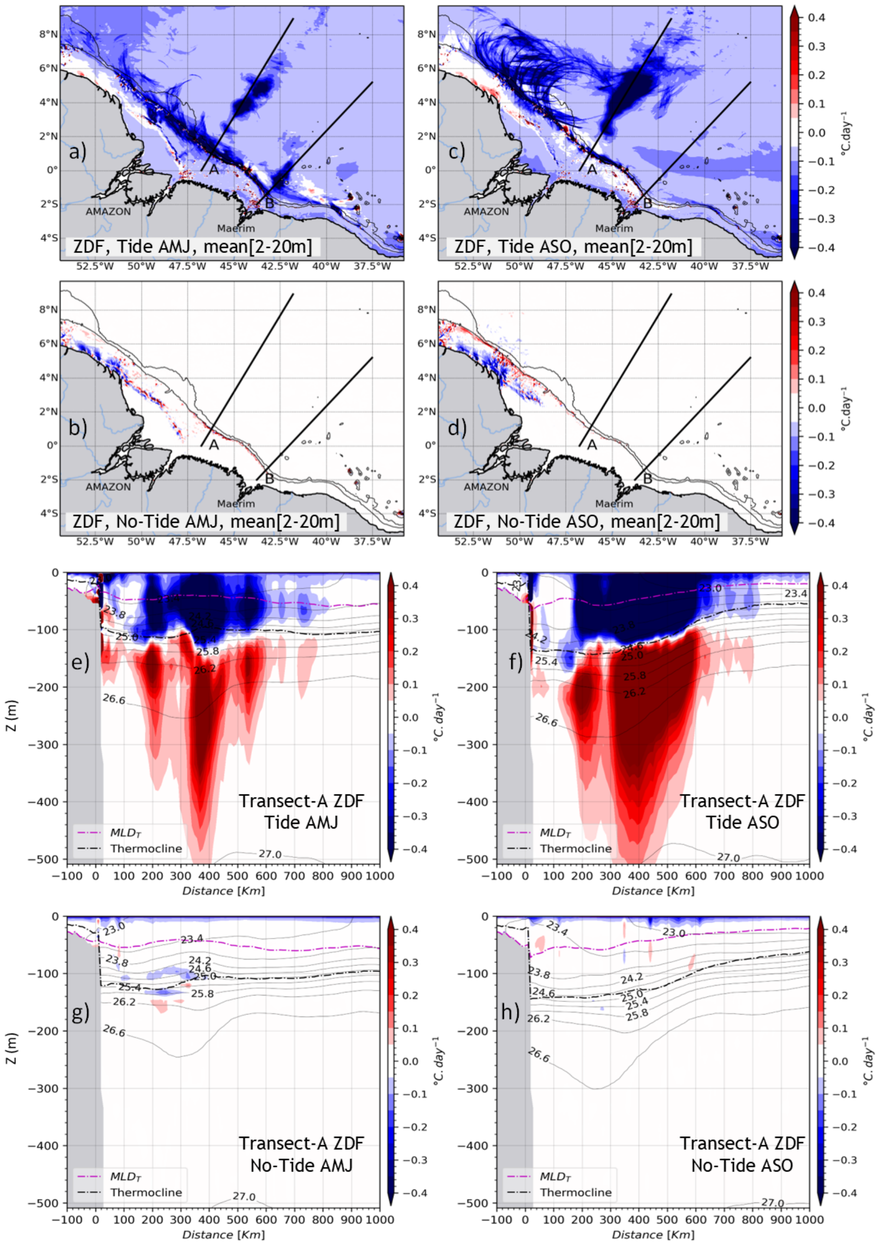

<ins>Figure 8</ins>: The vertical diffusion <ins>tendency </ins>of temperature (ZDF) for both seasons~~, respectively~~ ~~AMJ (left panel) and ASO (right panel). Vertical~~<ins>. The vertical</ins> mean between 2–20 m for AMJ

a mis en forme : Espace Avant : 0 pt, Après : 0 pt

season in tidal (a) and non-tidal (~~c~~b) simulation; then for ASO season in tidal (~~b~~c) and non-tidal (d) simulations. ~~Black thin contours are, from the coast to open ocean, 200 m and 2000 m isobaths. Vertical section~~ Vertical sections of ZDF following the transect A for AMJ season in the tidal (e~~) and~~), for ASO season in non-tidal (~~g~~f) simulations; then for AMJ season in the non-tidal (g) and for ASO season in ~~tidal (f) and no~~the non-tidal (h) ~~simulation~~simulations. The black and magenta ~~ticker dot~~ dashed lines are the thermocline depth and MLD respectively ~~thermocline depth and mixed layer depth. Thin~~. Solid black ~~contours are for~~lines represent the density ~~anomaly~~(σ_θ) isocontours.

a mis en forme : Police :13 pt, Non Italique

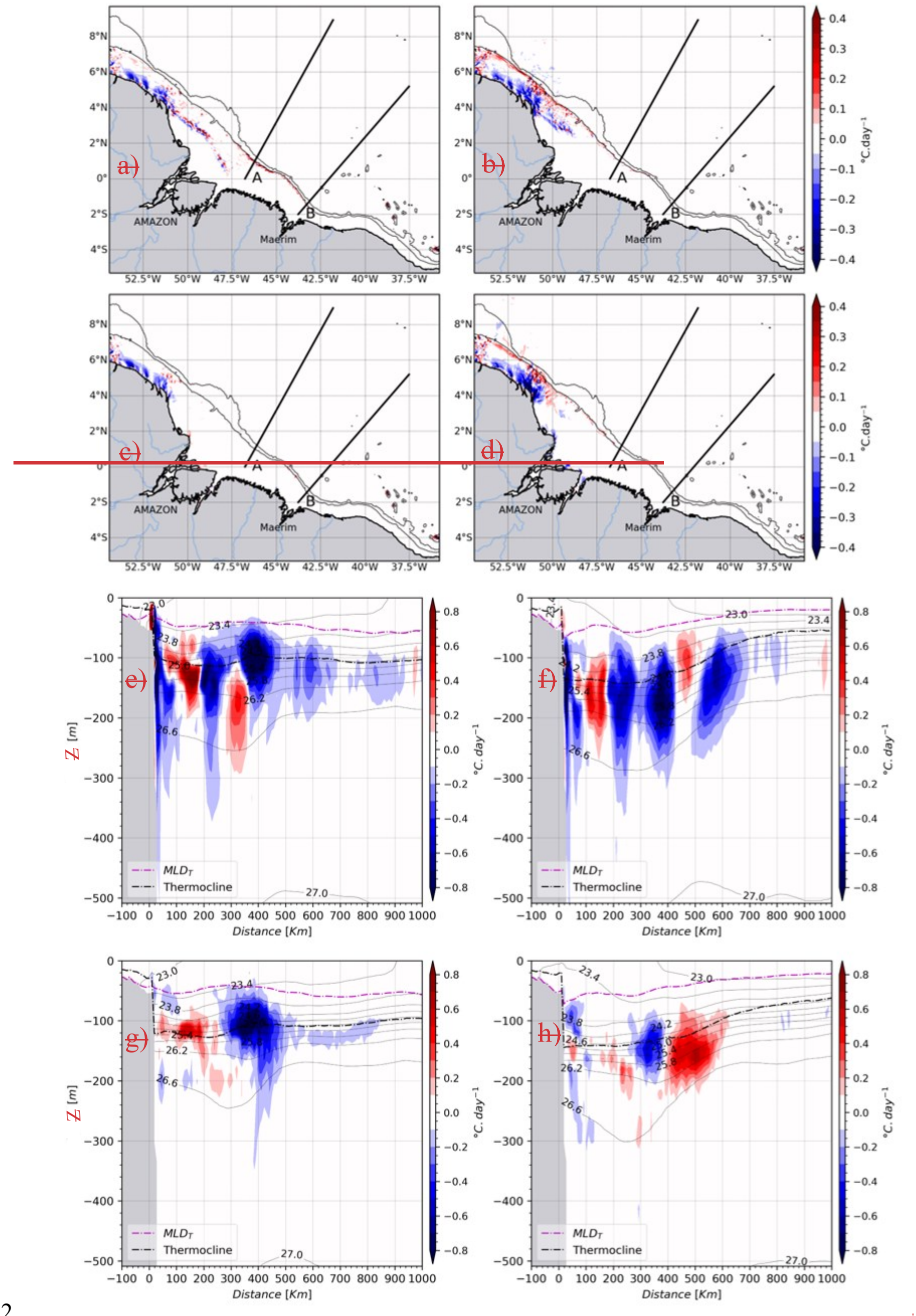
~~a)~~
~~b)~~
~~c)~~
~~d)~~
~~e)~~
~~f)~~
~~g)~~
~~h)~~
8°N
6°N
4°N
2°N
0°
2°S
4°S
52.5°W
50°W
47.5°W
45°W
42.5°W
40°W
37.5°W
A
B
AMAZON
Maerim
°C.day⁻¹
0.4
0.3
0.2
0.1
0.0
−0.1
−0.2
−0.3
−0.4
~~Z~~ [m]
Distance [Km]
°C. day⁻¹
0.8
0.6
0.4
0.2
0.0
−0.2
−0.4
−0.6
−0.8
MLD_T
Thermocline
23.0
23.4
23.8
26.2
26.6
27.0

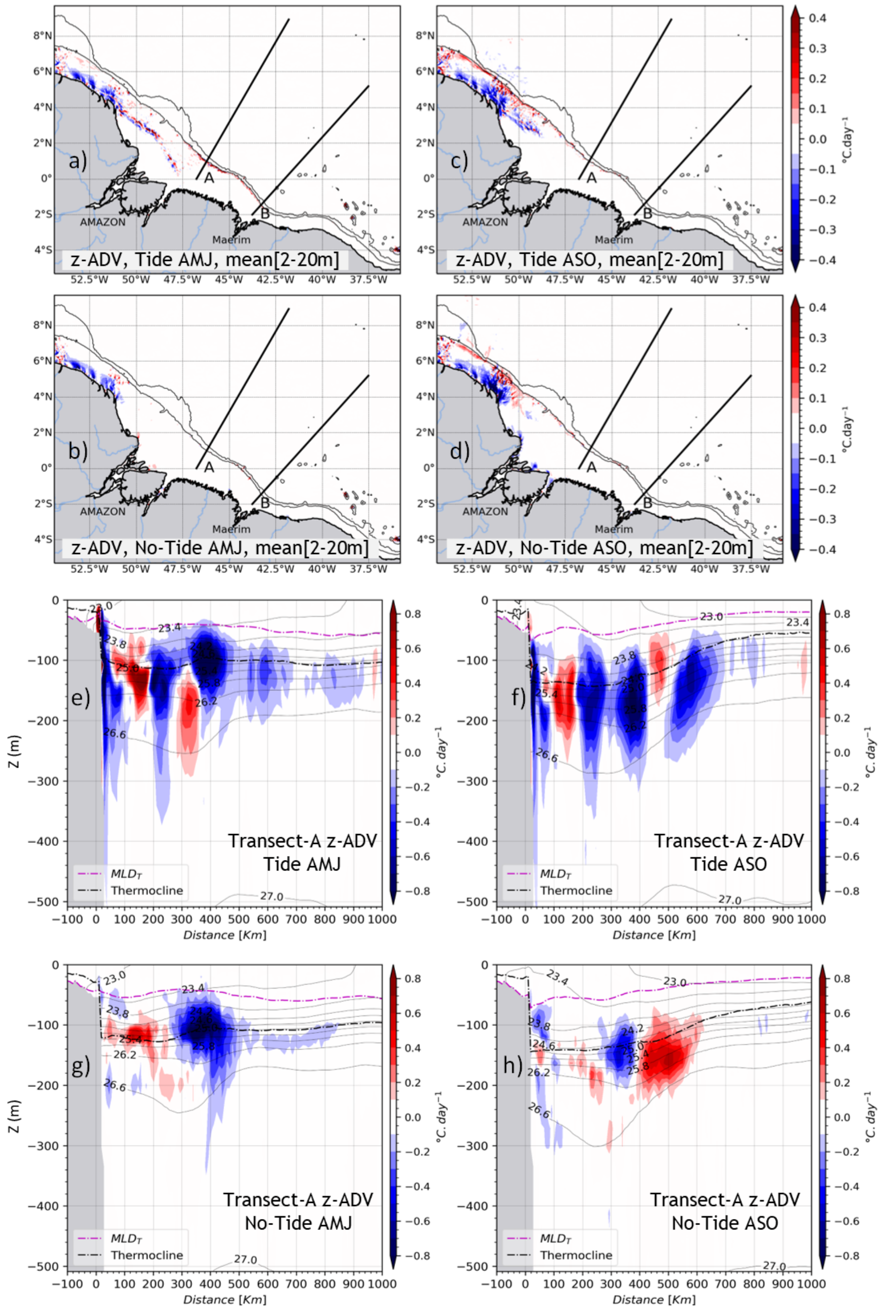
a)
z-ADV, Tide AMJ, mean[2-20m]
c)
z-ADV, Tide ASO, mean[2-20m]
b)
z-ADV, No-Tide AMJ, mean[2-20m]
d)
z-ADV, No-Tide ASO, mean[2-20m]
A
B
AMAZON
Maerim
8°N
6°N
4°N
2°N
0°
2°S
4°S
52.5°W
50°W
47.5°W
45°W
42.5°W
40°W
37.5°W
°C.day⁻¹
e)
Transect-A z-ADV Tide AMJ
f)
Transect-A z-ADV Tide ASO
g)
Transect-A z-ADV No-Tide AMJ
h)
Transect-A z-ADV No-Tide ASO
MLD_T
Thermocline
Z (m)
Distance [Km]
°C. day⁻¹

Figure ~~7~~9: same as figure ~~6~~8, but for the vertical advection tendency of temperature (z–ADV).

a mis en forme : Police :Non Italique

a mis en forme : Espace Avant : 0 pt, Après : 0 pt

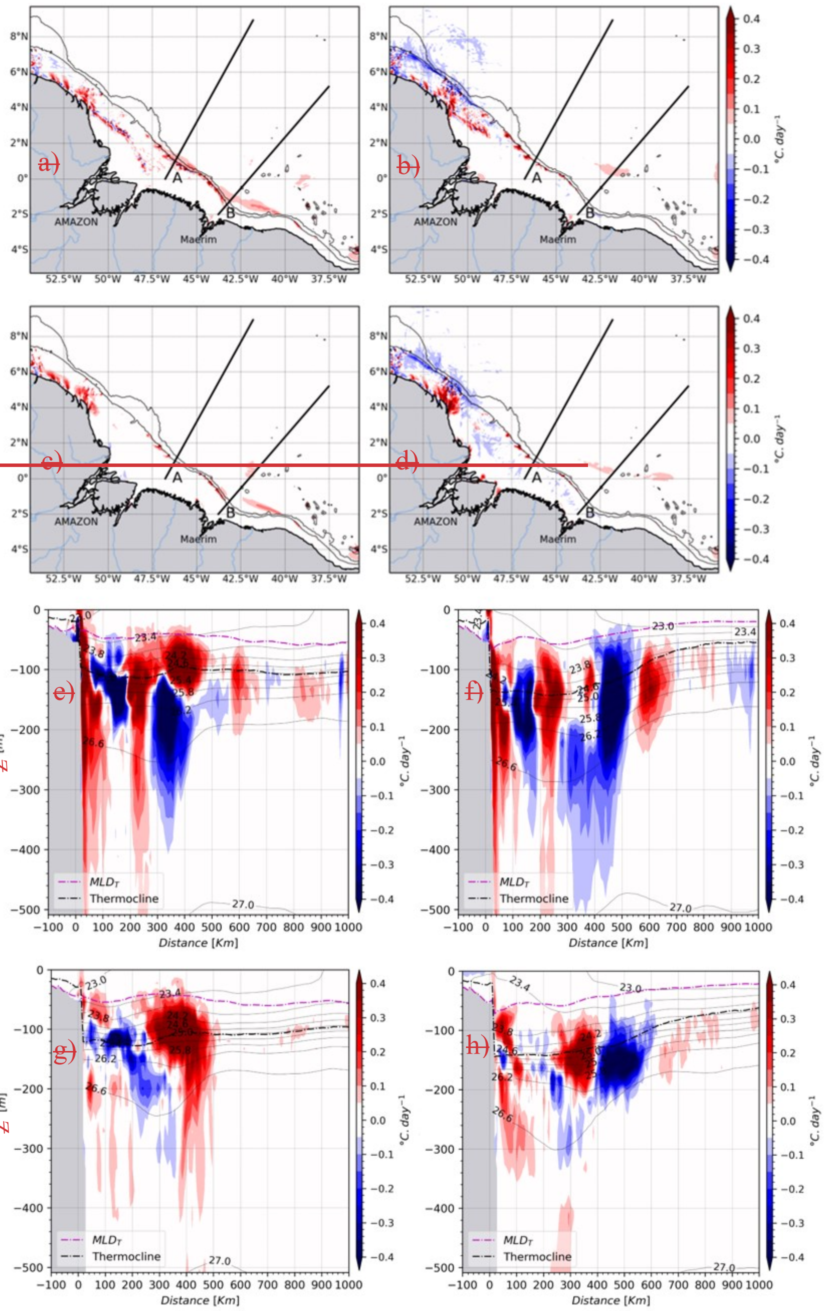
~~a)~~
~~b)~~
~~c)~~
~~d)~~
~~e)~~
~~f)~~
~~g)~~
~~h)~~
A
B
AMAZON
Maerim
8°N
6°N
4°N
2°N
0°
2°S
4°S
52.5°W
50°W
47.5°W
45°W
42.5°W
40°W
37.5°W
°C. day⁻¹
0.4
0.3
0.2
0.1
0.0
−0.1
−0.2
−0.3
−0.4
~~Z~~ [m]
Distance [Km]
MLD_T
Thermocline
23.0
23.4
23.8
25.0
25.8
26.2
26.6
27.0

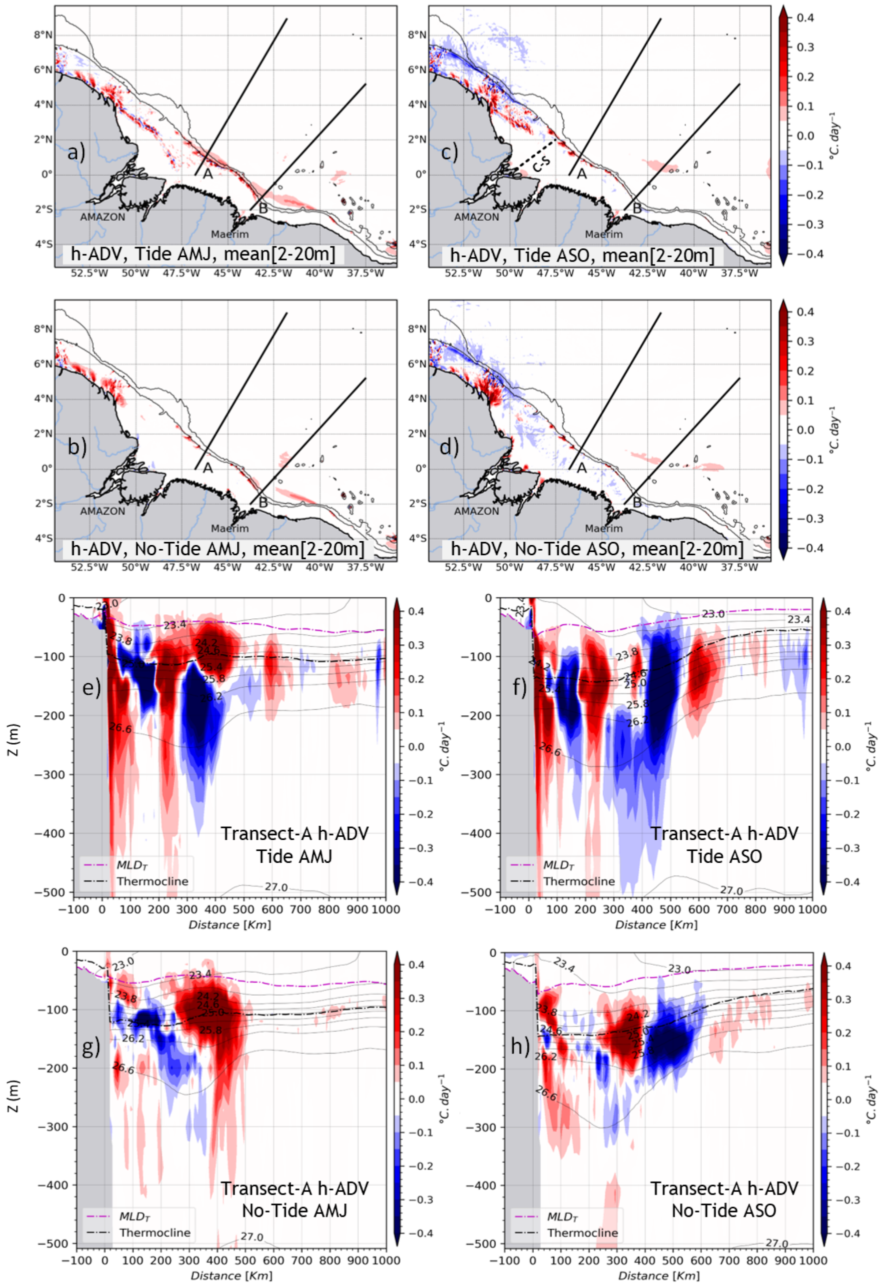
a)
h-ADV, Tide AMJ, mean[2-20m]
c)
h-ADV, Tide ASO, mean[2-20m]
b)
h-ADV, No-Tide AMJ, mean[2-20m]
d)
h-ADV, No-Tide ASO, mean[2-20m]
AMAZON
Maerim
A
B
C-S
8°N
6°N
4°N
2°N
0°
2°S
4°S
52.5°W
50°W
47.5°W
45°W
42.5°W
40°W
37.5°W
°C. day⁻¹
0.4
0.3
0.2
0.1
0.0
−0.1
−0.2
−0.3
−0.4
e)
Transect-A h-ADV
Tide AMJ
f)
Transect-A h-ADV
Tide ASO
g)
Transect-A h-ADV
No-Tide AMJ
h)
Transect-A h-ADV
No-Tide ASO
MLD_T
Thermocline
Z (m)
Distance [Km]
23.0
23.4
23.8
24.2
24.6
25.0
25.4
25.8
26.2
26.6
27.0
0
−100
−200
−300
−400
−500
−100
0
100
200
300
400
500
600
700
800
900
1000

Figure ~~8~~10: same as figure ~~6~~8 but for the horizontal advection of temperature (h-ADV = x–ADV + y–ADV). The dashed line from the Amazon River mouth toward the outer shelf in the panel (b) indicates the cross-shore transect (C-S) used further on.

a mis en forme : Police :Non Italique

a mis en forme : Espace Avant : 12 pt, Après : 12 pt

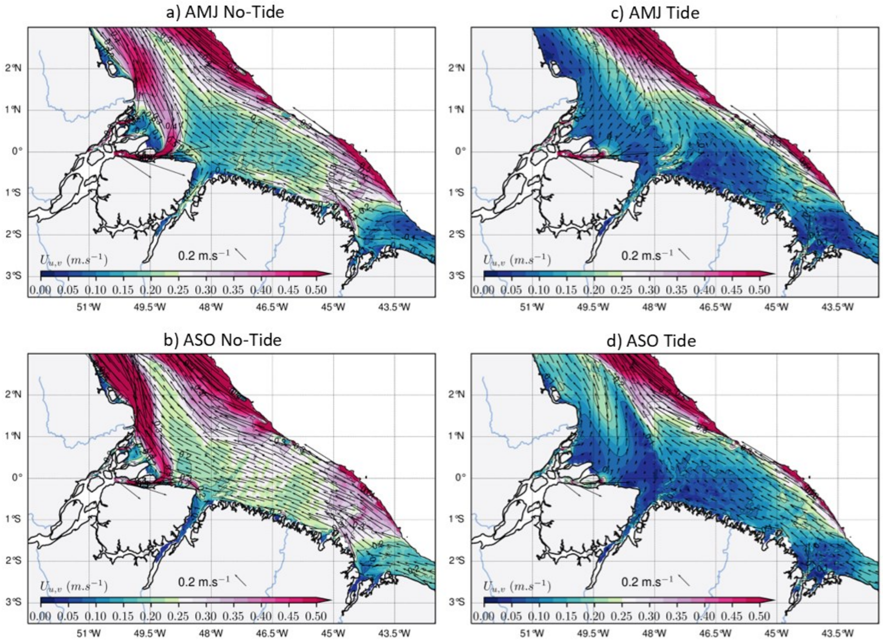

Figure 11: The seasonal mean of the current ($U_{u,v}$) at the shelf averaged between the surface and 50 m: the non-tidal simulation in the left panels and the tidal simulation in the right panels. The upper panels stand for the AMJ season, while the lower stand for the ASO season. The color shading is the modulus of the current and the black arrows represent its direction. Values beyond the 200 m isobath are masked.

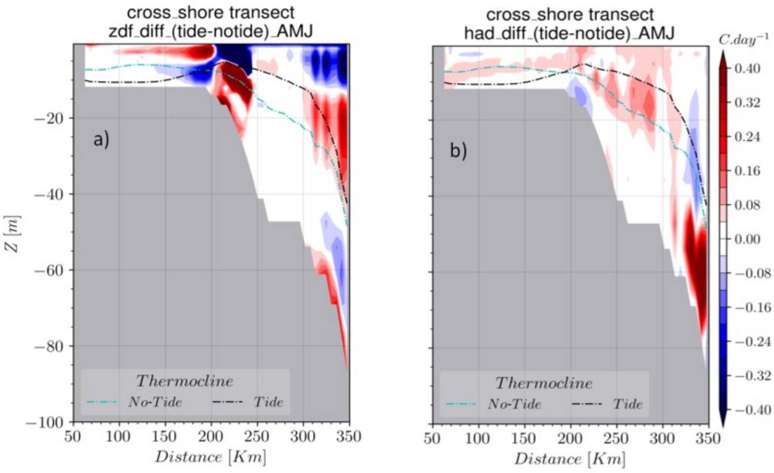

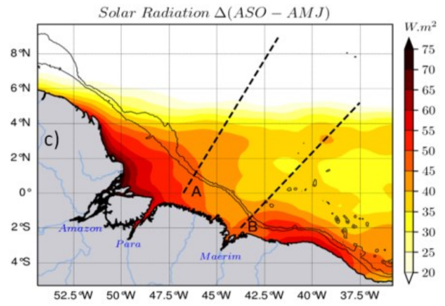

Solar radiation (Qs) increases in the ASO season:
> 30 W.m² offshore
> 60 W.m² over the shelf

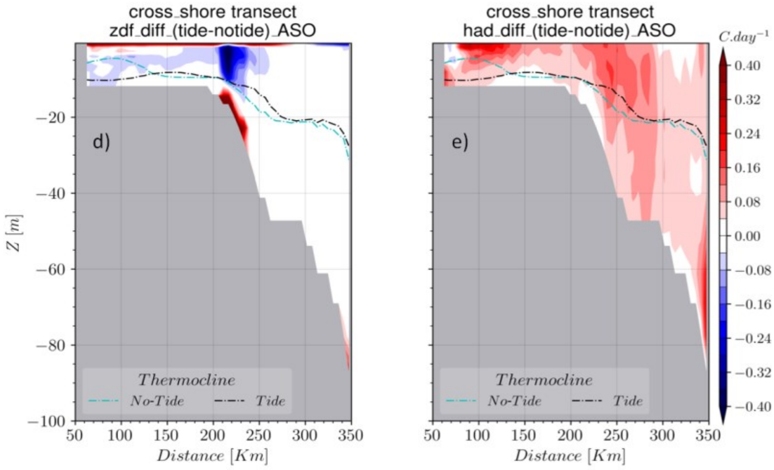

Figure 12: The cross-shore transect of ZDF anomaly for (a) AMJ and (b) ASO seasons, then for h-ADV anomaly for (d) AMJ and (e) ASO seasons ; (c) Difference in solar radiation between ASO and AMJ seasons. Solar radiation increases during the ASO season, with greater intensity on the shelf.

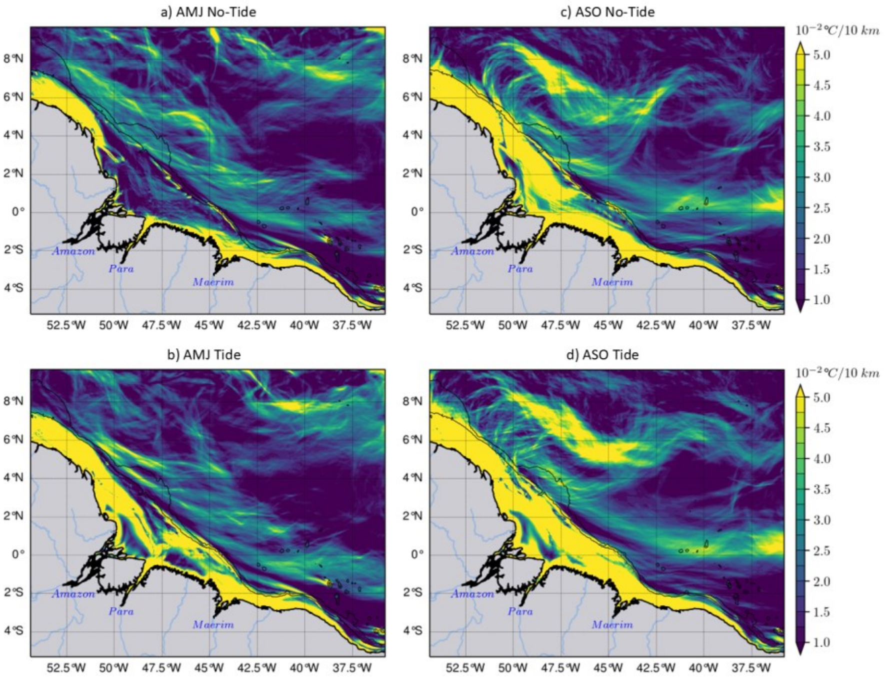

Figure 13 : The horizontal gradient of the Temperature (∇T) averaged between 2–20 m : the AMJ season in the left panels and ASO season in the right panels, the simulations without the tides in the upper panels, and with tides in the lower panels. During the ASO season, the NBC retroflects and eddy activity intensifies in the north-west. Therefore, ∇T emphasizes eddy-like fronts at the same location as eddy-like patterns in ZDF (see Fig.8b).

a mis en forme : Taquets de tabulation : 4,77 cm,Gauche

a mis en forme : Couleur de police : Texte 1